University of Alberta

Evaluation of Electric Cable Shovel Digging Force and Analysis of its Trajectory in Athabasca Oil Sands

By

Mostafa Hatami

A thesis submitted to the faculty of Graduate Studies and Research
in partial fulfillment of the requirements for the degree of
Master of Science
in
Mining Engineering

Department of Civil and Environmental Engineering
Edmonton, Alberta
Spring 2008

Library and Archives Canada

Published Heritage Branch

395 Wellington Street
Ottawa ON K1A 0N4
Canada

Bibliothèque et Archives Canada

Direction du Patrimoine de l'édition

395, rue Wellington
Ottawa ON K1A 0N4
Canada

Your file Votre référence
ISBN: 978-0-494-45817-4
Our file Notre référence
ISBN: 978-0-494-45817-4

NOTICE:
The author has granted a non-exclusive license allowing Library and Archives Canada to reproduce, publish, archive, preserve, conserve, communicate to the public by telecommunication or on the Internet, loan, distribute and sell theses worldwide, for commercial or non-commercial purposes, in microform, paper, electronic and/or any other formats.

The author retains copyright ownership and moral rights in this thesis. Neither the thesis nor substantial extracts from it may be printed or otherwise reproduced without the author's permission.

AVIS:
L'auteur a accordé une licence non exclusive permettant à la Bibliothèque et Archives Canada de reproduire, publier, archiver, sauvegarder, conserver, transmettre au public par télécommunication ou par l'Internet, prêter, distribuer et vendre des thèses partout dans le monde, à des fins commerciales ou autres, sur support microforme, papier, électronique et/ou autres formats.

L'auteur conserve la propriété du droit d'auteur et des droits moraux qui protège cette thèse. Ni la thèse ni des extraits substantiels de celle-ci ne doivent être imprimés ou autrement reproduits sans son autorisation.

In compliance with the Canadian Privacy Act some supporting forms may have been removed from this thesis.

While these forms may be included in the document page count, their removal does not represent any loss of content from the thesis.

Conformément à la loi canadienne sur la protection de la vie privée, quelques formulaires secondaires ont été enlevés de cette thèse.

Bien que ces formulaires aient inclus dans la pagination, il n'y aura aucun contenu manquant.

Canada

Abstract

With a transition from continuous mining with such excavators like draglines and bucket wheel excavators to truck and shovel application in Athabasca oil sands in 1990's research interests has been grown up on improvement of the shovel productivity as well as its availability through different approaches. Some studies been done on soil behaviour and requirements to overcome on the shear strengths and material diggability. Some other focused on equipment itself and to evaluate the stresses generated during the excavation cycle and improvements in metallurgy of the parts. There is also another spectrum of research, which looks at the forces in swing, crowd and hoist. In this paper in order to evaluate the performance of Bucyrus 495H series electric cable shovel, the hoist, crowd, and swing AC motors variables has been collected and post processed to measure and evaluate the digging trajectory, cutting force and its direction.

Acknowledgments

I would like to thank my advisor Josef Szymanski for helping me throughout my research project. I thank David Lang and Carl Gilmore from Bucyrus International Inc. for their authorization and technical support on this project. I also thank Ken Furem from Siemens for his valuable information of MIDAS application and data interpretation. I am especially grateful to Mike DiMarco and Matt Mayers from Shell Canada Energy for their valuable support on my research and arrangement with Bucyrus. Also, I thank Shell Canada Energy and Albian Sands Energy that allowed me to have close monitoring from the operation and receiving the production data.

Finally, I would like to thank my wife Leila for her patience and constant support.

Confidentiality Statement

Due the sensitivity of the input data being used in this report and data proprietary, all output results has been normalized and un-scaled to prevent the confidential information of manufacturer being disclosed. For this regard the letter of data proprietary agreement signed between Bucyrus International and me.

Table of Contents

1 INTRODUCTION 1
1.1 Problem Statement 1
1.2 Research Objectives 1
1.3 Methodology 2

2 BUCYRUS ELECTRIC CABLE SHOVELS 5
2.1 Introduction 5
2.2 History 6
2.3 Dimensions with 495HF/HR Models 7
2.4 Machine Components 8
2.4.1 Shovel Hoist System 13
2.4.2 Shovel Crowd System 13
2.4.3 Shovel Swing System 14
2.4.4 Shovel Propel System 14
2.4.5 Lower Carriage 15
2.4.6 Shovel Dipper 15
2.4.7 Saddle Block 17
2.5 Unique Features with 495HF/HR Models 18
2.5.1 Electrical 18
2.5.2 Structures 18
2.5.3 Planetary Drives 19
2.5.4 Swing 19
2.5.5 Hoist 20
2.5.6 Crowd 20
2.5.7 Operator Cab 20
2.5.8 Dipper 20
2.5.9 Safety 20

3 KINEMATICS AND DYNAMICS OF ELECTRIC ROPE SHOVEL 22
3.1 Cable Shovel Motions Overview 22
3.2 Lifting and Delivery Mechanism 23
3.3 Cable Shovel Kinematics 26
3.4 Cable Shovel Dynamics 28
3.5 Motion Rates of the Lifting and Delivery Mechanisms 37

4 MIDAS SOFTWARE APPLICATION 41

4.1 Overview 41
4.2 MIDAS Software 44
4.3 MIDAS Desktop Application in This Research 46

5 DIGGING TECHNIQUES AND CUTTING TRAJECTORY EVALUATION 52
5.1 Digging Methods 52
5.1.1 Double Back-Up 53
5.1.2 Modified Drive-By 53
5.2 Rake Angle 56
5.3 Shovel Position to Digging Face 59
5.4 Shovel Dipper Positions at Digging Face 59
5.5 Digging Envelope 60
5.6 Force Vectors 63
5.7 MIDAS Data Post Processing 64

6 CONCLUSION AND RECOMMENDATIONS 66
6.1 Conclusion 66
6.1.1 Data Interpretation and Monitoring 67
6.1.2 Dig Cycle and Load Identification 67
6.1.3 Dig Profile Evaluation 68
6.2 Conclusion Summary 79
6.3 Recommendations 80

REFERENCES 84

APPENDIX A: BUCYRUS-ERIE COMPANY SHOVEL PRODUCTION HISTORY 86

APPENDIX B: BUCYRUS ELECTRIC SHOVELS SPEC. SHEETS 89

APPENDIX C: SOIL PHYSICAL-PHYSICOMECHANICAL PROPERTIES 94

APPENDIX D: DYNAMICS BEHAVIOUR OF CABLE SHOVEL 112

APPENDIX E: MIDAS POST PROCESSED DATA SHEETS 122

APPENDIX F: AC MOTOR FORMULAS AND CALCULATIONS 127

List of Tables

Table 1: Key Components in the Three Main Sections of a Shovel 12

Table 2: Bucyrus Dipper Capacities 16

Table 3: Dipper Fill Factor 17

Table 4: Theorical Cycle Time and Outputs of Cable Shovel According to the Ease of Digging 17

Table 5: Bucyrus International Inc. Shovel Production History 87

Table 6: HF BUCYRUS ELECTRIC CABLE SHOVEL SPECIFICATION SHEET 90

Table 7: Values of E for Different Soils 98

Table 8: Transient Shear Strength of Frozen Soils 99

Table 9: Angle of Repose for t = - 10 °C 100

Table 10: Values of Angles of Internal Friction φ_2 100

Table 11: Classification of Soils for Roads 101

Table 12: Specific Resistance to Cutting, k, and Digging, k_1 for Excavator 110

Table 13: Normalized Raw Data to be Reportable to Public 126

List of Figures

Figure 1: Trajectory Assessment Research Flowchart 4

Figure 2: Bucyrus 495B-HF Electric Cable Shovel 7

Figure 3: Bucyrus Electric Cable Shovel Typical Dimensions Working Ranges and Weight 8

Figure 4: 495HR Deck Plan View 9

Figure 5: Major Shovel Components 11

Figure 6: Hoist-Crowd Ropes Assembly in Cable Shovel 11

Figure 7: Illustration of Bucyrus Lower Works 12

Figure 8: Front and Rear View of Dipper 16

Figure 9: Shovel Dipper Angle Nomenclature 19

Figure 10: Shovel Dig & Load Motions 23

Figure 11: Lifting and Delivery Mechanisms 24

Figure 12: Cable Shovel Schematic of Lifting and Delivery 26

Figure 13: Cable Shovel Kinematics Diagram - $\theta 3$: Hoist Angle; 2Π-$\theta 4$: Crowd Angle 27

Figure 14: Handle Free-Body and Elements of Shovel Dynamics (Frimpong S. et al., 2005) 29

Figure 15: a) General Layout of Forces on Shovel Digging Parts b) Dimensional of the Forces 33

Figure 16: Determination of Lifting (Hoist) Force 35

Figure 17: Schematics of Forces in Three Major Bucket Positions 36

Figure 18: Hoist and Crowd Speeds Dimensions 38

Figure 19: Optimal Trajectory Pattern 40

Figure 20: MIDAS Desktop Snapshot 44

Figure 21: MIDAS Report Snapshot 45

Figure 22: Shovel KPI, Hoist Torque-Power-Speed 47

Figure 23: Shovel KPI, Crowd Torque-Power-Speed 47

Figure 24: Shovel KPI, Hoist & Crowd Power-Speed 48

Figure 25: Shovel KPI, Hoist & Swing Power 48

Figure 26: Shovel KPI, Hoist & Crowd & Swing Power 49

Figure 27: Dig Cycle with Regards to Hoist-Crowd Power 51

Figure 28: Double Back-Up "A" 54

Figure 29: Double Back-Up "B" 55
Figure 30: Modified Drive-By 56
Figure 31: Shovel Dipper Angle Nomenclature 57
Figure 32: Bad Shovel Position at Digging Face 58
Figure 33: Proper Shovel Position at Digging Face 58
Figure 34 : Cable Shovel Typical Trajectoy Patern 60
Figure 35: Typical Path of Dipper into Digging Face 61
Figure 36: Shovel Position at Digging face 61
Figure 37: Optimum Start Point for Dipper Entry 62
Figure 38: Cutting Forces Vectors on Dipper (Not to Scale) 64
Figure 39: Force Vectors on Three Main Positions (Not to Scale) 65
Figure 40: Dipper Load Trips 70
Figure 41: Digging Cycle Selection (Units are not in same scale) 71
Figure 42: Shovel Power Usage-Generate Vs. Dipper Loads (Units are not in same scale) 73
Figure 43: AC Motors Volt Amp Vs. Time 74
Figure 44: One Full Dig Cycle Trajectory 74
Figure 45: Cutting Force vs. Force Direction 78
Figure 46: Normalizing the Hoist Power 78
Figure 47: Sample Histogram of One Hour Digging 81
Figure 48: Dig Cycle Time Probability 82
Figure 49: Cutting AngleDistribution Chart 82
Figure 50: 495HF Bucyrus Electric Shovel Dimensions 91
Figure 51: Schematic Bucyrus 495HR Parts Names 93
Figure 52: Tubular Dipper Handle Design Versus Rack& Pinion 93
Figure 53: a) Relation Between Angle of Internal Friction and Moisture b) Dependence of Cohesion on Coefficient of Saturation by Water (degree of compaction) and moisture 97
Figure 54: Deformation of Soil Under Action of Wedge 103
Figure 55: Determination of Tooth Parameters 104
Figure 56: Additional Resistance to Cutting as Function of Area of Blunting at Different Cutting Depth 106
Figure 57: Digging Resistance Force Vectors 108

Figure 58: Crowd Free Body Diagram and Bucket Assembly (Awuah-Offei, K., 2004) 112

Figure 59: Interaction Between Dipper and Media (Frimpong S. et al., 2005)..... 119

Figure 60: Handle Free Body Geometry..... 123

Figure 61: Tooth Point Trajectory 124

List of Equations

Equation 1: Cartesian Position Equation 27
Equation 2: Velocity Calculation 28
Equation 3: Acceleration Calculation 28
Equation 4: Dynamics Equation of Cable Shovel (Frimpong S. et al., 2005) 30
Equation 5: Dynamic Equilibrium on Shovel Working Device 34
Equation 6: Equilibrium of Drums for Delivery 36
Equation 7: Optimal Trajectory Equation 39
Equation 8: Constant Cutting Angle Curvature 40
Equation 9: Porosity Calculation 94
Equation 10: Coulomb's Law 96
Equation 11: Modulus of Deformation of Soil 98
Equation 12: Tangential Resistance Force 107
Equation 13: Detailed Form of Tangential Equation 107
Equation 14: Summarized Form of Tangential Equation 107
Equation 15: Digging Resistance Normal Component 108
Equation 16: Normal Tooth Length 109
Equation 17: Summation of Forces in X-Y Directions 113
Equation 18: Result of Momens Around Centre of Mass of Handle 113
Equation 19: Correlation of Force X-Y Components 113
Equation 20: Position Vector of Centre of Mass of the Handle 114
Equation 21: Acceleration Characteristics of the Crowd Arm 114

1 INTRODUCTION

1.1 Problem Statement

The level of the operator's experience directly can affect productivity of digging equipment such as cable shovel. How to manage the dipper to penetrate in the face and have the best trajectory pattern determines the amount of the cutting forces that should overcome to the resistance forces. Varying occurrence of different types of soil layers also detect the optimum trajectory path. Having the knowledge of the soft and hard zones at face enables the operator to proactively controls the dipper movement, hence the better smoother penetration the less energy consumption and damage to parts caused by hugely generated stresses in boom and other mechanical parts of the shovel.

In the past there are many researches done on optimization of mechanical components of the shovel to improve the productivity by means of numerical and computer simulation modeling. It is rarely attempted to analysis the real data and come up with some mentorship to the shovel operator on how to run the machine in proper way according to the environment, experimental data, and material type the excavator digs into the dirt. Goal of this research is to measure the cutting forces during the digging cycle. Collecting the input current and voltage data from swing, hoist, and crowd can do this. The readings being captured by means of an installed device innovated by Siemens on Bucyrus cable shovels at Albian Sands Energy oil sands Muskeg River Mine.

1.2 Research Objectives

This research was focused on the review of the Bucyrus electric shovel components and calculating the cutting forces by employing different shift and operator inputs. To accomplish this, the geometry of trajectory was studied and physics rules applied. The objectives of the research included of:

- Exploiting Bucyrus International Inc. electric cable shovel components and different machinery groups, and the trajectory pattern configuration. An optimized introduced trajectory evolves the reduction in cutting forces as well as dig cycle time and increase of productivity and significant cost saving due to reduction of required maintenance.
- Introduction and review of MIDAS real-time data acquisition device and the developed database to interpret the Midas information.
- Applying physics and geometry to calculate the cutting forces at the dipper. This could not be approached without having the known force vectors of the crowd and hoist forces that can be measured off the output data from Midas software.
- Evaluation of the best trajectory patterns according to the variation of the cutting forces during the dig cycle.

1.3 Methodology

The trajectory pattern optimization could not be fulfilled without having a thorough performance monitoring study. In this research, the cable electric shovel current and voltage data from swing, hoist and crowd motors of Bucyrus 495HF (High Floatation) series were being collected. Siemens has introduced a unique technology called MIDAS Data Acquisition System, with which all real-time machine's operating data can be recorded in a database. Once ample information from different dig cycles via the installed device on the shovel received, these data need to be post processed since the MIDAS software does not report all necessary key information to be imported into equations for this study of digging trajectory evaluation. For this regard some design manufacturing data is required to translate outputs of the software; Therefore, I visited the manufacturer production line as well as staying among the engineering design team to have close hands on communication with key personnel. Once all necessary design information was collected, data post processing on MIDAS database started. This was not practical without contacting the Siemens representative who directly involved in development of the MIDAS to interpret a huge database with missing

columns' headers. In this research in order to run the analysis on the forces, the motion geometry of the dipper has been reviewed to capture incorporating angles that must be added into the calculations. By assessing the trajectory at any given time/location and corresponding cutting forces one can say how to dig in oil sands with optimized adjustment of hoist and crowd motion to have the best result.

Numerical simulation results, Frimpong et al. (2006) says, For a constant hoist rope retraction speed, the optimum dipper trajectory is defined for crowd arm extension speeds and vice versa. Also, the digging time for crowd arm extension and hoist rope retraction speeds sampled from a uniform distribution between 0.15 and 0.35 m/s follows a triangular distribution with minimum 6.12 s, mode 7.26 s and maximum 13.7 s. Using these results, production engineers can parameterize shovel excavation schemes for optimum production performance. Researches have been performed on shovel performance monitoring and identification of the key performance indicators so far. "It was found that hoist and crowd motor responses could be used to identify different shovel activities, especially the dig cycle," said Sibba Pantnayak PhD student in mining engineering at university of Alberta. It is also seen in this theses study with the similar result. Analysis of the digging trajectory proves that it can directly be affected by operator's experience and significantly influence the shovel performance. Many studies been done to identify the types of forces and reaction between the shovel and earth to determine the ground diggability characteristics. As one of those references in this research it can be mentioned the mechanics for earthmoving work, the theory and calculations (T.V. Alekseeva, R.I. Voitsekhovskii, N.A. Ul'yanov, K.A. Artem'ev). This book includes of soil properties and machine moving parts interactions with soil as well as delivery mechanisms for the shovel. With application of microprocessor-based monitoring systems such as those invented by Siemens, it is viable to measure shovel performance parameters with high level of precision. Of those of shovel performance factors it can be cited the cycle time (dig-swing-dump), dipper payload and fill factor, and power and energy usage during the dig cycle. A paper by Hansen (2001) states measurement of dipper payload to find diggability of

electric shovel. Shovel parameters for instance hoist rope position, crowd arm extension, hoist armature current and voltage, hoist field current, crowd armature voltage and current have been monitored and reported by Hendricks (1990) and Hendricks et al. (1989). Karpuz et al. (1992) calculated the loading and digging cycle time, dipper fill factor, and power on the main drive AC motor to discover the effect of intensity of cut and blasting on shovel performance. The following diagram algorithm in Figure 1 shows the steps pursued in this study to come up with final results.

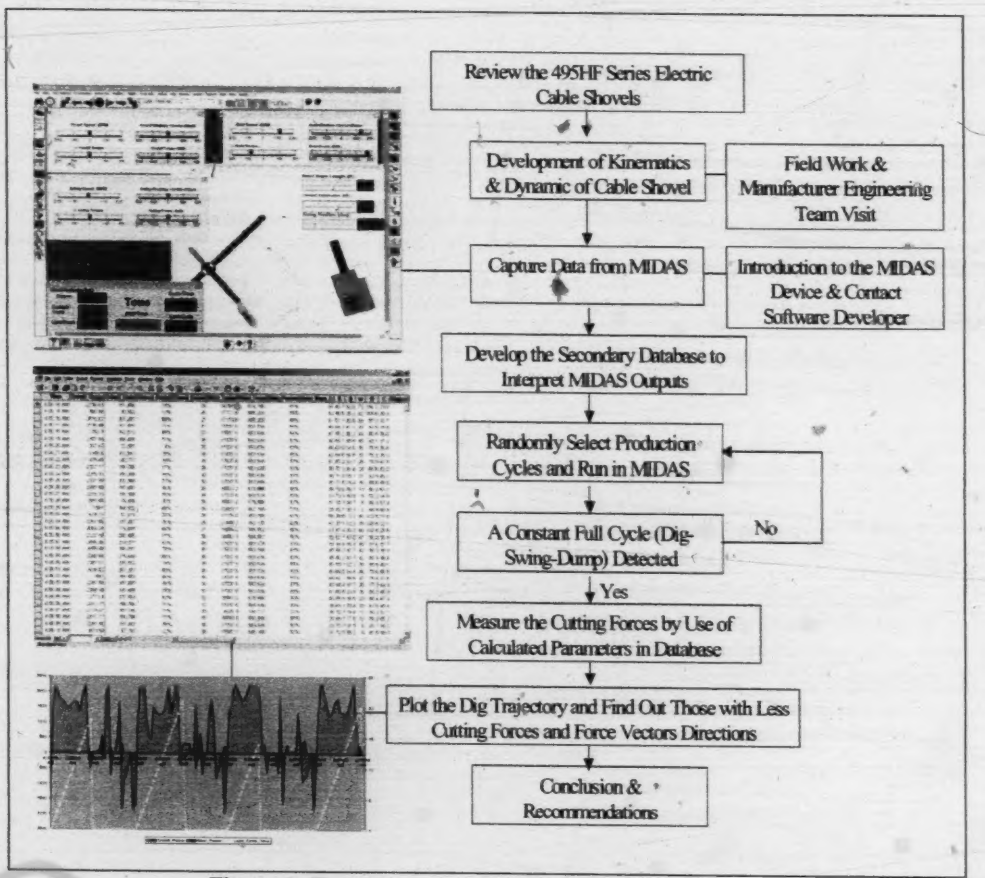
Review the 495HF Series Electric Cable Shovels
Development of Kinematics & Dynamic of Cable Shovel
Field Work & Manufacturer Engineering Team Visit
Capture Data from MIDAS
Introduction to the MIDAS Device & Contact Software Developer
Develop the Secondary Database to Interpret MIDAS Outputs
Randomly Select Production Cycles and Run in MIDAS
A Constant Full Cycle (Dig-Swing-Dump) Detected
No
Yes
Measure the Cutting Forces by Use of Calculated Parameters in Database
Plot the Dig Trajectory and Find Out Those with Less Cutting Forces and Force Vectors Directions
Conclusion & Recommendations

Figure 1: Trajectory Assessment Research Flowchart

2 BUCYRUS ELECTRIC CABLE SHOVELS

2.1 Introduction

Most of Canada's oil sands are found in Alberta, and the highest quality resources are the Athabasca deposits of northern Alberta. The mineable Athabasca oil sands are found in thick seams 17 to 50 m below surface, making them ideal for open pits. Hydraulic face shovels and backhoes, and electric shovels load the bitumen ore into the largest haul trucks available. Shovels are the major key element in bulk earth excavation in open pit mining nowadays. The competition in the mining industry caused to shift the operations toward truck and shovel techniques in early 1990s. This has led to the development of today's ultra size haul trucks with payloads of up to 400 short tons (e.g. CAT 797B, LIEBHERR 282B, KOMATSU 930e Series), and electric shovels carrying bucket loads of 100 to 120 short tons (e.g. Bucyrus 495H Series, P&H 4100 Series). There are 600 large electric rope shovels working worldwide today (Gilewicz, 1999). Large shovels are more or less defined by dipper capacities of 25 cubic meters and higher. Over 150 of those 600 units (25%) are the ultra-large shovels like the Bucyrus 495 and the P&H 4100.

Electric shovel is the name given to electrically powered rope shovels. They are the modern equivalent of steam shovel, and operate in an identical fashion. The Bucyrus-Erie 495 series is derived from a set of shovels built based on different applications. 495-B HR – Hard Rock, 495-B HF – High Floatation, and 495-B HD – Heavy Duty. 495-B HF is widely being used in oil sands mining operations. Albian Sands Energy a joint venture of Shell Canada (60%), Chevron Texaco (20%), and Western Oil Sands (20%) has employed this type of cable shovel successfully in its oil sands production. Figure 2 shows a typical operation in oil sands mine with the truck back up operation. 495 series has a proven history of outstanding productivity and the "HR" version incorporates new and innovative technologies, which enhance its capabilities. The 495 employ the Siemens AC - IGBT electric drive system. The AC system eradicates brushes; fuses and RPC

components that are high maintenance items on DC drive machines. An entirely modularized electrical room ships directly to the field to facilitate the erection process. Each 495H series equipped with two optional monitoring systems, AccuLoad and MIDAS. AccuLoad is setting industry standards for precise weighing of each individual dipper load. MIDAS provides a means for production tracking and maintains ongoing detailed records of the various machine motions and activities. The resulting digital history of the machines operation allows managers to track and set benchmarks for improving productivity.

The shovel can be used in all types of material excavation in a spectrum of very soft to toughest ores. Shovels are able to yield consistent and high production by a combination of rugged construction and pivotal dig load motion.

2.2 History

The first generations of the steam excavators were developed in early 1800's and being used for dredging. In 1835 shovels were mounted on rail cars to assist with railway construction. In 1925 first heavy duty, self propelled, full revolving shovel was developed for use in quarrying and mining. The driving force in all shovels was steam until mid 1900's when the DC motors were introduced into the market and shovels were equipped to either steam or electric power force. This continued by 1979 that technology introduced AC motors to be used on shovel due to advantages of the AC current over the DC for heavy-duty applications. Steam and electric shovels are the two types of shovels manufactured by Bucyrus International Inc. Stripping, electric, and hydraulic shovels are types that being used in the industry for many years. Mentioned sequence incorporates with the size of each excavator. As an example, one can be mentioned of Bucyrus 1950-B with 105 cubic yard (81 cubic meter) to be used in stripping and Bucyrus 495-B or 595-B with capacities of 53-57 cubic yard (41-44 cubic meter) for mining operations. A brief history of Bucyrus production and different models is given in Appendix A.86

2.3 Dimensions with 495HF/HR Models

Figure 3 shows the typical section of the shovel dimensions. It is advantageous to be familiar with the terms in this report might be used that sources from this picture of the Bucyrus engineering design definitions on different parts and functions of the machine. Also Figure 4 shows the schematic view plan of 495HR deck assembly showing all major components on this shovel structure. In appendix B it is also illustrated of a 495HF dimensions for better appreciation of the current valid sizes on Bucyrus electric shovels.

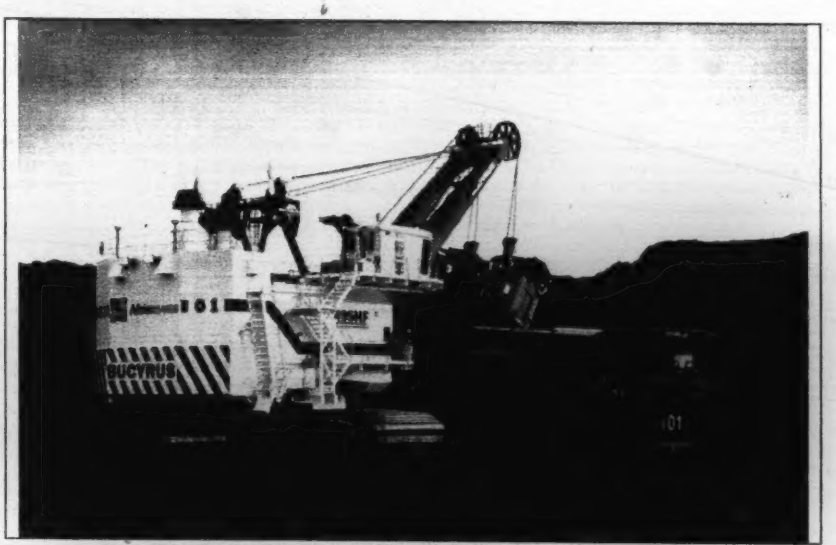

Figure 2: Bucyrus 495B-HF Electric Cable Shovel

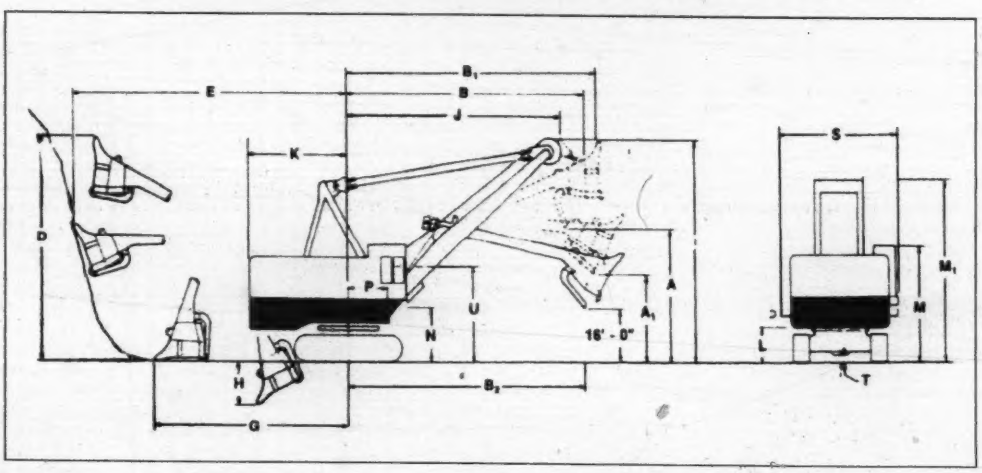

CODE	DIMENSION
A	Dumping height – maximum
A_1	Dumping height at maximum radius – B_1
B	Dumping radius at maximum height – A_1
B_1	Dumping radius – maximum
B_2	Dumping radius at 16'0" dumping height
D	Cutting height – maximum
E	Cutting radius – maximum
G	Radius of level floor
H	Digging depth below ground level – maximum
I	Clearance height – boom point sheaves
J	Clearance radius – boom point sheaves
K	Clearance radius – revolving frame
L	Clearance under frame – to ground
M	Clearance height top of house
M_1	Height of A-frame
N	Height of boom foot above ground level
P	Distance – boom foot to center of rotation
S	Overall width of machinery house and operator's cab
T	Clearance under lowest point in truck frame
U	Operator's eye level

Figure 3: Bucyrus Electric Cable Shovel Typical Dimensions Working Ranges and Weight

2.4 Machine Components

Each electric cable shovel is included of three major sections. Front end, revolving frame, and lower works. Table 1 gives key components found in the

three main sections of a shovel. Figure 5 shows an overview of major parts of a cable shovel.

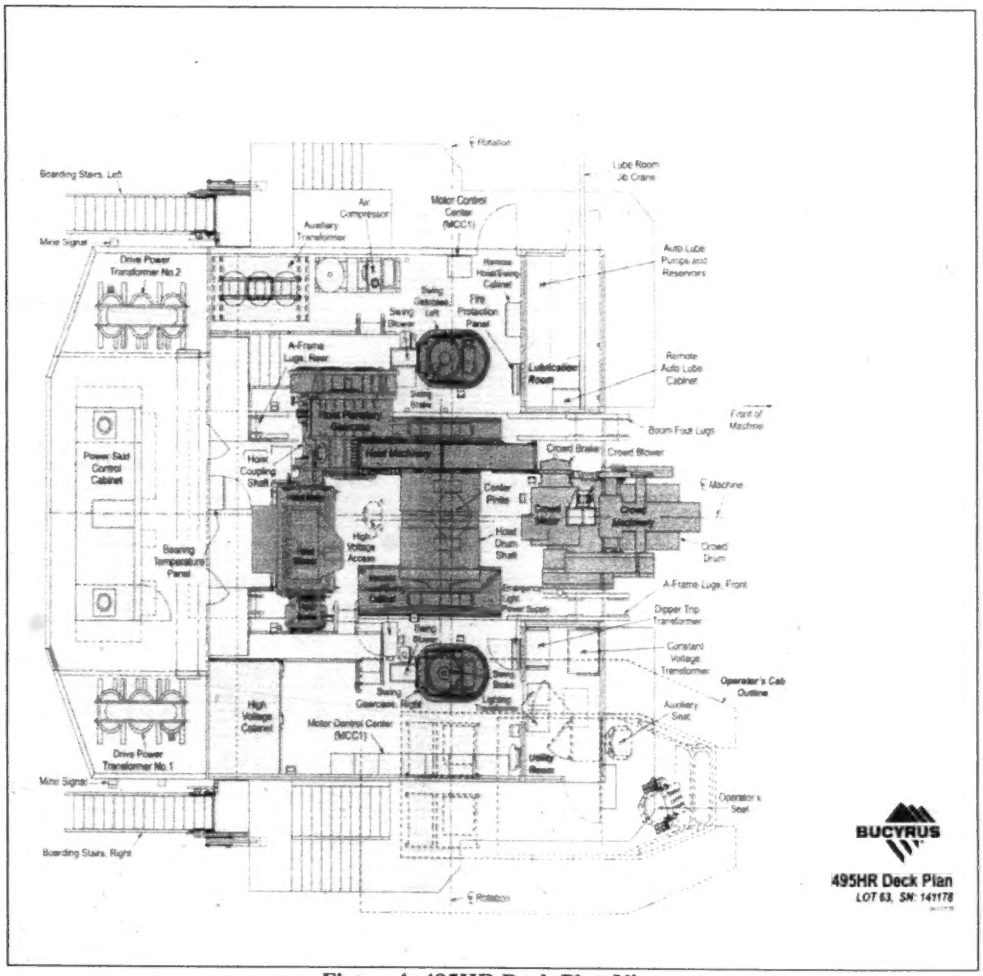

Figure 4: 495HR Deck Plan View

The three sets of ropes at several parts of the shovel being installed to facilitate transfer of the forces and energy toward the dipper. These can be counted as hoist and crowd ropes. However, boom structural suspension strands hold the boom assembly – Figure 6 - and acts as a safety relief valve while the operator of the shovel over exceeds the crowd into the face causing the dipper handle to push the boom upward. Also dipper trip rope is another one that plays important roll in shovels production to enable the latch lever operational to release the door while dumping dirt into the haul trucks.

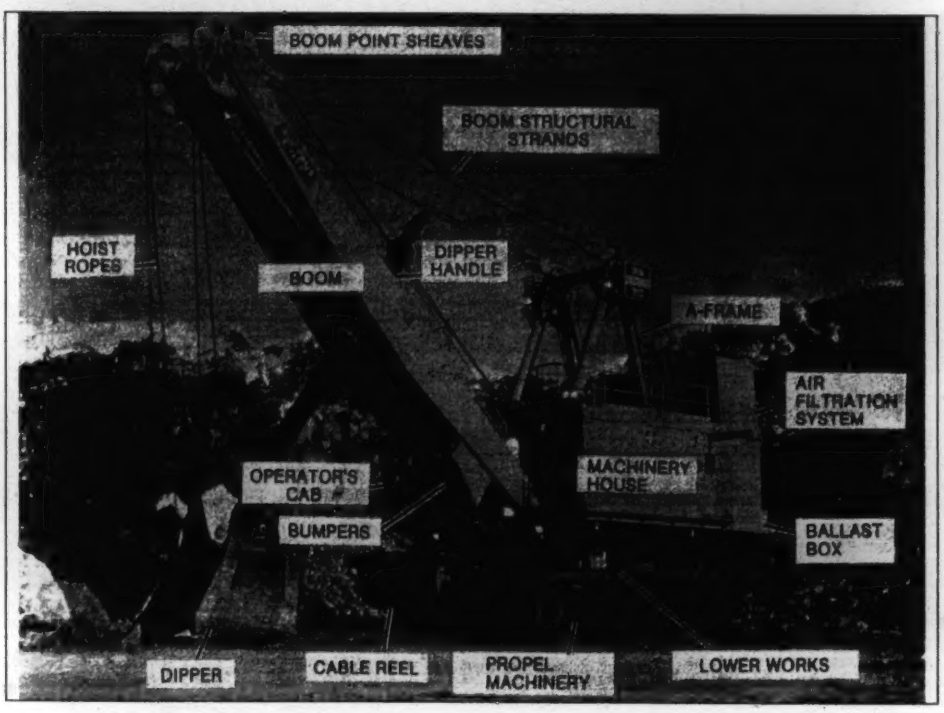

Figure 5: Major Shovel Components

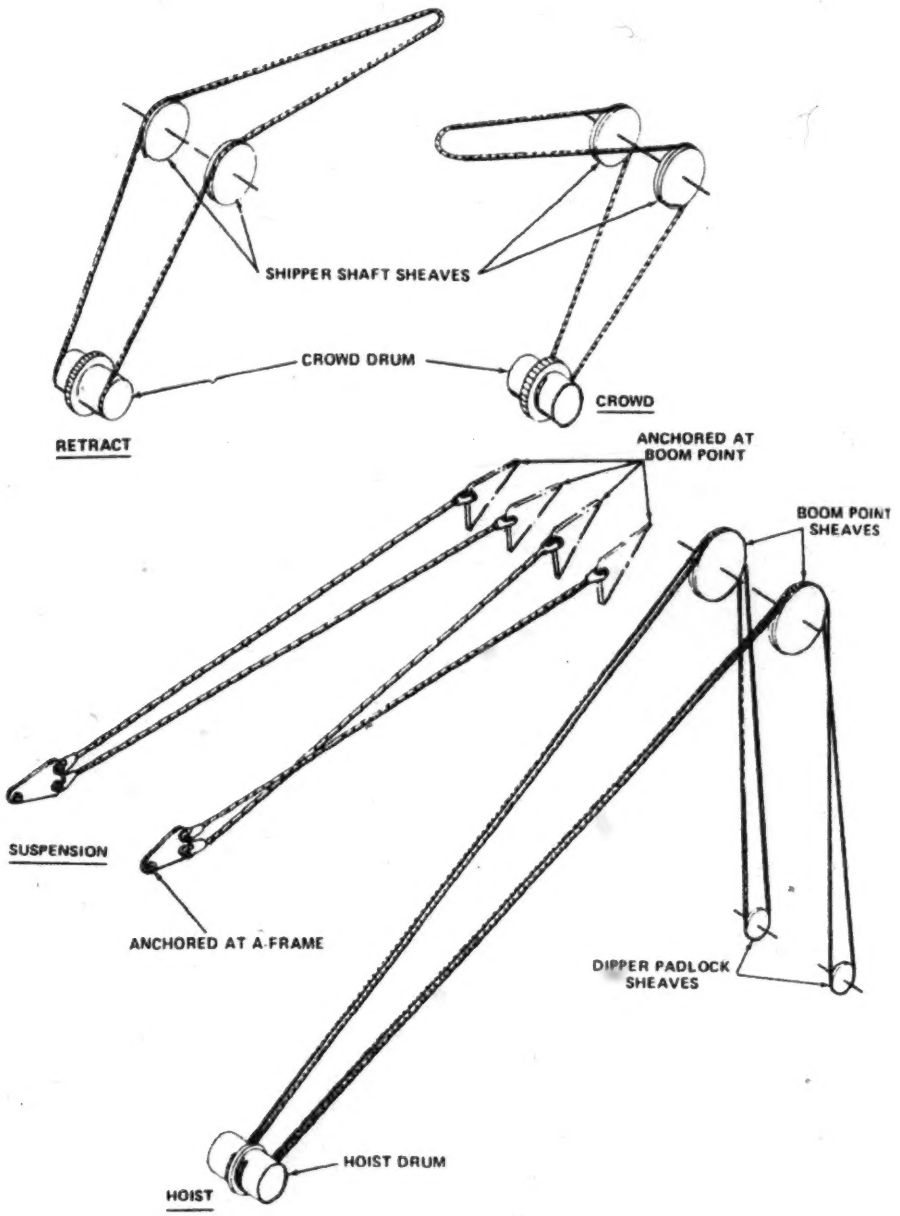

Figure 6: Hoist-Crowd Ropes Assembly in Cable Shovel

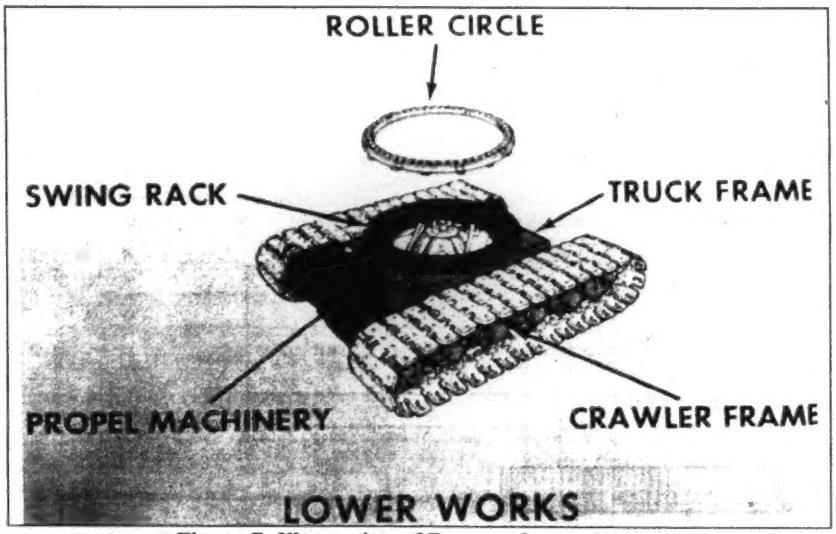

Figure 7: Illustration of Bucyrus Lower Works

TABLE 1: KEY COMPONENTS IN THE THREE MAIN SECTIONS OF A SHOVEL

SHOVEL SECTION	COMPONENTS
Front End	Boom Shipper Shaft Assembly Dipper Handle and Dipper
Revolving Frame	Hoist Machinery Crowd Machinery Swing Machinery Operator Controls MG Set Electrical Cabinets Lubrication and Air Systems
Lower Works	Truck Frame Side Frames Propel System Swing Circle Crawler Track Assembly

Figure 7 shows the illustration of lower works of a Bucyrus electric shovel. More detail information of 495HF series that can be published publicly is presented in Appendix B. 89

2.4.1 Shovel Hoist System

The hoist system is consisted of a variable speed, reversible. The AC motor draws its power from AC generator. While the dipper dig in the face and requires hoisting upward, the hoist AC motor consumes power but once the hoist reverts down then the AC motor through the AC generator produces electricity and deliver it back to the mine network. The hoist mechanism plays the major roll during the digging cycle. The hoist rope transfers the force from the hoist drum towards the dipper padlock sheaves through boom point sheaves. There is a shut down switch enforces the hoist to stop if the boom starts to jump up from the current position (it supposed to be a stationary part). This prevents any damage to the suspension strands. On 495H series a 70" (177.8 cm) hoist drum is installed for extended rope life. The gearing system is called dual output planetary hoist mechanism that reduces required maintenance compare to the single pinion design.

2.4.2 Shovel Crowd System

The shovel crowd system is designed to control dipper penetration in the bank. The crowd motion, like the hoist is involved in transmitting power to the dipper and is subject to shock or impact loading methods generally used to achieve the crowd and retract motion of the dipper handle. The dipper handle assembly is presented in the market in two different types, wire rope system and rack and pinion system. 495H series are equipped with the wire rope crowd system, which is included with dipper handle that traveling through the saddle block as well as crowd and retract ropes woven around the crowd drum and transfer the energy through the shipper shaft sheaves towards the crowd rope adjusting mechanism and retract rope take-up mechanism. The stick carrying the bucket is hinged between the two main chords of the boom at about half of its length. To be able to vary the digging radius and to position the bucket at the right place over the dump

body of the mining truck the stick can glide forward and backwards in its saddle block. This motion is achieved by a set of ropes. Thus and because of the fact that the stick is tubular allows it to revolve around its centre line to compensate for forces that are applied on the digging lip off the centre of the bucket during the digging cycle. As it is already shown in Figure 6 the generated force by the crowd AC motor directly transferred through the crowd rope to the dipper. In this function the force only being changed in direction around the shipper shaft sheaves. 495H series is equipped to deck mounted automatic rope crowd take-up system with which it reduces the maintenance preparation and downtime while enhancing the maintenance safety. A 60" (152.4 cm) crowd drum with hardened and grounded gearing is installed in front of hoist machinery very at the front-end of shovel. One of the advantages of having the deck mounted rope crowd is what the extra weight off the boom and cause improvement on swing time and easier maintenance. The crowd mechanism consists of a double rope drum each carrying two ropes - one to extend the stick, one to retract it.

2.4.3 Shovel Swing System

The swing motion is designed to facilitate the loading aspect of the shovel production cycle. The shovel can swing or revolve the upper works and front end of the machine through 360° in either direction but ideally the swing arc does not exceed 90° for efficient operation during regular digging. Pinions on the end of the final swing shaft mesh with the large swing rack on the truck frame, causing the rotating frame to revolve, or swing around the centre point when power is applied. The swing motion from the bank to the dump truck consists of acceleration, maximum speed, deceleration and plug to stop. 495H series applies the dual output planetary swing system.

2.4.4 Shovel Propel System

The prime function of this system is to give the shovel mobility. Due to the mega tonnage of shovel weight (i.e. 1,344,000 kilograms), it is geared very low with top

speeds of ½ to 1 mph (1.6 kilometres per hour). There are two separate propel motors installed on the lower works of the shovel.

2.4.5 Lower Carriage

The HF version of Bucyrus' 495 series shovels is designed for low ground bearing pressure applications. This means that there have to be wide crawlers to distribute the massive weight of 1450 tonnes to an area as big as possible. On the shovel the track shoes measure 3.5 meters.

2.4.6 Shovel Dipper

For any given capacity, the dipper weight varies depend on the type of duty for which they are designed. The dipper weight is normally dictated by:

- Rock abrasive quality
- Diggability of material
- Maintenance policy of the operation

Figure 8 shows front and rear of a dipper respectively. In Figure 9, typical dipper angle nomenclature has been shown. In order to interpret the forces at the dipper tooth, it is better to have a better understanding of the geometry of dipper and status of coordinate system at different spots on the dipper. Hence, the following terms being reviewed:

Rake Angle: the angle formed by the intersection of the centreline through the dipper handle and a line drawn from the tip of the tooth on the outside of the dipper to the bottom of the heel. This angle is normally set at approximately 65°.

Digging Angle: the angle formed by the intersection of the dipper handle centreline and the line drawn along the top of the shovel tooth. This angle is normally set at 45°. Shortening or lengthening the pitch braces can change either of these angles.

Dipper Width: the wider the lip, the faster the fill time but the lower the dipper penetration

Dipper Height: the lower the height, then the less the swell factor in certain cases

Dipper Depth: the shallower the dipper, the greater the fill factor

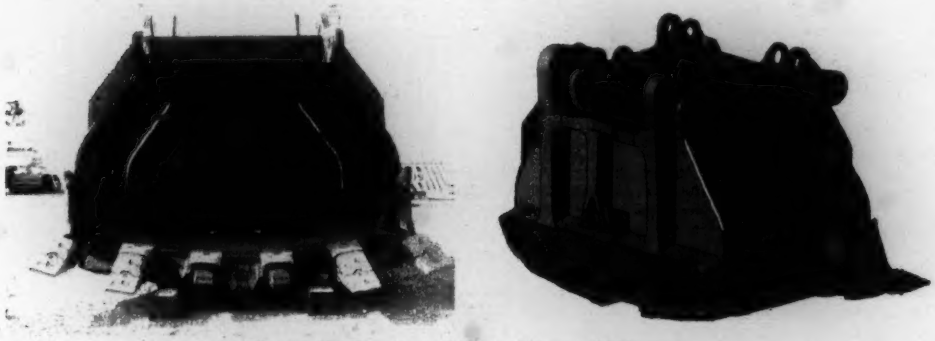

Figure 8: Front and Rear View of Dipper

Designed dipper by Bucyrus has a unique feature of optimized geometry for easier bank penetration and reducing drag. The so-called "Fast Fill" design incorporates slanted rear corners to eliminate the voids for 100% or more fill factor. The current spectrum of dipper capacities manufactured by Bucyrus is shown in Table 2.

TABLE 2: BUCYRUS DIPPER CAPACITIES

Model	Dipper Capacity (m^3)	Dipper Capacity (Yd^3)
180	5.7-17.6	7-23
201	18.4-39	24-51
495	26.8-61.2	35-80
795	53.5-68.8	70-90

Depend on the type of material shovel digging in, the fill factor in the dipper varying as the softer material fills in the bucket easier than the hard broken lumps

such as rocks. Karpuz. et al. on their study of performance assessment of the hydraulic and cable shovel tabularized the given summary in Table 3.

TABLE 3: DIPPER FILL FACTOR

Ease of Digging	Fill Factor %
Easy	> 95
Medium	90 – 95
Moderately Difficult	80 – 90
Difficult	70 – 80
Very Difficult	< 70

It was also introduced by Karpuz et al, 1992 that how diggability varies as well as the bucket size and material type as shown in Table 4.

TABLE 4: THEORICAL CYCLE TIME AND OUTPUTS OF CABLE SHOVEL ACCORDING TO THE EASE OF DIGGING

		Easy Digging		Medium Digging		Moderately Dif. Dig.		Difficult Digging	
Bucket Size yd3	Bucket Size m3	Cycle Time S	Output m3/h	Cycle Time S	Output m3/h	Cycle Time S	Output m3/h	Cycle Time S	Output m3/h
4.5	3.4	20	591	25	464	28	371	32	294
10	7.6	23	1165	27	933	31	754	32	603
10.5	8	23	1212	27	972	31	787	34	629
15	11.5	25	1630	29	1319	33	1074	36	863
17	13	25	1813	29	1471	33	1200	36	965
20	15.3	26	2091	30	1701	34	1391	37	1120
25	19.1	26	2584	30	2106	34	1724	37	1389

2.4.7 Saddle Block

Saddle block enables the movement of the dipper handle on the boom and transfer the cutting forces into the dipper tooth. Bucyrus shovels have a low inertia front end. The front end of these shovels increase in weight as the physical extension is

increased. Added strength or weight is needed to overcome the anticipated stresses and torque encountered in the normal course of digging. These stresses include those produced by gravity acting on the front-end equipment as well as unequal or off-centre loading of the dipper lip caused by irregularities in the bank or premature withdrawal and entry of the dipper while the swing motion is employed. The result is torsional stresses applied to the dipper handle, shipper shaft assembly and the boom structure. To minimize this effect, the front-end design of Bucyrus shovels are applied with a single tubular dipper handle, which has freedom to rotate in a saddle block. Additional anti-torsion assistance is also available in the hoist ropes.

2.5 Unique Features with 495HF/HR Models

2.5.1 Electrical

- AC IGBT fuseless electric drive system
- AC brushless motors. The AC system eliminates brushes, fuses and RPC components that are high maintenance items on DC drive machines
- MIDAS, AccuLoad, and AccessDirect; operational data acquisition, storage, transmittal, retrieval and analysis systems
- AccessDirectTM is a revolutionary approach to remote machine diagnostics. AccessDirect allows for direct access to a machine's electrical system by a Bucyrus engineer anywhere in the world. AccessDirect not only allows an engineer to view what is occurring on a machine to make a diagnosis, but in many cases adjustments or repairs can be made without the need of going to the machine.

2.5.2 Structures

- Extensive use of Finite Element Analysis in structural design
- Thermally stress relieved major structures
- Profile and toe grinding techniques in selective high stress areas
- White painted structural interiors for ease of field inspection

- Built-in interior boom ladders facilities in-the-air inspections
- Cold weather steels on outside skin plates of all major structures

2.5.3 Planetary Drives

- For swing, hoist, and propel motions

2.5.4 Swing

- Four swing pinions drive into the swing rack for reduced tooth loading and prolonged life
- Positioning of pinions results in even load distribution over full swing rack circumference. Swing rack rotation for even wear is not required
- Swing scrapers remove material build-up from the track keeping ring gear free of dirt and damage

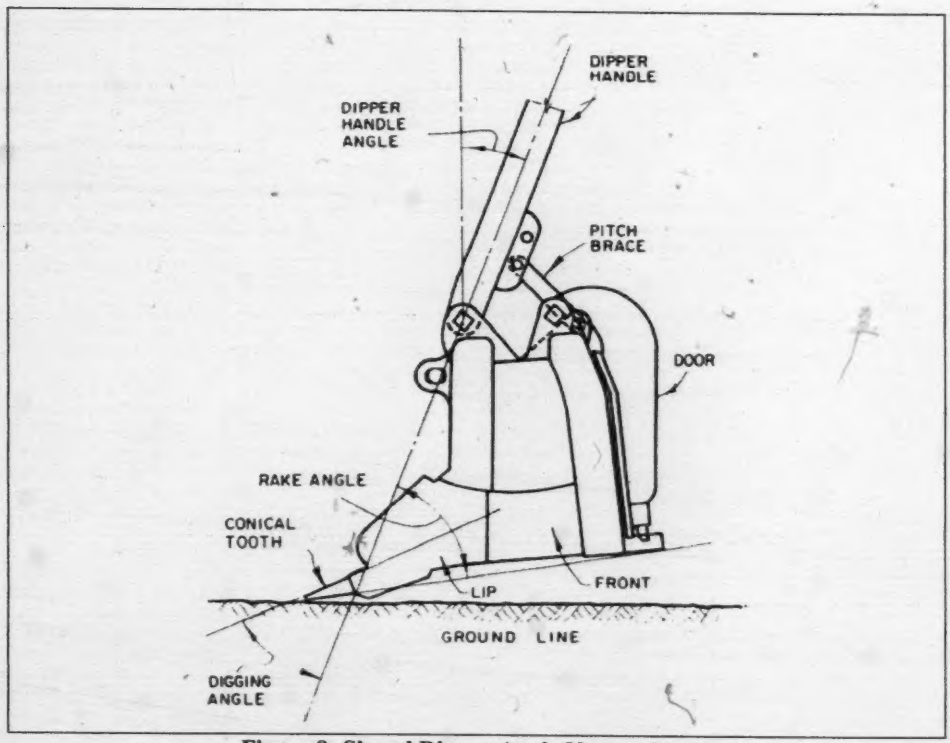

Figure 9: Shovel Dipper Angle Nomenclature

2.5.5 Hoist

- HoistBoss™ planetary hoist, which offers superior load capacity, improved drum gear and pinion life, and supports increased rope life

2.5.6 Crowd

- Rope crowd reduces front end weight and vibration which supports external boom suspension life
- Tubular dipper handle for torsion free structural loading
- Hydraulic/worm drive crowd rope adjustor is accessible from machinery house roof
- Adjustment free saddle block system

2.5.7 Operator Cab

- State-of-the-art operator cabin with dual access/egress doors, exceptional workforce and truck visibility and ergonomic design for operator comport and safety

2.5.8 Dipper

- Thermally stress relieved door, body bowl, and back
- Tilted latch bar to reduce heeling and increase track clearance
- There is variety of the dipper size introduced by Bucyrus on cable shovels. The addition of a Bucyrus 59 cubic yard capacity dipper at Albian Sands makes this the most productive electric rope shovel available in its class on the market today

2.5.9 Safety

- Stored Energy Warning signs applied throughout, at appropriate locations
- Forty-five degree rear facing boarding stairs supplied as standard equipment
- Optional second boarding means is available
- Second operators cab access door is provided for safety egress

- Non-skid grating and roof surfaces
- Caterpillar handrail mounting clamps help eliminate vibration induced weld cracks

Reliability and ease of maintenance are key ingredients of the 495 design. A few of the numerous features include a third rail swing system (which uses larger, wider, flangeless lower rollers) and lowered swing planetary to provide for improved maintainability and ease of maintenance. A low inertia boom design is an exclusive feature of Bucyrus' rope crowd machines and allows for greater operator control and visibility when swinging. In addition, design enhancements in all structural areas and increased horsepower in key digging motions, allows the 495 High Performance shovel to provide payload ratings at the top of its class.

3 KINEMATICS AND DYNAMICS OF ELECTRIC ROPE SHOVEL

3.1 Cable Shovel Motions Overview

Figure 10 demonstrates the major shovel parts motions with which a shovel dig into the face and depend upon the applied amount of the forces on these different movements the productivity of the shovel can directly be affected. In fact, in engineering design and data monitoring of shovel hoist and crowd, the force vectors being evaluated to measure the design and operating cutting forces / resistances at face; hence, in this study all crowd motions deemed positive as well as hoist. Also all retract and lowering the hoist rope considered negative values. Prior to start discussion about the kinematics and force vectors on electric cable shovel, it is beneficial to introduce the mechanical properties of the soil in essence of what researched by Alekseeva et al. (1985). This will lead the research on better understanding to find out the relationship between the soil cutting resistances versus the dipper cutting force vectors. Prior to proceed with the rest of report I strongly recommend to have a quick review on appendix C concerning the some of important soil properties and behaviours to dig/cut.

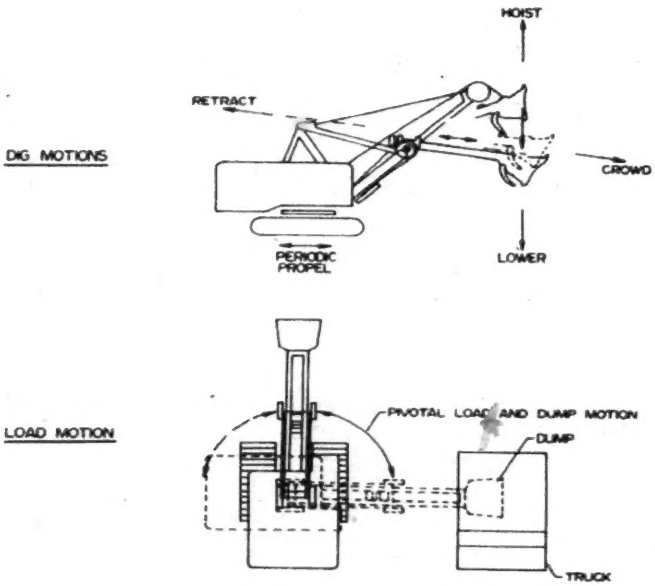

Figure 10: Shovel Dig & Load Motions

3.2 Lifting and Delivery Mechanism

The ratio of the rates of lifting and delivery clarifies the direction of the motion of dipper at any given time while the bucket dig in the face. In shovel with single-motor drive, independent, dependent or combined mechanisms are being considered. In multi-motor drive, independent delivery is usually used. Figure 11 shows different lifting and delivery mechanisms and following is a summary of each case. From these set of diagrams the reader can observe that the hoist drum of the main winch and driving sprocket-chain wheel for delivery are located on one shaft or on two different shafts if twin-shaft main winch is used. By applying the clutches system, we can make a link between the hoist and crowd motions.

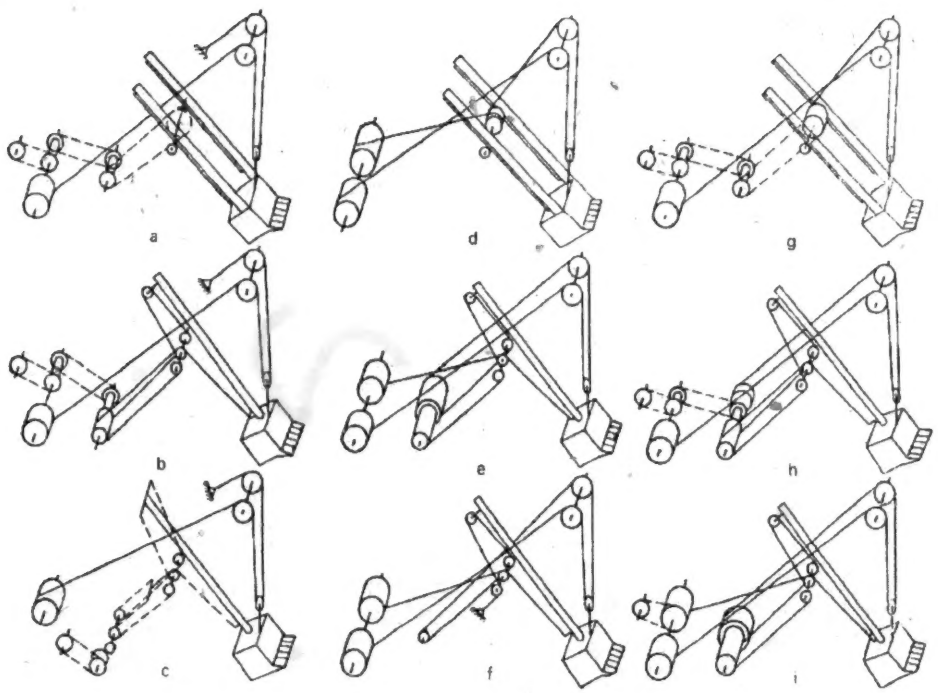

Figure 11: Lifting and Delivery Mechanisms

When we have the rack and pinion drive (Figure 11-a). The torque of main winch shaft transmitted through the reversible chain drive to the drum or shaft, which is located at the pivot hinge of the jib and connected to the crank by the rack and pinion drive.

Figure 11-b and c show the cable and pulley or chain mechanism. In this case the delivery mechanisms where the chain drive or cable system directly joins the star-wheel or cable drum to the shaft of the main winch with the delivery shaft of the saddle bearing or with the crank handle. The axles with chain sprocket wheels or cable blocks are installed instead of the shaft or the drum at the jib pivot hinge.

Figure 11-d shows a double drum rack and pinion dependent delivery system.

Figure 11- e illustrates dependent or coupled delivery mechanism in cable system while Figure 11-f shows the same mechanism with rack and pinion derives. With Figure 11-f, blocks with the rear end, coupled to the crank handle, tighten the end

of hoist cable. In these two cases, the tension in the hoisting cable influences extend of the handle. The function of the return cable on the reciprocating drum that is joint to the front of the handle, affects the drawing-in mechanism.

Figure 11-g and h show the combined delivery mechanism. In these cases, the crowding force is generated from both the shaft of the main drum as well as the hoist cable. By disengaging the clutch on the sprocket of the delivery system on the main winch, the system acts as independent delivery mechanism. By engaging the clutch then both dependent and independent delivery mechanism become actively functional.

Figure 11-i shows dependent crowding of which development in the design has been done for improvement in kinematics mechanisms of hoist and delivery. With this improvement in design, dipper follows closely to the optimum cutting trajectory. The reversible drum is connected to the main winch reversing-shaft of the auxiliary chain drive. This is perfect measure to control the speed of the cable on the drum when it unwinds during digging.

By engaging the clutches of the hoist drum and reversing shaft of the main winch, we can keep the ratio of the hoist/crowd rate constant. Having said that, by this mean we also able to control the movement of the dipper along the specified trajectory we are looking for. There are safety measures in the crowd/retreat mechanism that prevents receiving damage to the system if the handle seizes and does not retreat back. This can be either gained by application of safety clutch on auxiliary chain drive or by installation of locking devices to control the clutches and brakes.

The ratio of hoist over crowd rates is constant as long as the shape of hoist drum is cylindrical; otherwise, conical shape of the hoist drum causes a variable ratio. In independent deliver method, large cutting angle with negative clearance angles, or slippage of the clutches and brakes lead to unproductive digging process with loss of energy that reach only 30% or more of the total power for the drive.

3.3 Cable Shovel Kinematics

As earlier shown in Figure 10, the motion on dipper derives from the hoist and crowd forces being transmitted via the ropes which wind and un-wind on the hoist / crowd drums. This is basically two-dimensional motion (Figure 12). Point S is the main coordinate system origin (X_0,Y_0). And there is also another coordinate origin centre at point O. Angular displacements are positive in anti clockwise direction (trigonometrically expressed). The linear displacements of R_1 and R_2 (i.e. the boom length between boom point sheave and shipper shaft and the boom point sheave radius) are fixed lengths, as these are not changing during shovel operation.

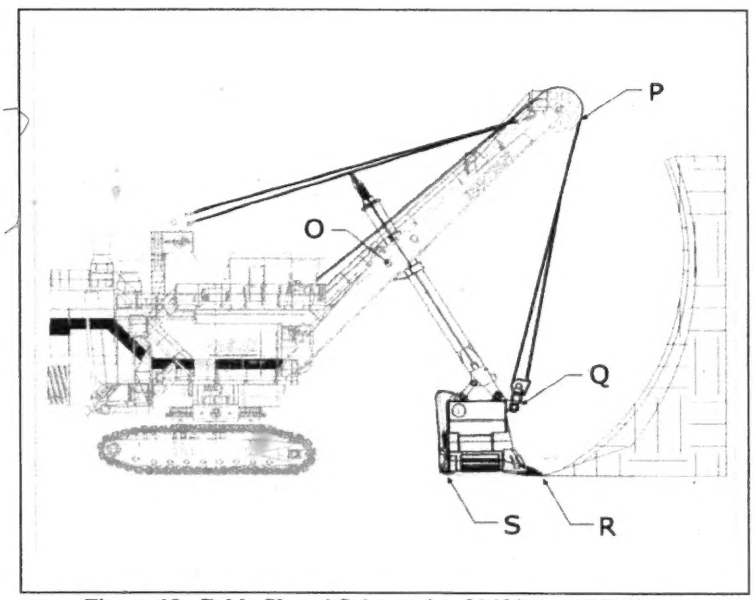

Figure 12: Cable Shovel Schematic of Lifting and Delivery

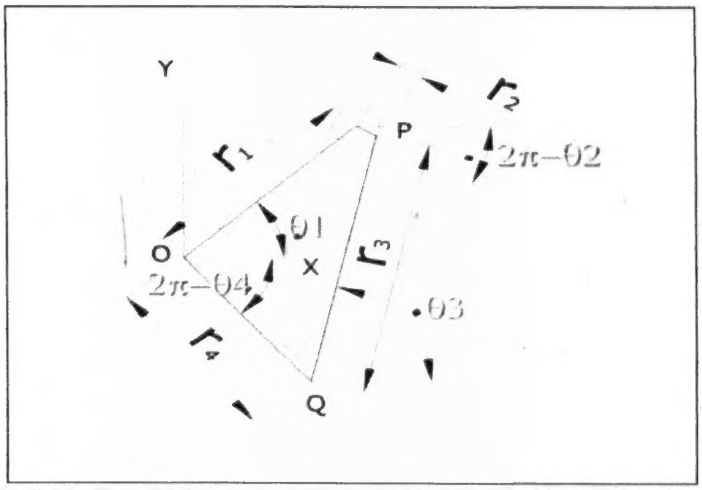

Figure 13: Cable Shovel Kinematics Diagram - θ3: Hoist Angle; 2Π-θ4: Crowd Angle

By sketching the position of the major parts in digging (hoist, crowd, and dipper) and put these together in a schematic diagram (Figure 13, Awuah-Offei, K., 2004), the following correlation among the linear displacements can be considered (Awuah-Offei, K., 2004):

$R_1+R_2=R_3+R_4$

By application of the X-Y coordinate system (Cartesian), the position equations (Equation 1) can be derived, Awuah-Offei, K., 2004:

Equation 1: Cartesian Position Equation

$$r_1 Cos\theta_1 + r_2 Cos\theta_2 = r_3 Cos\theta_3 + r_4 Cos\theta_4$$

$$r_1 Sin\theta_1 + r_2 Sin\theta_2 = r_3 Sin\theta_3 + r_4 Sin\theta_4$$

To calculate the kinematics equations for velocity and acceleration of shovel moving components into the dig process (Equation 2, first degree differentiation over Equation 1) and (Equation 3, second degree differentiation over Equation 1) are introduced (Awuah-Offei, K., 2004):

Equation 2: Velocity Calculation

$$\begin{bmatrix} r_3 s_3 - r_2 s_2 & r_4 s_4 \\ r_3 c_3 - r_2 c_2 & r_4 c_4 \end{bmatrix} \begin{pmatrix} \omega_3 \\ \omega_4 \end{pmatrix} = \begin{pmatrix} c_3 \dot{r}_3 + c_4 \dot{r}_4 \\ -s_3 \dot{r}_3 - s_4 \dot{r}_4 \end{pmatrix}$$

Equation 3: Acceleration Calculation

$$\begin{bmatrix} r_3 s_3 - r_2 s_2 & r_4 s_4 \\ r_3 c_3 - r_2 c_2 & r_4 c_4 \end{bmatrix} \begin{pmatrix} \alpha_3 \\ \alpha_4 \end{pmatrix} = \begin{pmatrix} (c_2 r_2 \omega_3 - c_3 r_3 \omega_3 - 2 s_3 \dot{r}_3)\omega_3 - (c_4 r_4 \omega_4 + 2 s_4 \dot{r}_4)\omega_4 + c_3 \ddot{r}_3 + c_4 \ddot{r}_4 \\ (s_3 r_3 \omega_3 - s_2 r_2 \omega_3 - 2 c_3 \dot{r}_3)\omega_3 - (s_4 r_4 \omega_4 - 2 c_4 \dot{r}_4)\omega_4 - s_3 \ddot{r}_3 - s_4 \ddot{r}_4 \end{pmatrix}$$

While: $\theta_2 = \theta_3 - \dfrac{2\Pi}{3}$ And $\omega_2 = \omega_3$

Where $\dot{r} = \dfrac{dr}{dt}$, $\ddot{r} = \dfrac{d^2 r}{dt^2}$;

$\omega = \dfrac{d\theta}{dt}$, $\alpha = \dfrac{d^2 \theta}{dt^2}$.

3.4 Cable Shovel Dynamics

Before jump into the discussion of dynamic equations for the cable shovel system of handle and dipper it lets to have quick look at Figure 14. There are joints on the system of handle-boom connection that each joint can be overlaid with a local coordinates although these local coordinates are being linked together through Newton-Euler dynamics equations (Frimpong S. et al., 2005) by application of transformation matrixes.

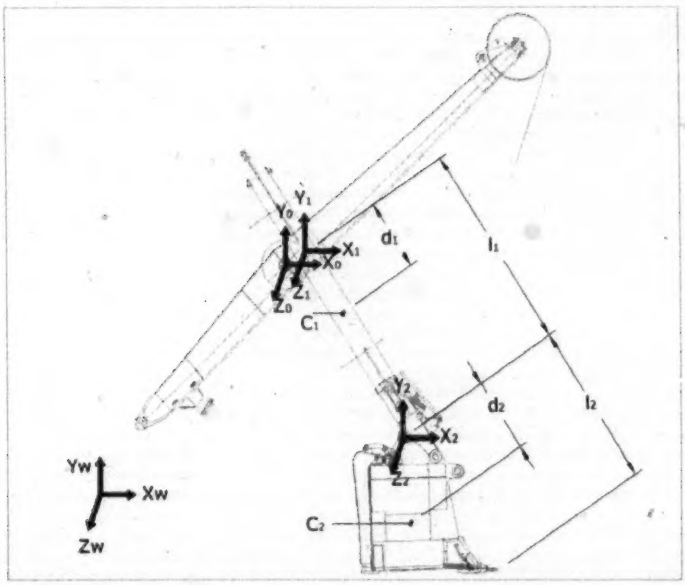

Figure 14: Handle Free-Body and Elements of Shovel Dynamics (Frimpong S. et al., 2005)

Nomenclature to above figure:

C_1 centre of mass for handle whereas C_2 is the centre of mass for the bucket;

d_1 linear displacement between C_1 and O_1, d_2 linear displacement between C_2 and O_2;

l_1 length of crowd arm from pivotal point connection point between arm and dipper;

l_2 length between dipper tip and connect point of arm and dipper.

Since in my research area of interest is only focused on the trajectory overview and optimization, hence only the forces interaction between the face and dipper in vertical motion for a duty cycle studied and evaluated. For this reason the crowd handle as well as boom being incorporated into the dynamics evaluation to the digging process. The dynamics equations for cable shovel are given in the following (Frimpong S. et al., 2005):

Equation 4: Dynamics Equation of Cable Shovel (Frimpong S. et al., 2005)

$$D(\Theta)\ddot{\Theta}+C(\Theta,\dot{\Theta})\dot{\Theta}+G(\Theta)=F-F_{Load}(F_t,F_n)$$

Where Θ is a vector of generalized variables, $D(\Theta)$ is generalized inertial matrix, $C(\Theta,\dot{\Theta})$ is generalized Coriolisand and centripetal effects, $G(\Theta)$ is gravity;

F is crowd and hoist effect;

$F_{load}(F_t,F_n)= F_r$ is resistive force due to soil to dipper interaction, F_t is tangential resistance force vector reaction and F_n is normal force vector reaction;

And following is description of components of Equation 4 from which are derived from equations shown in Appendix D:

$$D(\Theta)=\begin{bmatrix} m_1+m_2 & -m_2 d_2 s_{2C_2} \\ -m_2 d_2 s_{2C_2} & I_{ZZ1}+I_{ZZ2}+m_1 d_1^2+m_2(l_1^2+2l_1 d_1 c_{2c_2}+d_1^2) \end{bmatrix}$$

$$C(\Theta,\dot{\Theta})=\begin{bmatrix} 0 & -(m_1 d_1+m_2(l_1+d_2 c_{2c_2}))\dot{\theta}_1 \\ 2(m_1 d_1+m_2(l_1+d_2 c_{2c_2}))\dot{\theta}_1 & 0 \end{bmatrix}$$

$$G(\Theta)=\begin{bmatrix} (m_1+m_2)gs_1 \\ (m_1 d_1 c_1+m_2(l_1 c_1+d_2 c_{12_{c_2}}))g \end{bmatrix}$$

$$F_{Load}(F_t,F_n)=\begin{bmatrix} F_t c_{2\theta_b}-F_n s_{2\theta_b} \\ F_t(l_1+l_2)s_{2\theta_b}+F_n(l_1+l_2)c_{2\theta_b} \end{bmatrix}=F_r$$

Where m_1 is mass of crowd arm;

m_2 is mass of dipper;

Ci and Si are $\text{Cos}\theta_i$ and $\text{Sin}\theta_i$ respectively;

I_{zz1} is momentum of inertia of crowd arm about centeroidal axis parallel to Z_1-axis;

I_{zz2} is momentum of inertia of dipper about centeroidal axis parallel to Z_2-axis;

θ_i is angular displacement;

$\dot{\theta}_i$ is velocity of joint (i=1 for crowd and I=2 for dipper);

$\ddot{\theta}_i$ is acceleration of joint (i=1 for crowd and I=2 for dipper);

Force F provided in Equation 4, is an outcome of the hoist and crowd forces at the dipper tip. This force must overcome to the two different group of forces that eventually cause to dipper penetrate in the face (required digging force):

Soil resistance forces, $F_{Load}(F_t, F_n)$, which is been driven by physical and mechanical properties of soil need to be excavated. Based on following experimental equation mentioned by Frimpong S. et al., 2005 in their report article referenced to Zelenin et al. the resistive force during digging can be measured:

$$F_r = 10C_0 d^{1.35}(1+2.6w)(1+0.0075\beta)(1+0.03s)e_z k_z$$

Where C_0 is compactness and cutting resistance index;

d is depth of cutting;

w is length of horizontal chip;

β is the angle of cutting;

s is the cutting edge index;

e_z is the tool plate thickness and k_z is the index for the type of cutting;

Dynamic parts including the inertial effect $D(\Theta)$, Croriolis and centripetal effect $C(\Theta,\dot{\Theta})$, and gravities $G(\Theta)$. The first and third effects are directly related to the geometry and material type of the dipper handle and dipper itself while the second one is concerned to kinematics and dynamics effect of digging strategies including the digging profile (trajectory pattern) and time distribution during the digging operation.

Although there could be some other factors directly or indirectly affecting determination of the magnitude of required break out force F, the above mentioned one are the main factors to be input in the dynamics of the shovel equations.

As shown in Figure 15-a existing loads / forces on the handle and bucket of a shovel of which follow a trajectory pattern in the face of open cut are illustrated in the image for better identifying the geometrical positions of shovel digging components. Following explanatory lines are description of the parameters being shown in this layout. The G_b is the bucket weight, G_h is the handle weight, Ge is the weigh of the earth, S_n is lifting (hoist) force, S_c is the delivery (crowd) force, P1 is the tangential vector of digging resistance force to the trajectory of digging, P2 is the normal vector of the resistance force to the trajectory of digging, and N is the reaction of the saddle bearing on the handle at the shipper shaft point. If during the operation the crowding is stopped while the operation of the shovel continues, then Sc is considered as a reacting force.

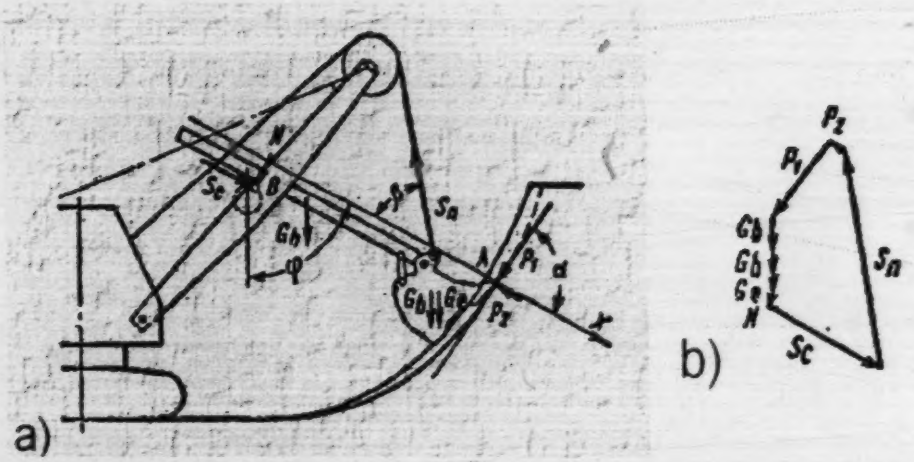

Figure 15: a) General Layout of Forces on Shovel Digging Parts b) Dimensional of the Forces

Figure 15-b shows the simplified force vector diagram with their real vector direction. In this chapter it is discussed how to interpret and use the dimensional vector system in conjunction with other available data such as forces values generated by AC motors. All these diagrams are a function of time and depend of the position of the bucket in the face the direction and angles of the forces are different.

According to the second law of Newton, for a system of forces we can define the static and dynamic state of equilibrium. Whenever the system is stopped with no movement, we can apply the static equilibrium around deemed origin the same for all different conditions. If digging parts being considered during the excavation of shovel, but with consistent speed and no acceleration, then one can apply the dynamic equilibrium around the origin centre. Based on equilibrium law, summation of all forces in two axis (X-X' and Y-Y') must be equalled to zero the same as momentum summations around the origin point. In this case summation of momentums around the shipper shaft (deemed the centre for handle evolution) must be equal to zero. Depend on the number of unknowns we can get maximum of three equation from the geometry of moving parts – crowd and hoist system – and per any given time we can numerically calculate the amount of digging forces at the teeth of bucket to the face. Since the digging force must be greater than the

digging resistance to allow the bucket to penetrate into the soil and complete the digging cycle; hence, the measured values for the forces can be deemed the same for resistive forces to the digging. The outcome of applying the Newton second law under the state of equilibrium is shown in Equation 5:

Equation 5: Dynamic Equilibrium on Shovel Working Device

$$\Sigma X = (G_h + G_b + G_e)Cos\varphi - P_1 Cos\alpha - P_2 Sin\alpha - S_n Cos\beta + S_c = 0$$

$$\Sigma M_B = G_h r_h + G_b r_b + G_e r_e + P_1 r_2 + S_n r_1 = 0$$

Where r is the moment arm of appropriate force relative to point B;

φ is the angle of rotation of the handle with respect to vertical position;

α is the angle between digging resistance force P1 and axis X (crowd alignment);

β is the angle between the hoist rope and the X axis (crowd).

From this equation with two unknowns and two equations the arguments P_1 and P_2 can be easily calculated at any given time. This is practical as long as the operating values of crowd S_c and hoist S_n forces are known and measured for us.

To determine the design value of the lifting force (S_n), the situation in which the dipper handle is horizontal to the face (Figure 16) and is half way advance of the crowd handle being considered. In this case, the hoisting force as well as tangential resistance force to trajectory is vertical and the normal resistance force is horizontal passing through the shipper shaft (point B). The bucket is in its highest weight full of cut soil while the digging resistance forces (P_1 and P_2) are their design values. There is also maximum value for the hoist that can be gained (Alekseeva et al.) during the digging operation. The maximum lifting force $S_{n\,max}$ can be derived from the following ratios:

$S_{n\ldots max} \approx \frac{S_n}{0.65}$ When single motor derive;

$S_{n...\max} \approx \frac{S_n}{0.8} \xleftrightarrow{TO} \frac{S_n}{0.7}$ When multiple-motor derive functioning on direct current the braking force.

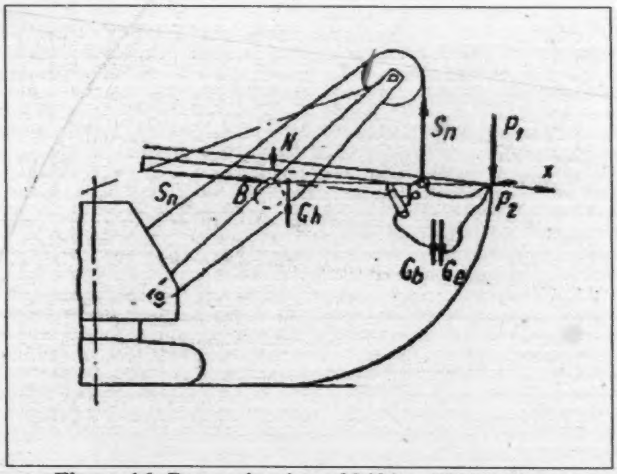

Figure 16: Determination of Lifting (Hoist) Force

In Figure 17 three main positions of the bucket are shown. These spots are used to determine and measure the design delivery force (crowd). These three positions can be described as following:

Position I: the beginning of the dig process. In this state, the cutting edge drawn from the bucket teeth toward the shipper shaft (B) is vertical and bucket is at the closest safe distance to the front end of the crawlers. The value of the lifting force (hoist) is its design value. Also between the cutting resistance vector the ratio of P2/P1=0.1 simplifies the system of forces equilibrium with empty bucket (Ge=0). At this position the angle of inclination between the boom and horizontal axis is between 50°-60°.

Position II: which is called the end of digging cycle while the bucket approaches its maximum weigh full of dug out soil. At this situation, the crowd is at its maximum extend and the cutting edge of shovel is horizontal passing through the shipper shaft (point B). Likewise the position I, the hoist value (S_n) equals to the design value. And the P2 to P1 ration is equal to 0.1. The angle of boom inclination to the horizontal direction to be deemed 45° with no reaction from soil (i.e. zero values for P1 and P2).

Position III: bucket is at highest elevation to the face, crowd at maximum extent, no ground reaction (P1=P2=0) and boom angle of inclination between 55°-60°.

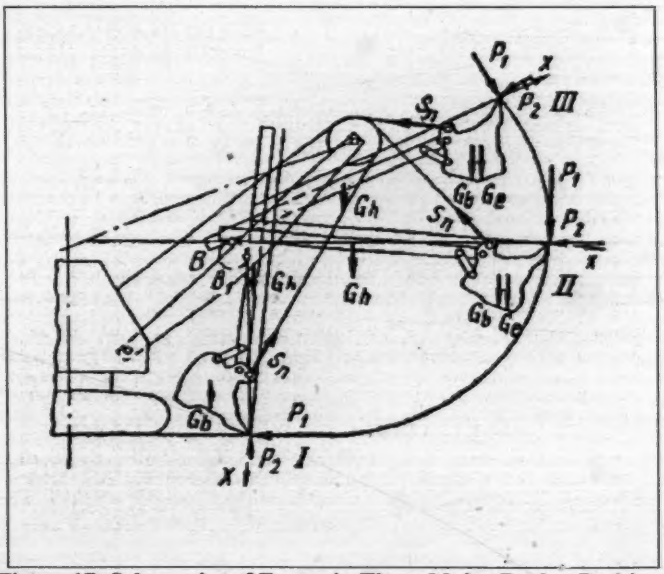

Figure 17: Schematics of Forces in Three Major Bucket Positions

The maximum delivery force $S_{C...max}$ with braking can also be calculated while the P2/P1=0.2. for the condition of dependent delivery force when we have the combined forces of delivery and lifting, the following Equation 6 can be applied to calculate one of each at a time by having the other as known parameter:

Equation 6: Equilibrium of Drums for Delivery

$$\frac{Sc}{K_c \eta_b \eta_d} * \frac{D_c}{2} = \frac{S_n}{K_L} \eta_p \eta_d \frac{D_a}{2}$$

Where ηb, ηd and ηp are coefficients of the block, drum and lifting pulley;

Dc is the diameter of delivery drum (Crowd Drum);

Da is the diameter of auxiliary drum;

Kc is the number of the pulleys for delivery;

K_L is the number of the pulleys for lifting.

If K_L=2, Kc=1 and $\eta_p = \frac{2\eta_b}{1+\eta_b}$; Equation 6 can be simplified in the following format:

$$\frac{D_a}{D_c} = \frac{S_c}{S_n} = \frac{1+\eta_b}{\eta^2{}_a \eta^3{}_b}$$

In a dependent crowding this ratio is between 2.15-2.2 and for combined delivery it equals to 1.4. Also the rates of lifting and delivery forces are described by the speeds of these functions (V_L and V_e). In case of independent delivery, V_e=0.8* V_L. Due to exceeding of the delivery speed required for digging, we can control it by applying the engaged and braked crowd mechanism.

When we have the combined crowding, the independent part of delivery acts as idling the dipper handle, the speed of independent delivery is assumed from this ratio: Ve =(0.8-0.9)* V_L.

In dependent delivery mechanism (dependent part of combined crowding), above-mentioned ratio of speeds, are no longer to be captured by kinematics of the mechanism. In such case, in measuring the ratio the shape of the face as well as the interaction of the generated forces on handle with the dipper are being considered.

3.5 Motion Rates of the Lifting and Delivery Mechanisms

By having the ratio of lifting and delivery rates (hoist and crowd speeds - V_L / Ve) the direction of motion of the dipper (trajectory) based on certain geometrical dimensions can be sketched out. For drawing an optimal trajectory knowing the value of this ratio is also required. A trajectory pattern is also depend upon the position of the shovel / dipper to the face, the rate of crowd extension and hoist rope retraction.

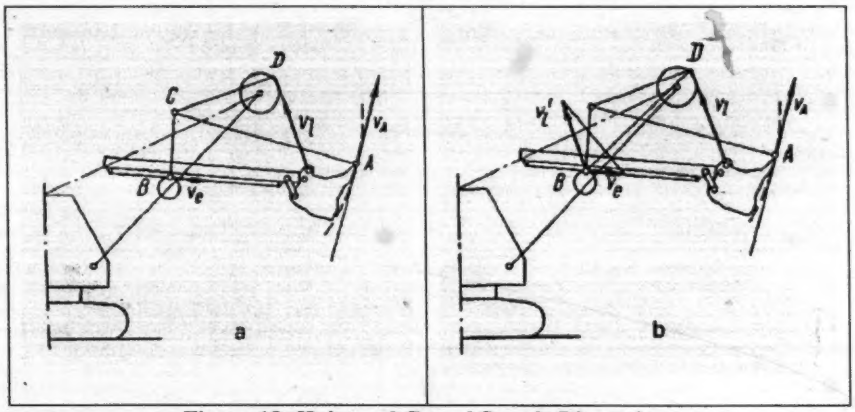

Figure 18: Hoist and Crowd Speeds Dimensions

For better appreciate the rates of hoisting and crowding, Figure 18 is giving the dimensional diagrams of speeds at given dipper position in the face. The dashed line is part of the trajectory pattern. The V_A is the bucket tangential speed to the trajectory. The point C is the centre of the rotation of the handle and it is derived by to perpendicular lines drawn to points A and B. When the hoist/crowd speeds ration is known, for a given dipper position at face, the direction of bucket teeth speed, which in turn can be deemed the same as cutting resistance vector tangent to the trajectory, determined. If draw a vector ($V_l^{'}$) equal with the same direction to V_l from point B and connect the two vectors V_c and $V_l^{'}$. Then draw a perpendicular line from B to this connector line and extend it till hit the V_l on the sheave (point D). From D drop a normal line to the direction of V_l. Point C will be gained by intersecting this line and the normal line drawn from B to handle. Connecting the C to A and normal to AC is the direction of V_A.

Based on the Euclidean geometry, the ratio of speeds and ratio of segments CA, CB, and CD are equal:

$$V_c:V_l:V_A=CB:CD:CA$$

From above speeds – segments relationship at any given dipper position when travels in optimum trajectory one can measure the values of the speed rates of hoist and crowd. The trajectory equation is described in Equation 7 by help of the illustrated diagrams in Figure 19:

Equation 7: Optimal Trajectory Equation

$$\rho = \rho_0 e^{\varphi Cot\psi}$$

When we talk about the optimal trajectory it is in terms of energy consumed and this is while the dipper moves in face with smallest cutting angle when the rear clearance angle is not less than 5°-7°. The ratio of V_L / Ve in optimum trajectory state is:

0.55 – 0.6 at the upper part of the face with small to medium boom size;

2 – 3 or more at the lower part of the face. Practically, if the ratio rest in the range of between 0.6 – 0.8 the applicable angles of cutting can be gained.

By referencing to Figure 19, and consideration of the origin (O) at shipper shaft and OA is the radius vector. , above equation can be explained as:

Where ρ and ρ_0 are correspondingly the immediate and initial values of the radius vector of point A assuming with centre at point O;

φ is the angle of rotation of the radius vector from the initial position;

ψ is the angle between the radius vector and the tangent to the dipper trajectory

Figure 19 also can be used in determination of the curve fit the purpose of having a constant cutting angle in Cartesian coordinates system (Equation 8):

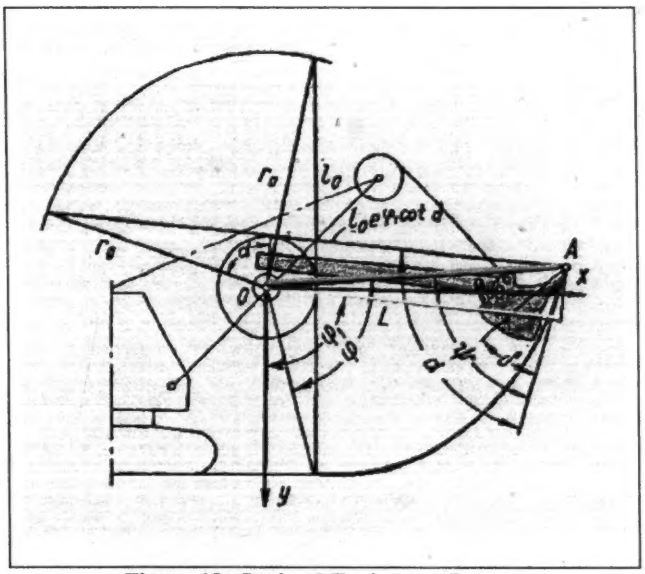

Figure 19: Optimal Trajectory Pattern

Equation 8: Constant Cutting Angle Curvature

$$\begin{cases} X = r_0 Cos(\alpha + \varphi_1) + l_0 e^{\varphi_1 Cot\alpha Sin\varphi_1} \\ Y = r_0 Sin(\alpha + \varphi_1) - l_0 e^{\varphi_1 Cot\alpha Cos\varphi_1} \end{cases}$$

Or in polar system by:

$$L = L_0 (2e^{\varphi_1 Cot\alpha} - 1)$$

$$r_0 = \frac{R}{Cos\,\psi}$$

Where φ1 is the angle of rotation of the handle from the initial position;

L_0 and L are the initial and momentary values of stick deflection.

4 MIDAS SOFTWARE APPLICATION

4.1 Overview

Electric cable shovels manufactured by Bucyrus conducted big achievements on their productivity improvements by using Siemens instrumentation installed on shovels. Siemens innovation of AC Drive System to the mining industry in 1980 accomplished a significant progress in its development trend. Siemens has played a major role in integrity of the shovel performance by installing state of the art devices and instrumentation on the shovels to capture all operating data, which are vital for optimization, performance measure and duty cycles reduction. All these are required to improve productivity, which in turn serves the operating cost reduction and has direct impact on maintenance schedule and cost as well. SIMINE is the AC drive and automation solution developed by Siemens which this innovation take advantage of the Insulated Gate Bipolar Transistor (IGBT) technology that eventually cause a lot of cost savings by reducing the operating costs and productivity improvement. There are some advantages using the AC drive versus the DC drive (Siemens web site):

AC drive can operate faster than the DC drive. AC induction motors allow higher stall torque, faster acceleration, and higher speeds in field weakening. This results in a larger area under the speed and/or torque curve and shorter machine cycle times. This creates higher productivity on the shovel operation.

IGBT shovel drive systems operate routinely at above 98% availability. Mean Time Between Failure (MTBF) is in the thousands of hours and Mean Time To Repair (MTTR) is typically less than one hour. This will keep the benchmark values high over the life of machine.

AC motors, unlike DC, have no brushes or commutators to wear out or to be maintained. IGBT power requires minimal maintenance.

In today mining industry with large electric shovels, a peak of more than 3.5 MW can be consumed. Active IGBT rectifiers known as Active Front Ends (AFEs).

uninterrupted operation even during line voltage fluctuations, provides unity machine power factor and a total harmonic distortion of less than 5% while improving dynamic machine performance. Increased AC system efficiency combined with unity or leading power factor reduces energy costs. This, plus maintenance savings and smart controls, lowers machine operating costs over the complete life cycle.

Some interesting facts about the IGBT inverters which is controlled by SIBAS control unit, that while operator engage the brakes on either moving parts of machine the inverters send power from the motors back to the DC link and hence the AC motors act as power generators. There are Intelligent Diagnostics devices presented by Siemens to the market that can be found on Bucyrus electric cable shovels. These are included of:

Onboard Maintenance Computer: that is a diagnostic system to identify any faulty part on the shovel and enables mechanics to source out the failure easily.

SiRAS (Siemens Remote Access System) Remote Diagnostics: that is a remote access to the shovel on board computer and by application of this device engineers and experts can simply follow the shovel operation for several reasons such as monitoring, troubleshooting, and maintenance. Siemens SIRAS allows the technician to send software updates through the Internet to the shovel. Using this system reduces the maintenance cost and increase system availability.

MIDAS (Monitoring Interaction Diagnostic Analysis Service) a performance measure device: with which allows the technicians closely monitor the shovel performance in real time or by reviewing the logged data. MIDAS saves huge amount of fieldwork need to be done in terms of data collection to analyse the shovel and operator performance. MIDAS captures set of comprehensive information regarding to shovel production, motions such as crowd and hoist lengths, mechanical, and electrical including the hoist, crowd, and swing motors RPM's, powers, torques, voltage, and current. MIDAS records operating features of the machine per any given second in the working shift and reports them into the mine computer system. This software in general can be said capturers all input

and output signals and show them in a meaningful way. One of the benefits of this software is to monitor the shovel operating cycle times and evaluate different operators performance and attempt to make required corrections or improvement on their abilities to operate the shovel by providing more training courses or organizing team sessions and review the defects of operators jobs and enforce them to use lessons learned from all this.

As mentioned above, engineers and technicians by means of the SiRAS can get hooked up into the shovel computer and monitor and analyse all shovel performance key indicators via the MIDAS software that I'm going to bring more information into the text about this application that played the major role in my research to help me with operating data collection. It is not only matter of data management but also review the shovel historical data as a measure to double check the output of the computations done by different geometrical formulas. As per Patnayak S. et al. 2005, in their experimental research has been done on P&H cable shovel performance, performance indicators of the shovel including the dig cycle time, hoist and crowd motors' power and energy are being captured and assessed by use of different methods such as intelligent monitoring system or digital camera recording. This is while I have applied state of the art technology like MIDAS which reports back a very high precise operating information of the shovel and have put all results together in charts and tables for de-bottlenecking of power usage in shovel. This won't be possible unless a comprehensive study being done to evaluate the performance of dig cycle that directly is an effect of the operator's accomplishment of having a cost-production effective shift.

4.2 MIDAS Software

MIDAS is developed by Siemens and installed on Bucyrus electric cable shovels operating in Albian Sands Energy mines. This application is divided to two different software. The MIDAS Desktop and MIDAS Report. Under the first one all data being captured by means of data transfer of SiRAS remote technology. All collected information can be either monitored live in MIDAS Desktop (Figure 20) (Appendix E) or can be loaded into the MIDAS Report (Figure 21) for post data processing and performance measure of the shovel.

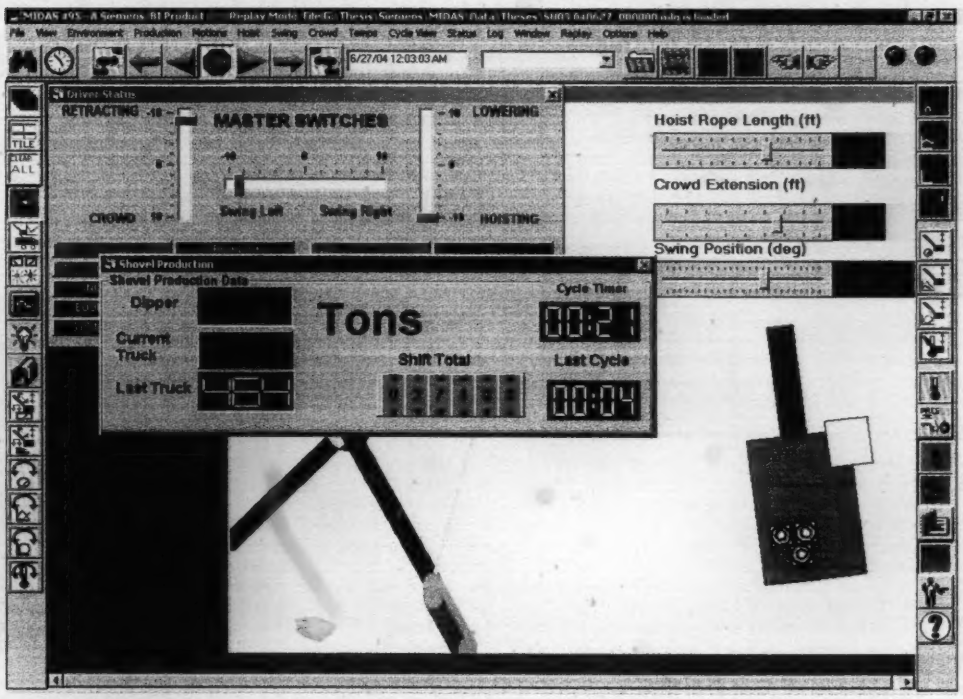

Figure 20: MIDAS Desktop Snapshot

In this research, by use of the Replay mode of MIDAS Desktop, I was able to manage to run the QC on the developed geometrical formulas to calculate the break out forces at any given time/second of the digging cycle. In this report the key performance indicators values (crowd-hoist-swing power, torque%, voltage, etc.), been extracted from the native ASCII coded-database of MIDAS Desktop.

By help of Siemens technicians I was able to decode the ASCII file and develop my Access database based on the introduced equations in next chapter. For the reason of data proprietary and confidentiality, all output numbers are being normalized in a scale of 1-10 or 0-100%. MIDAS Report has minimal share in my study and I have tried to develop my own analysis method since that software does not report the outputs required for the cutting forces measurement. As it was mentioned in this chapter, this software is only designated somehow for performance measure of the shovel.

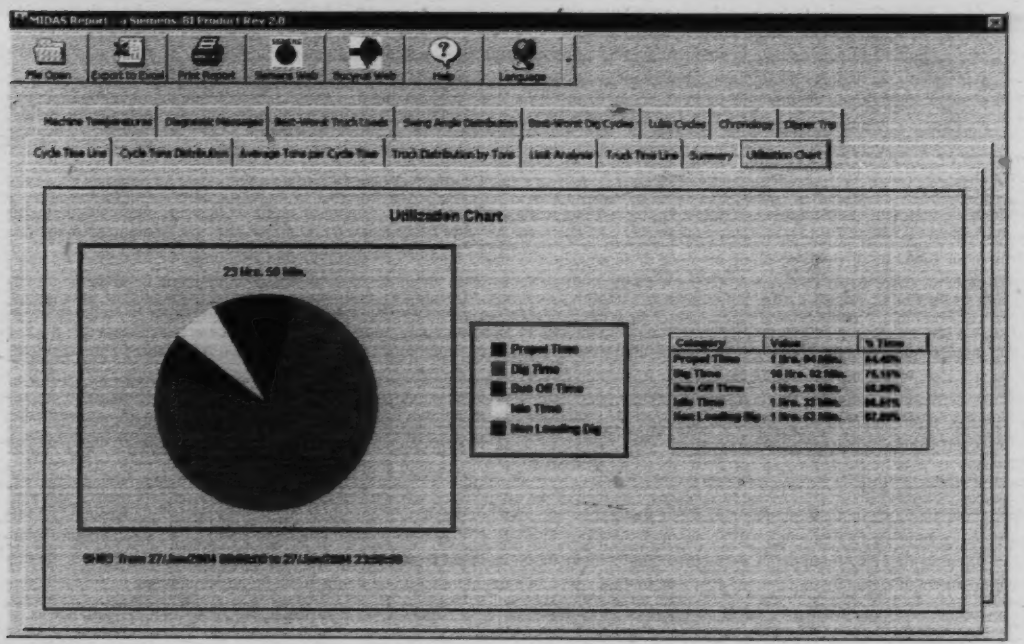

Figure 21: MIDAS Report Snapshot

The MIDAS Reports program summarizes shovel data from a machine log file and displays the data as a collection of visually appealing and easy to understand charts and graphs, which in turn I found it useful.

4.3 MIDAS Desktop Application in This Research

In order to fulfill this task, several different shifts' shovel operating data log files have been considered for the research. To appreciate how to interpret the dig cycle amongst these files, several plots (Figure 22 through Figure 26) have been made to investigate which of the performance indicators can be used in determining the beginning and end of the dig cycle.

Prior to proceed with application of the equations introduced in Chapter 3, it is required to determine the dig cycle that by knowing that we will be able to manage the spreadsheets to be used for digging force calculation in certain digging cycles. Compare to other research (Patnayak S. et al. 2005), which was practice for performance monitoring of electric cable shovel but under different purpose and algorithm; the DC motor armature voltage considered as measure of the beginning and end of the dig cycle. By plotting crowd, hoist, and swing powers and torques it can be apprehended that the swing power or torques has less affect on dig cycle determination since usually digging is swing free action. Nor the crowd extension proves any indication of where the dig cycle starts or ends. It is shown on the following figures that any time right before the dig cycle to start the crowd power flips in direction and that is when the hoist length is at its maximum value and hoist power shows a steady positive amount turned positive from a negative value. Hence, Figure 26 can be deemed as the best indicator for digging cycle determination with which the hoist-crowd powers and hoist extension can be used for any discrimination between the dig cycle start-end and other shovel activities including the idling and face preparation. As previously mentioned, in this report, MIDAS Desktop only used for QC of the data processing along side the camera recordings of the considered shovel operation while a secondary database developed for all necessary calculations to get the digging forces and trajectory coordinates.

Figure 22: Shovel KPI, Hoist Torque-Power-Speed

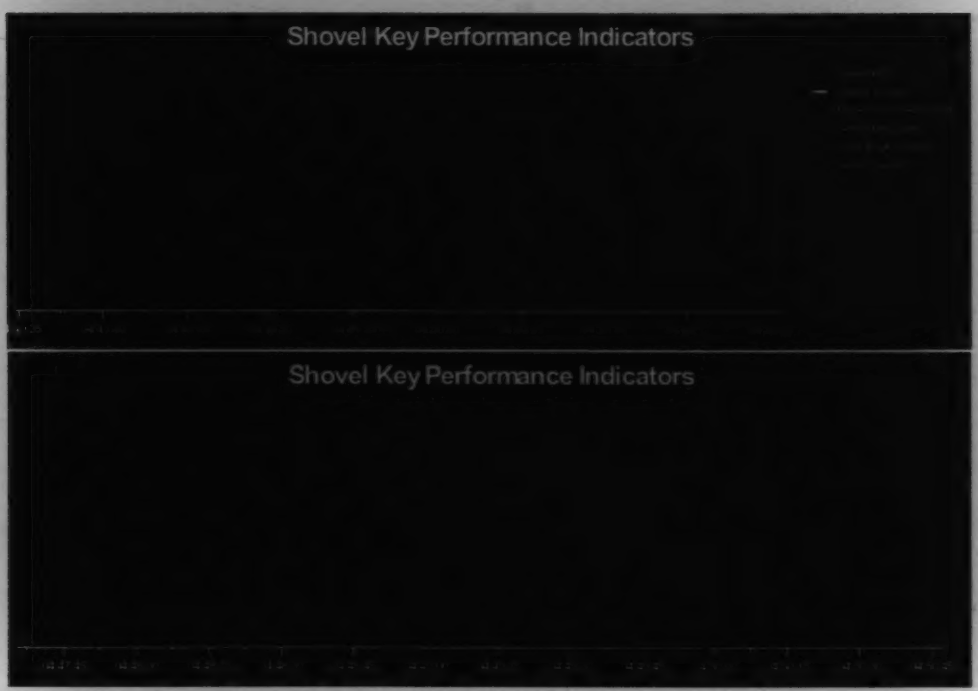

Figure 23: Shovel KPI, Crowd Torque-Power-Speed

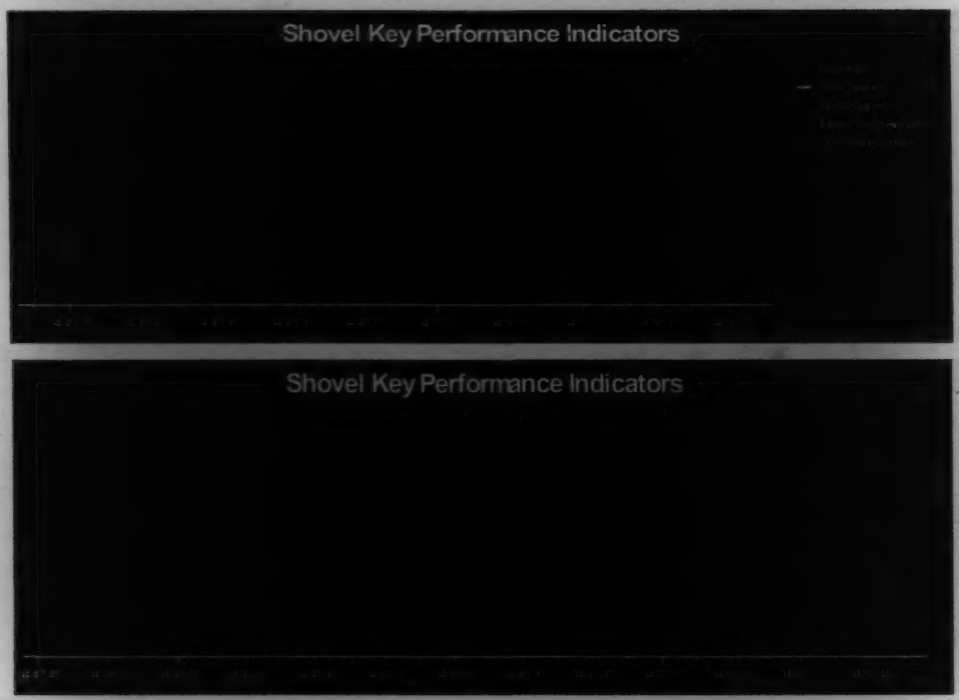

Figure 24: Shovel KPI, Hoist & Crowd Power-Speed

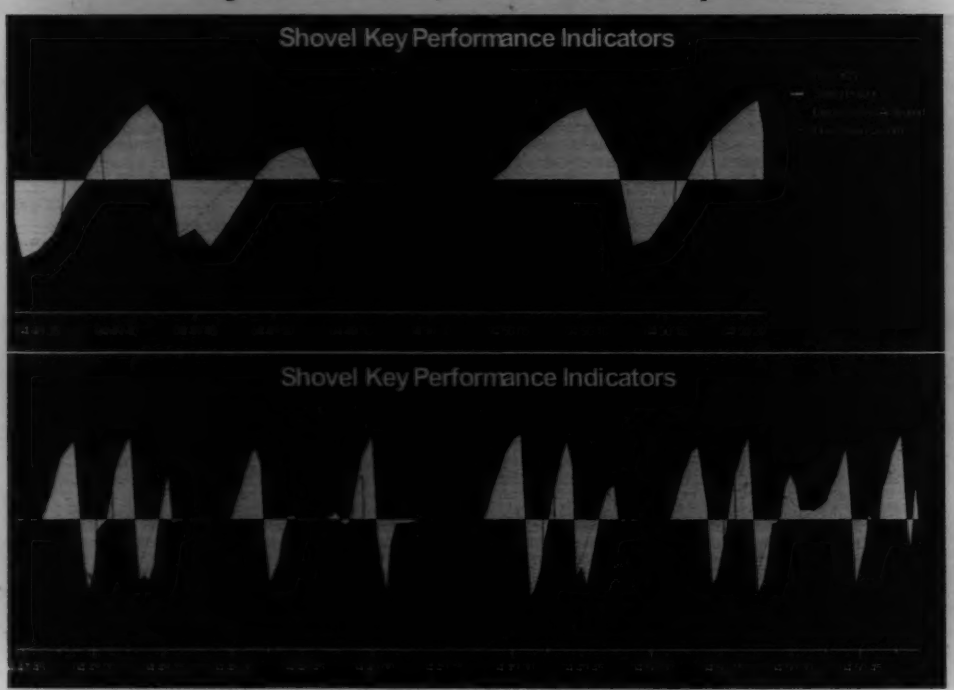

Figure 25: Shovel KPI, Hoist & Swing Power

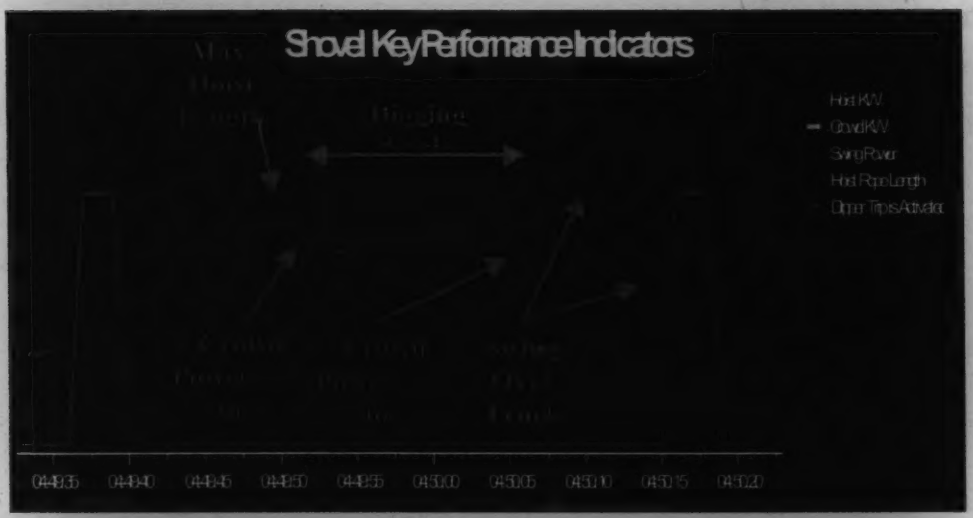

Figure 26: Shovel KPI, Hoist & Crowd & Swing Power

Figure 26 is the most logical graphic can be chosen is the process interpreter. As depicted on this figure, the relationship between the dipper door trip and start of the dig once the hoist length approaches its maximum length and crowd power changes its value from negative to positive. During the dig cycle the hoist power remains positively high indicating of the energy consumption to penetrate into face while the crowd force fluctuates but still remains on positive area meaning the energy being consumed on pushing the dipper into the face. And close to end of dig cycle the swing power increases from zero showing the shovel turn from face toward the hauling unit.

In all shovel motions it is deemed to for positive (+) values as the crowd extends forward of hoist length reduces (dipper moves upward) and negative (-) values implies for crowd retraction the same for hoist lowering (dipper moves downward). By evaluating the data summary from the developed database, one can mention that whenever the crowd rope extension is less than 24 feet (7.32 m) and hoist rope length is greater than 63 feet (19.20 m), the dipper hit the bumper, which in turn indicates a bad function of the operator. Figure 27 is an outcome of the post-processed data off the MIDAS operating log files. As shown in this figure, the dig cycle has been determined as follows. Anytime that the hoist length approaches its maximum length with a rapid change to reduce is being considered the beginning of the dig. This is; however, need to be carried on with another satisfying condition, which in turn is the constant change of the hoist power from negative to positive, meaning the dipper engaged in the soil removal and facing the resistance. It is also detected with the idle times and face clean ups during the duty cycle evaluation. These cycles are being disregarded in determination of the cutting forces.

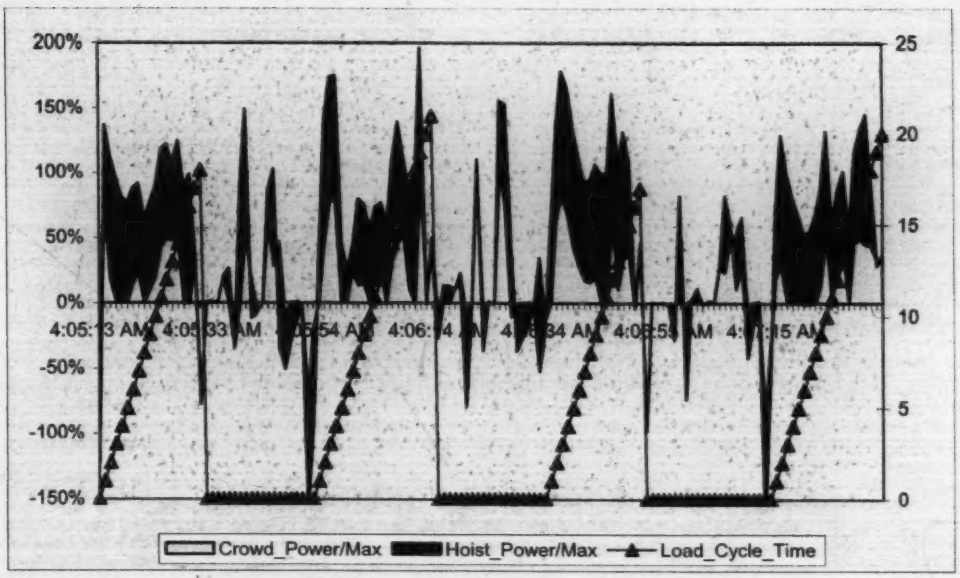

Figure 27: Dig Cycle with Regards to Hoist-Crowd Power

Once the dig cycle has been determined, the reported dipper load can be easily distributed during the dig cycle in the database. By recognition of the all parts weights at any given second, and by drawing the geometry diagram of the shovel handle free body, the digging forces has been computed according to the text in Chapter 3 that I described it in more detail in next Chapter.

5 DIGGING TECHNIQUES AND CUTTING TRAJECTORY EVALUATION

So far in this research different conditions that affect the dig cycle and in general shovel productivity have been discussed. Variety of equations, states of mechanical behaviour of gear including introduction of kinematics and dynamics of moving parts reviewed. The media interaction with dipper and its characteristics, which directly affects the dig cycle and production rate also studied. In this case we should not forget the main influence of operator's role in this business. If he fails to properly operate the unit, despite all mathematical measures, simulations and understanding of the environment we intend to tackle, no optimization can be gained.

Only with proper training programs to the shovel and truck operators a successful and safe production can be reached as ultimate goal of any production manager. In this section it is tried to review some hints of proper manners of operating the shovel while digging in the face.

5.1 Digging Methods

The digging methods partly relates to loading schemes. It is essential that shovel operator be familiar with these vantages of positioning the equipment in right spot to increase productivity and have less loss time due to face area maintenance required to be done by support equipment because of spills and bad operation of shovel in front of him. There are two major loading techniques as follows:

5.1.1 Double Back-Up

Known as double side loading while shovel productivity depends on trucks manoeuvre and positioning time.

5.1.1.1 Double Back-Up "A"

When shovels stand angular to the edge of a 90 degree angle face and two trucks approach on two sides of shovel while one truck is on vicinity of dug face (Figure 28). This scheme gives lower average swing angle compare to state "B". This in turn results significant amount of tons per year.

5.1.1.2 Double Back-Up "B"

When shovel stands perpendicular to the face and two trucks approach backward on sides of shovel (Figure 29).

Shovel relocation as shown in Figure 28-c and Figure 29-c parallel to the digging face in states "A" and "B" are slightly different. On both schemes the propel pattern is known as "basic saw-tooth" profile. On first situation, the tracks turn prior to backing out. Essentially system "A" has very low swing angle and moves up usually until a wider face in front of shovel becomes available.

5.1.2 Modified Drive-By

Known as single side loading is when the shovel progress in the face in one direction parallel to face and causes only one truck can be approached for loading. In this method there is always two open surfaces are available and gives better dipper penetration into fragmented mineable material (Figure 30).

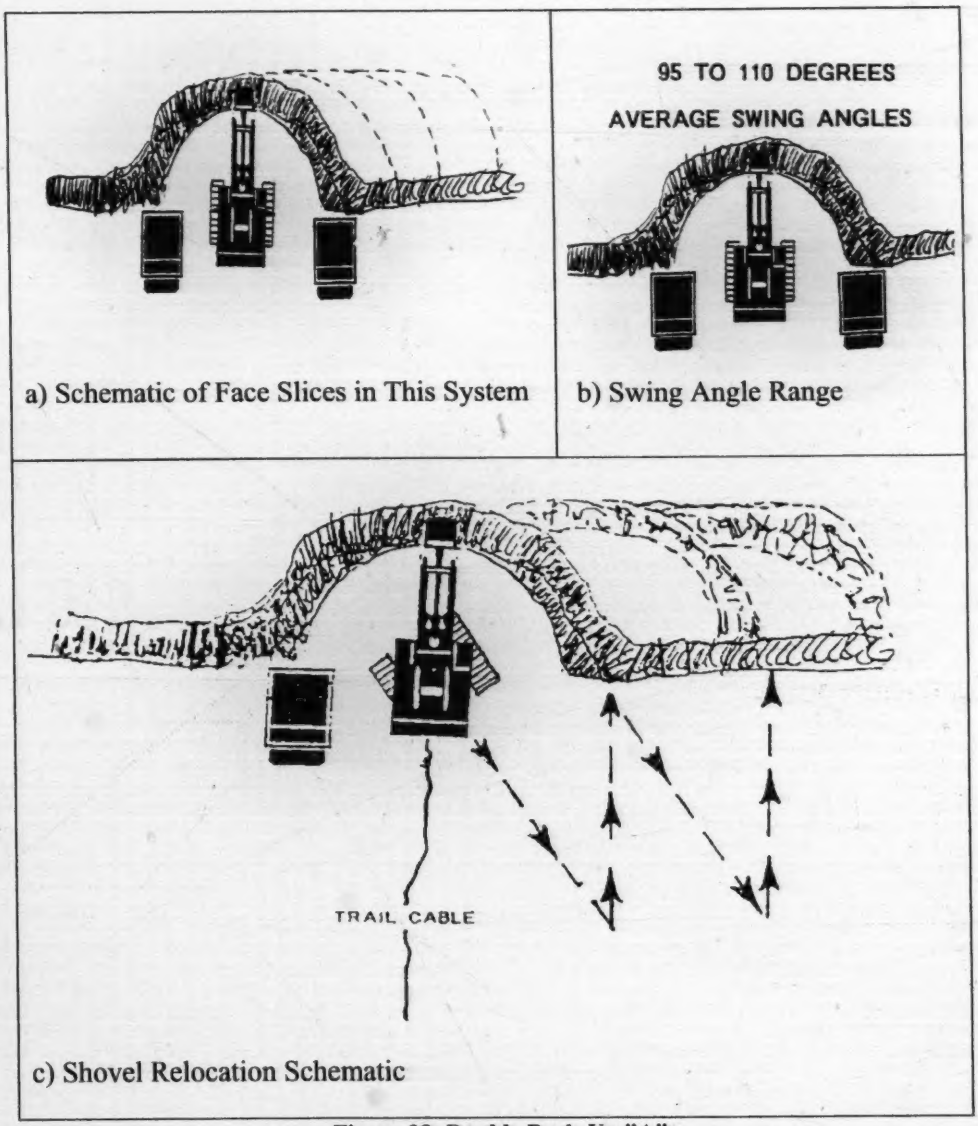

a) Schematic of Face Slices in This System

b) Swing Angle Range

c) Shovel Relocation Schematic

Figure 28: Double Back-Up "A"

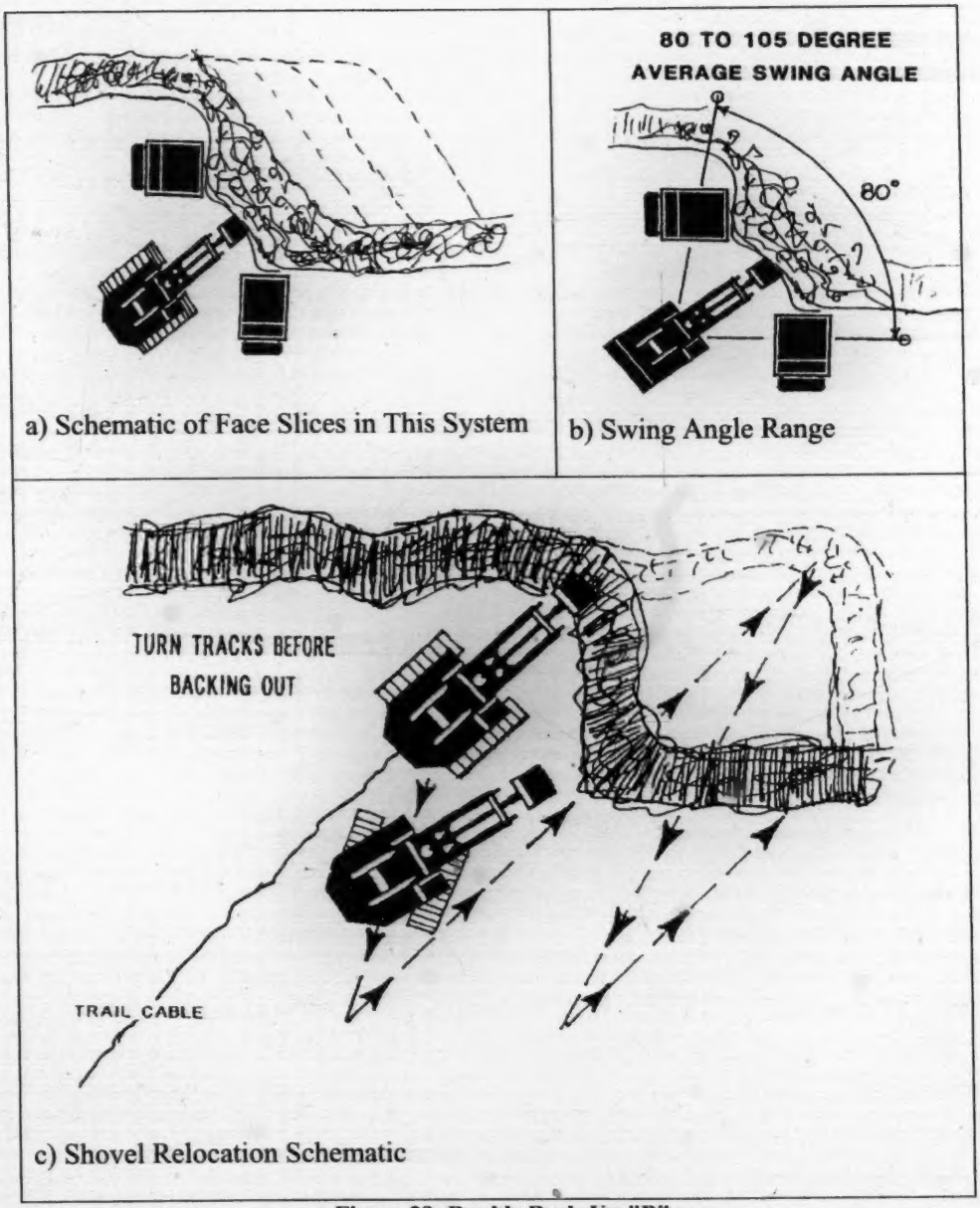

a) Schematic of Face Slices in This System

b) Swing Angle Range

c) Shovel Relocation Schematic

Figure 29: Double Back-Up "B"

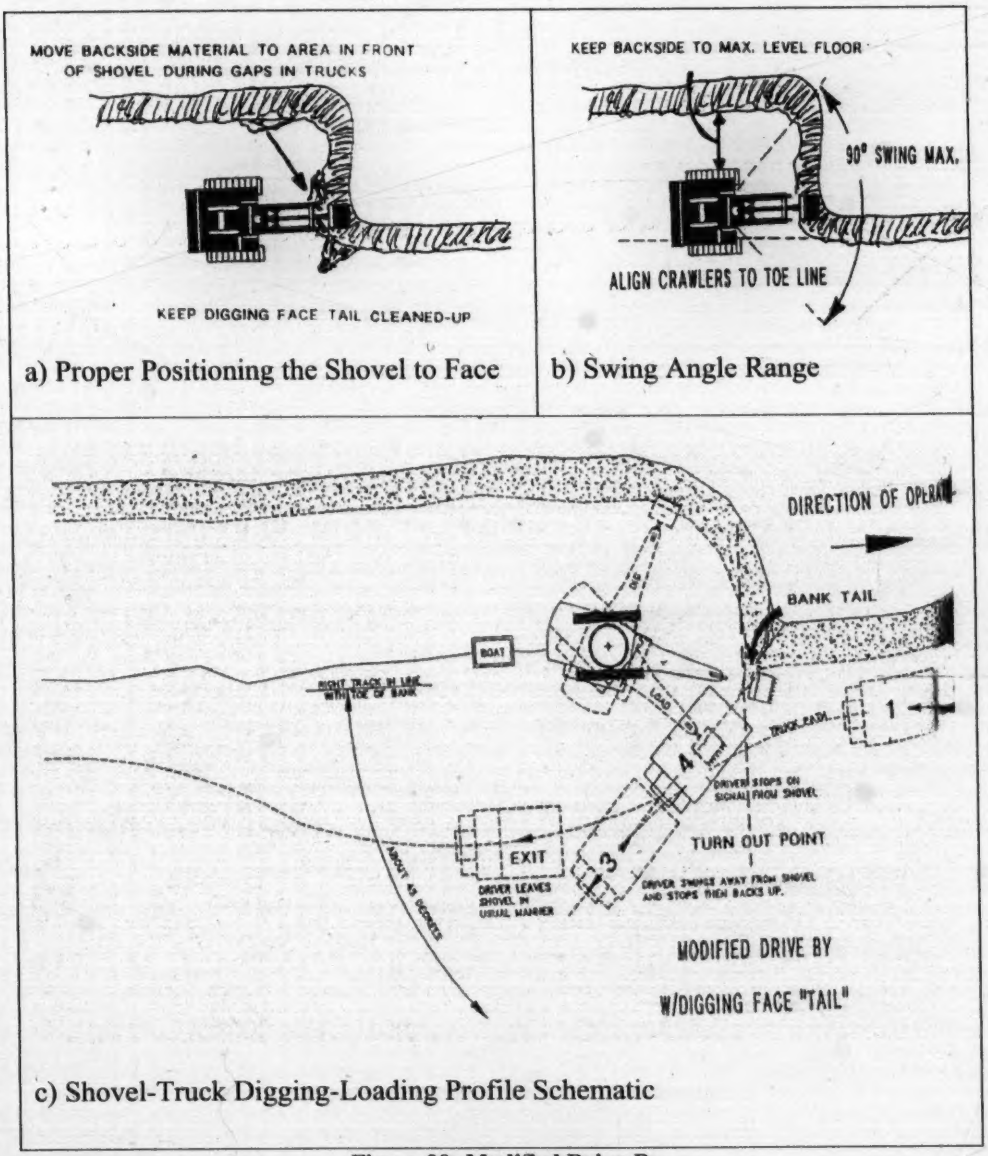
MOVE BACKSIDE MATERIAL TO AREA IN FRONT OF SHOVEL DURING GAPS IN TRUCKS
KEEP DIGGING FACE TAIL CLEANED-UP
a) Proper Positioning the Shovel to Face
KEEP BACKSIDE TO MAX. LEVEL FLOOR
90° SWING MAX.
ALIGN CRAWLERS TO TOE LINE
b) Swing Angle Range
DIRECTION OF OPERATION
BANK TAIL
BOAT
RIGHT TRACK IN LINE WITH TOE OF BANK
LOAD
TRUCK PATH
1
4
DRIVER STOPS ON SIGNAL FROM SHOVEL
TURN OUT POINT
EXIT
3
DRIVER LEAVES SHOVEL IN USUAL MANNER
DRIVER SWINGS AWAY FROM SHOVEL AND STOPS THEN BACKS UP.
ABOUT AS SHOWN
MODIFIED DRIVE BY
W/DIGGING FACE "TAIL"
c) Shovel-Truck Digging-Loading Profile Schematic

Figure 30: Modified Drive-By

5.2 Rake Angle

In chapter 2 the shovel dipper angle nomenclature partly reviewed and to address the best shovel dipper face penetration, it is beneficial to have better understanding of the optimum rake angle during digging. As shown in Figure 31,

the average of 62° rake angle and 5.5° lip angle are the best known angles to gain best dipper fill factor.

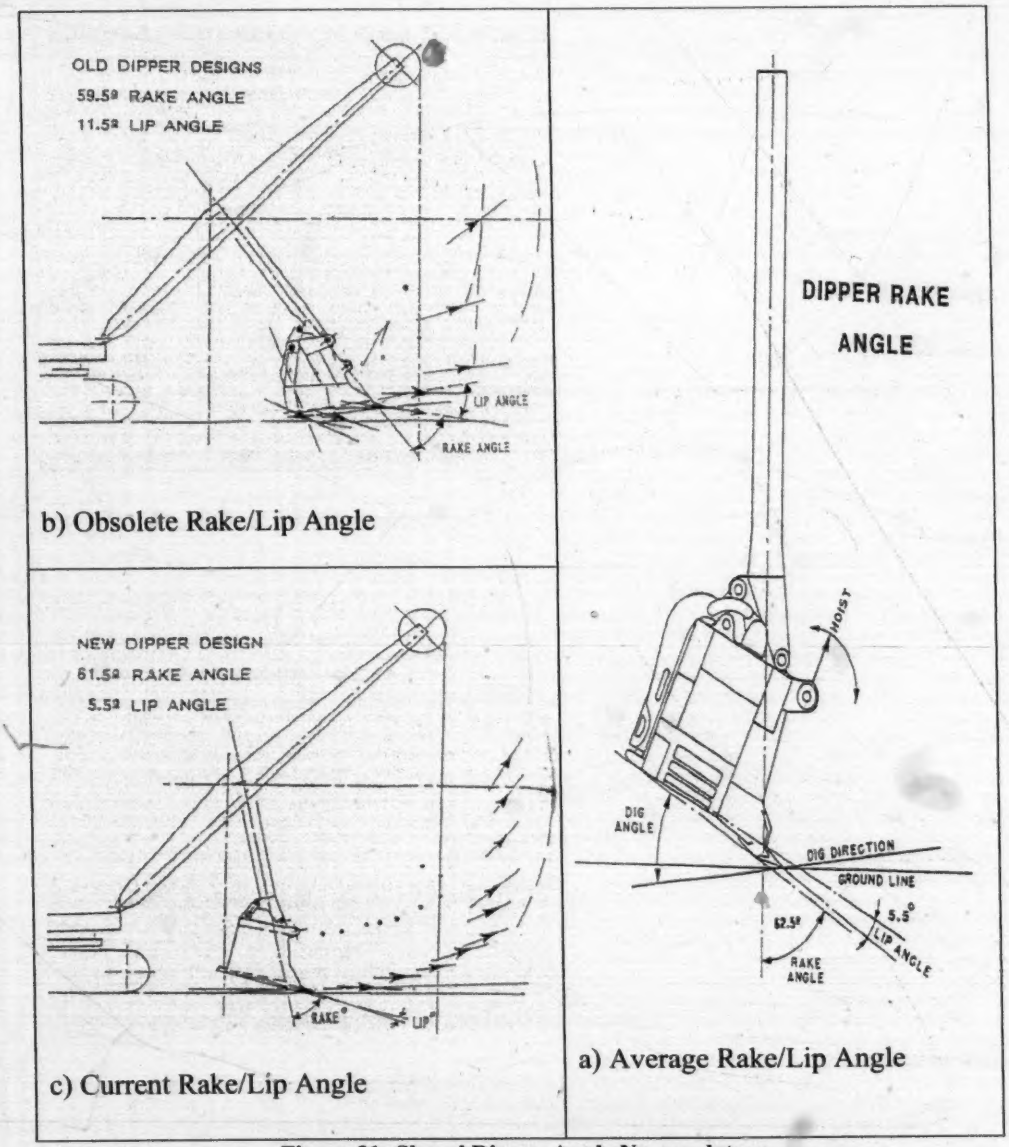

Figure 31: Shovel Dipper Angle Nomenclature

The dipper fill time (in turn fill factor) is directly related to the rake angle. In some mining operations the dipper angles are altered to reduce dipper front and heel band wear rates. By reduction on rake angle, the fill factor will be directly affected. The more sever the angle change, the greater the filling time and the lower fill factor. Alteration to rake angle cause the dipper teeth to be clawed into

the face rather than slicing through it. Due to dipper claw into the face shovel operator has to back up the shovel to release the dipper, hence lowers the fill factor during the dig cycle. Bucyrus shovels if properly positioned in front of face have set for a fill time of 7 to 10 seconds.

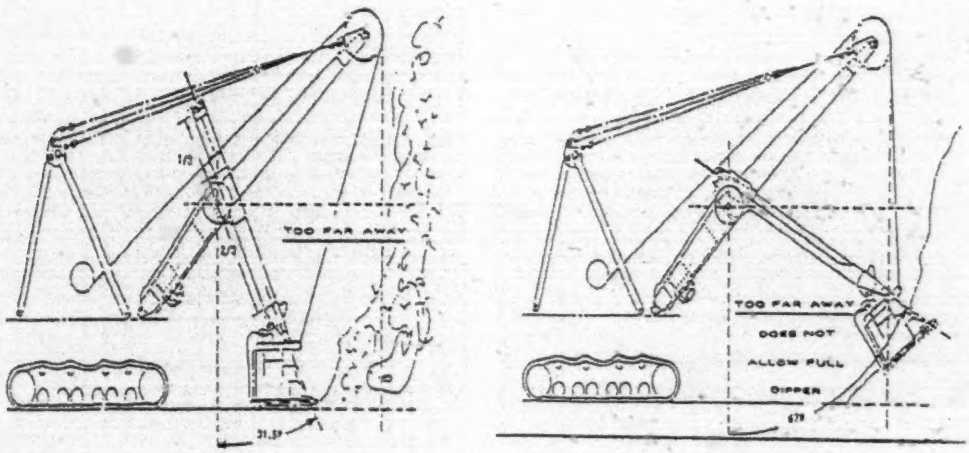

a) Shovel Too Far from Digging Face

b) Shovel Too Far from Digging Face

Figure 32: Bad Shovel Position at Digging Face

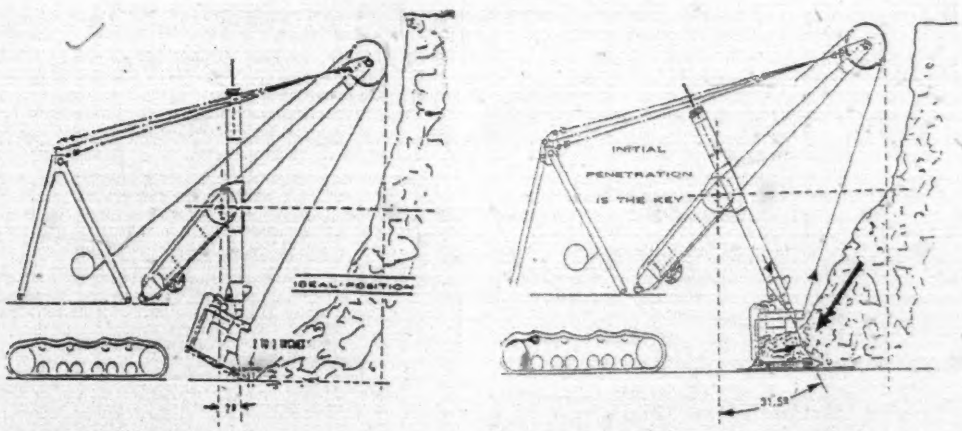

a) Teeth Tip 2"-3" to the Digging Face Toe

b) Handle Angle of 31.5° at Initial Penetration

Figure 33: Proper Shovel Position at Digging Face

5.3 Shovel Position to Digging Face

In the event the shovel locates too far from digging face (Figure 32) dipper will never gets filled adequately. Dipper filling time and fill factors are definitely tied to the shovel position at the digging face. Figure 33 depicts the shovel at the start point of the fill cycle. The handle in perfect world would be vertical and the tooth point at entry to the digging face. However, this positioning is not viable; hence, while the handle is situated in vertical position the dipper tooth points should be within 12 inches from dig face entry. During the increase of the handle angle outwards (about 7 degrees), the allowable distance for the tooth points to dig face entry decreases to 2 to 3 inches. This is vital to assure dipper penetration into the dig face productively to make the dipper as full as possible in one run of dig cycle.

5.4 Shovel Dipper Positions at Digging Face

Figure 34 shows the dipper in different main positions while digging in media. Position 1 is when the dipper locates in front of toe and ready to start digging. Position 2 is ramp up with dig process and position 3 is when the dipper is full (in a proper digging) or end of dig process and position 4 corresponds to the time of swinging toward the hauling unit. It is depicted that with combinations of crowding, hoisting, retracting, and lowering the dipper the trajectory can be shaped and whether operator have the competent control on this operation, the goal of having the best trajectory which in turn carries the maximum productivity can be approached. All this as mentioned before strictly depends on the operator level of training and experience as well as monitoring devices to measure the performance and mechanical behaviour of shovel at any given seconds of its operation. By post processing of actual collected data during shifts, production engineers are able to evaluate the shovel production performance and try to improve it in different ways.

5.5 Digging Envelope

As shown in Figure 35 the digging envelope is defined with the existing face surface and maximum reachable dipper penetration deep into face. It can be seen that Depends upon the operator's competency a under cut as shown on the figure can occur. By looking at the tooth point in the first dipper length of movement, if the shovel operator digs within the digging envelope the heel of the dipper will clear the digging face. The outer line of the digging envelope is the heeling path of the dipper as well as a completely extended handle. It can be seen that to tackle the face after operator place the dipper on the desirable dimensions from the shovel crawlers (start position –lowering applied), he applies the hoisting and crowding (position I) and then when the dipper is substantially filled he retreats the dipper to avoid trapping dipper in face (position II).

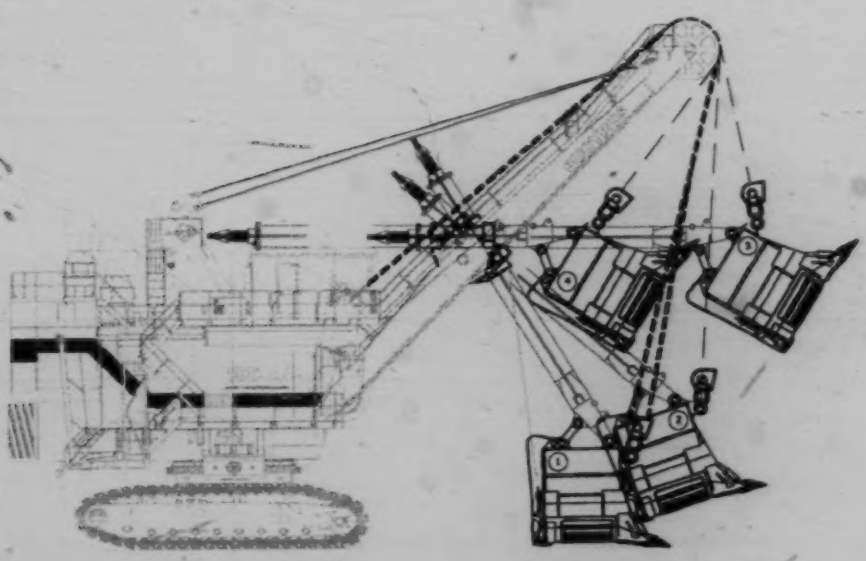

Figure 34 : Cable Shovel Typical Trajectoy Patern

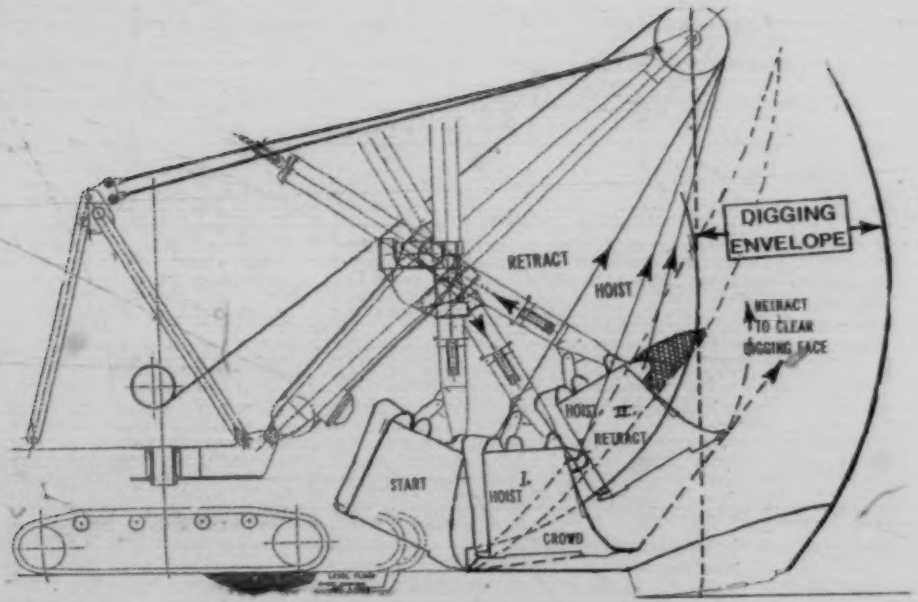

Figure 35: Typical Path of Dipper into Digging Face

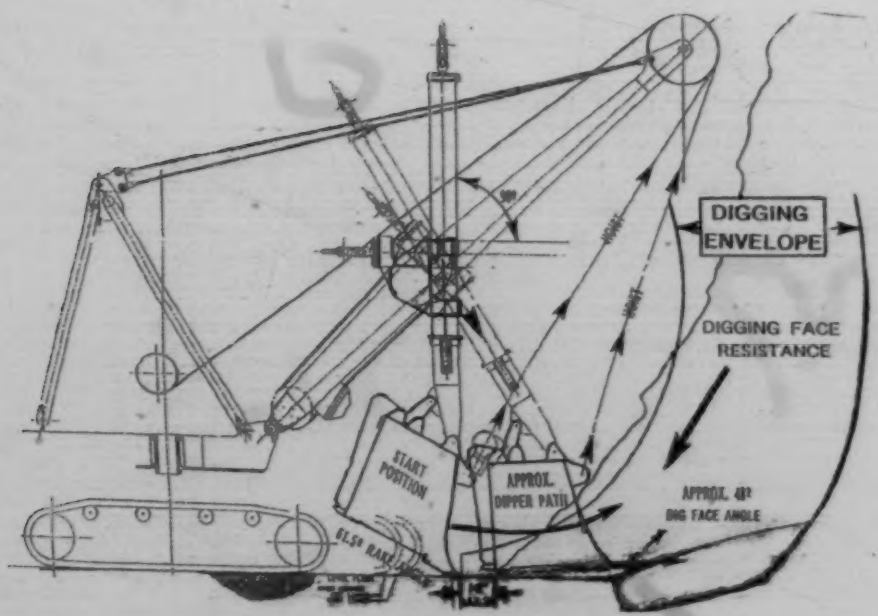

Figure 36: Shovel Position at Digging face

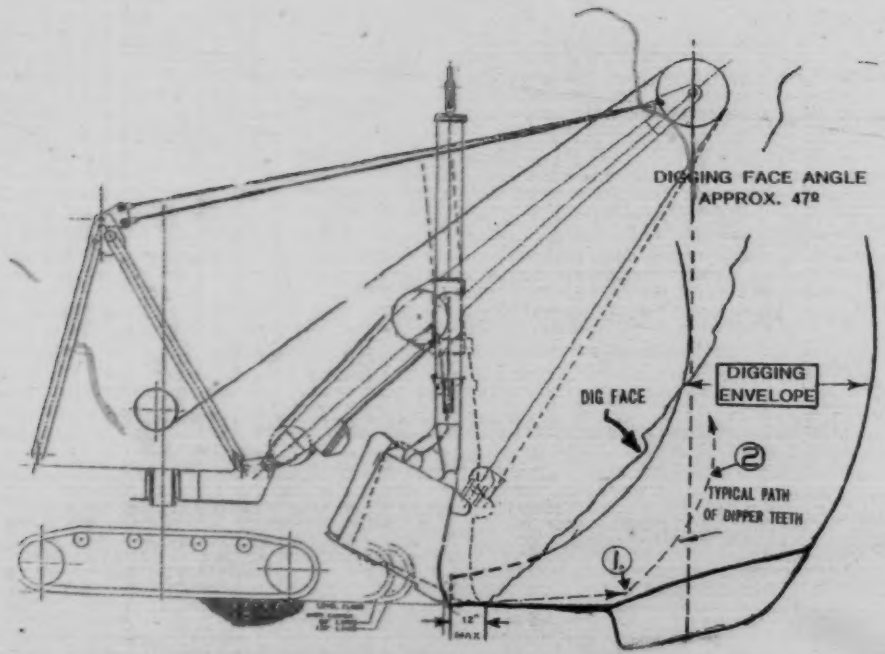

Figure 37: Optimum Start Point for Dipper Entry

Figure 36 represents the initial presentation into digging face. It is obvious from the digging profile how the digging resistance in the media reacts to the dipper penetration in the face; however, the amount and timing of applied two major forces (i.e. hoist and crowd) and their directions will determine the magnitude of the resistance force. If operator applies too much crowding in position II the dipper might trap in face and he then needs to retract and less hoist the release the dipper, hence the dipper poorly becomes full before reach to its maximum defined height (i.e. below shipper shaft horizontal line). Also, if operator keeps digging in the face above the shipper shaft height due to poor digging method, the spillage in front of face will be increased and productivity drops since the support dozer clearing time increases.

As illustrated on Figure 37 the optimum initial dipper teeth distance from face toe when the face angle is about 47° is about 12". While the shovel proceeds with digging in the face and slices of f the digging envelope taken out, depends on how the operator control the dipper teeth movement the final digging path (solid far line on Figure 37) can be either almost straight or under cut in this envelope.

5.6 Force Vectors

One of the quickest and simplest ways to interpret the status of forces on teeth of dipper at face is by drawing the force vectors that already been discussed in chapter 3 and as shown in Figure 38. Depend on what level of forces on crowd, retract, hoist or lowering applied the cutting force can be drawn. On this figure for instance, it looks that about 70% (optimum) of the crowd is applied and it is obvious that with bigger crowd force the direction of the cutting force is more toward the core of the face and no good. In other hand, if less crowd force is applied then the cutting force is more tend to be tangential to the trajectory and this manner also is not good. So that is verification of cutting force in any given seconds of the digging trajectory helps to better evaluate the cutting trajectory and bench mark the operator's performance on operating the shovel. According to wh[illegible] explained Figure 39 for three positions (I, II, and III) been developed. Based on the experimental as well as design variables, cutting force increases on an

empty dipper from position I through III while if the dipper is full this equation is in opposite direction.

5.7 MIDAS Data Post Processing

Recorded shovel operation data via MIDAS on different shifts and operators been post processed to verify the shovel KPI's differences and summarise the results to grade out each shift and operator. In chapter 4 the basics and fundamental of how to find out the best KPI already discussed. An Access Database being developed to input/translated the raw data received from Siemens representative at Albian Sands. And since the reporting outputs from MIDAS software could not provide this research with needed bench marks input, it was necessary to post process the MIDAS information in the mentioned database. Then the results exported to Excel spreadsheet to plot the results as summarised in Appendix E.

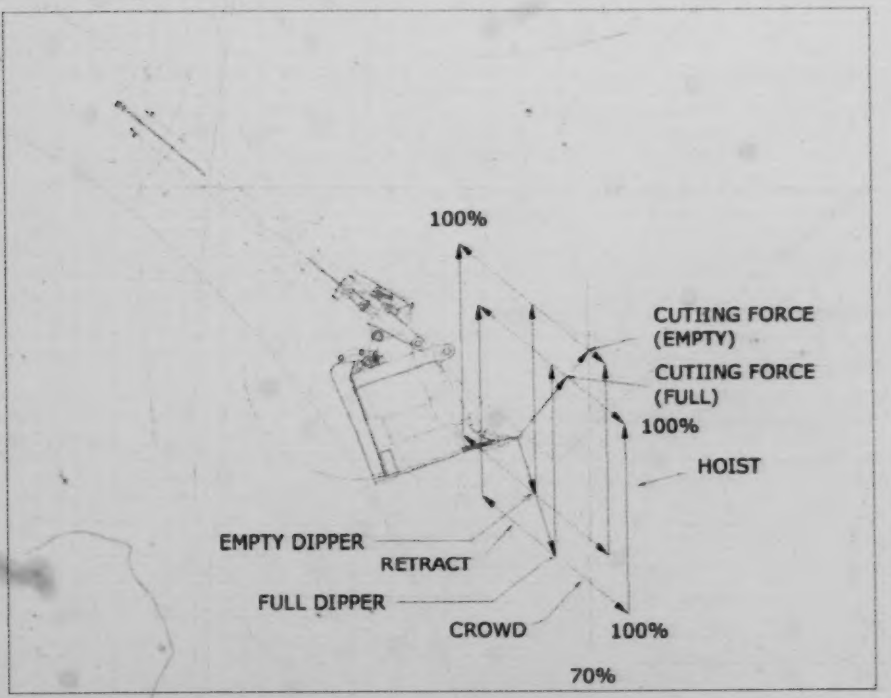

Figure 38: Cutting Forces Vectors on Dipper (Not to Scale)

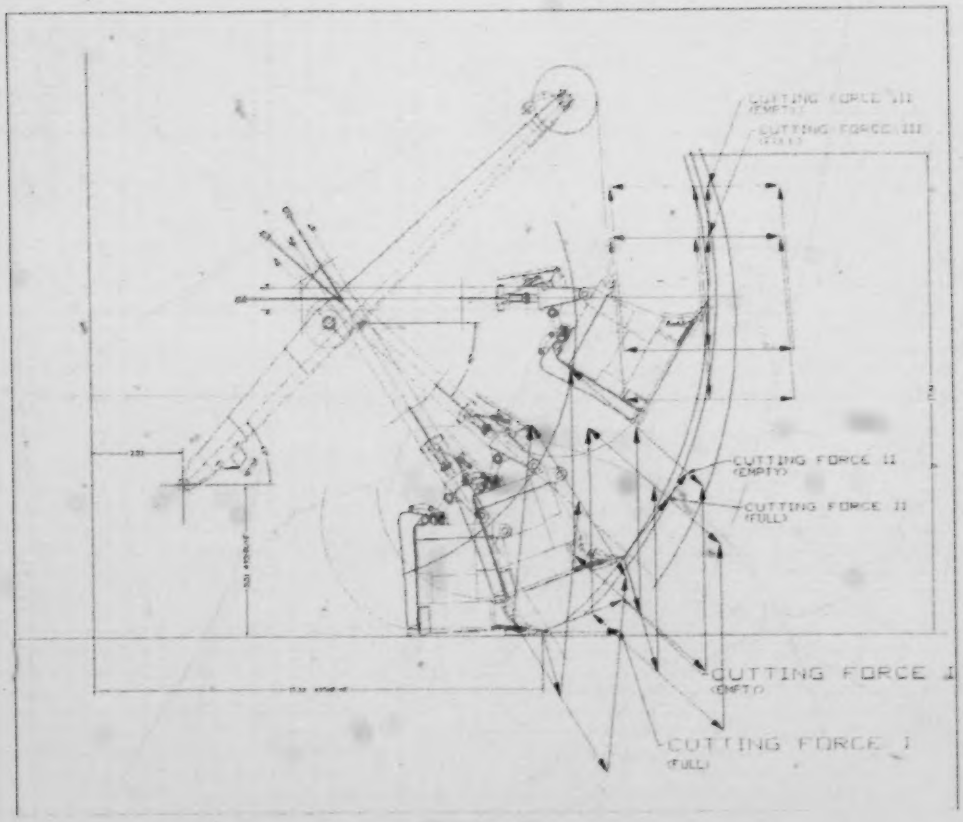

Figure 39: Force Vectors on Three Main Positions (Not to Scale)

6 CONCLUSION AND RECOMMENDATIONS

6.1 Conclusion

On previous chapters it is tried to introduce electric cable shovels in general including key operating parts and components as well as verification the variables that interact directly to shovel performance. Also it is attempted to review the dynamics and kinematics of cable shovel handle and dipper that play main role on transferring combination of forces from crowd, hoist, swing, and propelling as one effective force named as cutting force which has to be greater than the cutting face resistance force that is a reaction against dipper penetration into soil.

This research is focused on oil sands open pit mining with fleets of Bucyrus 495 electric cable shovels and 797B Caterpillar heavy haulers. With regards to huge dipper capacity of about average of 40 m3 (~100 short tons in oil sands of specific density of 2.08 t/bcm) it takes 4 dippers runs to substantially fill the trucks if a successful dig in the face gained otherwise it will take 5 dipper runs over to fill the box to maximum payload capacity of about 400 tons (380 tons exact); however, to increase the productivity, shovel operators usually over load the trucks that in turn cause escalation in operating cost due to spills off trucks on haul roads and increase of maintenance need on mine roads as well as damages to mechanical components of trucks as well as faster wear and tear on trucks tires that is part of big cost runs in mine operating expenses. Therefore, it can be seen that operator's level of competency is not only important on shovel productivity but also goes beyond and affect bigger picture of whole mine operation.

Having well trained shovel operators will help the operation to reduce extra work for support equipment need to police the shovel operating area to clear the front of face, which is result of spillage off the dipper or face during the cut cycle and this issue can be reduced and controlled by shovel operator.

6.1.1 Data Interpretation and Monitoring

This research study concentrated on real data collected by monitoring device called MIDAS that in previous chapters is already reviewed. By analysing the raw information and decoding them into understandable database language to the researcher, I then applied the design conversion factors provided by manufacturer to translate electric motors torques, current, voltages, and powers to hoist and crowd forces. It is deemed that swing has less effect to cutting (i.e. ignored cutting while swinging) hence the cutting force evaluation is considered in two-dimensional Cartesian coordinate system. In chapters of this report on a comprehensive approach the forces on handle and dipper was studied and studies done by others also been reviewed.

Mathematical relations to correlate these forces and measure the cutting force at any given second of dig cycle verified. With application a simple geometry of handle-dipper system, in developed database the varying angles followed and recorded. These angles are included with crowd and hoist angles at any given second of dipper travel time. Adjacent to database calculating digging key parameters, MIDAS Desktop software has been used to assure the quality and integrity of calculations as well as precision of outputs. To accomplish this task MIDAS Desktop been applied in a observation approach and database results sampled in a random basis on different shovel times and shifts to ensure measured cutting forces and their directions at face are rational and valid numbers.

6.1.2 Dig Cycle and Load Identification

Once the database was developed, it was essential to filter it down only to dig cycles as the rest of times were not relevant to goal of this research.

Figure 40 depicts that how the dipper gets filled in different dig cycles compare to different positions of the shovel to the face on different swing angles and why sometimes truck total load crosses its payload. As it is earlier mentioned, truck over loading causes operating problems such as spillage in front of face and along the haul roads. It is obvious that operator digging technique will affect a lot on

dipper fill factor. That is why on one full truckload cycle it takes four dipper travel-runs while on some other cycles it takes five runs to over fill the truck due to insufficient fill in dipper on some dig cycles. In this chapter it is shown that as a result how the trajectory profile looks like and how to instruct shovel operator to follow the best trajectory pattern to optimize and improve shovel production. It should be mentioned that with proper operating practice by shovel operator, shovel line electricity use also can be optimized and the same time the amount of generated electricity as a result of dipper lowering.

To identify the dig cycle in data based an algorithm based on criteria such as the maximization of the hoist rope length while sudden power direction change on crowd occurs has been considered. In this process shovel operating cycle time segregated to three components: dig in face, face preparation, and wait time for truck. With regards to full description and how to implement and use MIDAS and post processing raw data, Chapter 4 and Appendix E are best reference in this report. As a summary as shown in Figure 41 it is worthwhile once again to have a look to the graphics of behaviour of power curves on hoist, crowd, and swing during the dig cycle to re-cap what so-far is discussed. As illustrated in Chapter 5, digging envelope includes three major sections in which second dipper supposed to be substantially filled during the cut in the face. Algorithm in database calibrated to allocate a fragment of total dipper load in each cycle to every second of digging cycle. For simplicity, it is deemed equalized distribution of weight amongst the digging seconds. To precisely model the fill rate in dipper it requires a stand-alone research to fulfil this need.

6.1.3 Dig Profile Evaluation

Figure 42 is an example of one full dig cycle randomly taken from shovel production file. All factors such as time, season, hardness of ground, and coordinates of shovel are known parameters. The dig profile in this figure consists of five dipper travel times on the face to fill the truck box. Due to data privacy to the owner, all graphics re-scaled not to reflect the actual values, hence there is no scale correlation in graphs between charts.

Looking at this figure, it can be inferred that on first run the dipper over filled that in turn some can be spilled to the front of face. Opposite to this position the fifth run can be considered as less productive shut. Furthermore, early swinging on the face on the second run shows less captured material in dipper. The third and fourth dipper loads are close to the average of loaded dippers in this full cycle. It is obvious that in second run the crowd was over forced into the face, and that the operator had to retract to release the dipper from face and engaged the crowding again to compensate the lost second due to this to fill the dipper. Opposite to this position one can compare the first run with smoother dig cycle and as can be seen dipper is less upset in the face by applying more uniform crowding and hoisting together to gain best result. As a result interpreting this full dig cycle, I can say if operator was able to manage the dig to copy the first trajectory pattern over the rest of runs he might got the same result like the first one and might no need for fifth run; therefore, it could be a time saving and in turn increase of shovel productivity. However, to reach to this goal the environment surrounding the media also need to be considered such as under what circumstance we are digging the face whether it is frozen and etc. Even in these cases the operation can be well managed by applying the support equipment such that the frozen ground can be ripped in advance the shovel dipper come to that section.

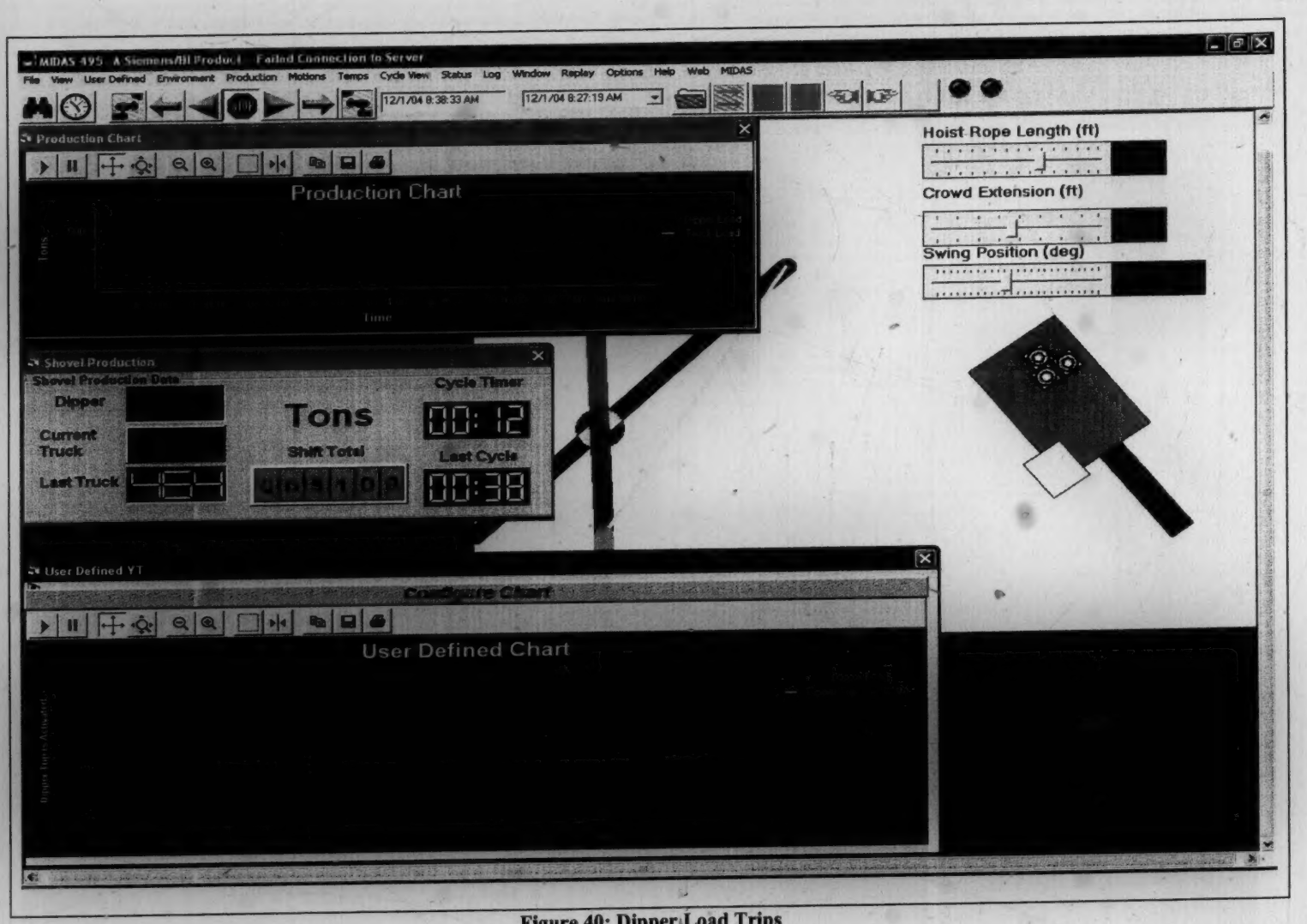

Figure 40: Dipper Load Trips

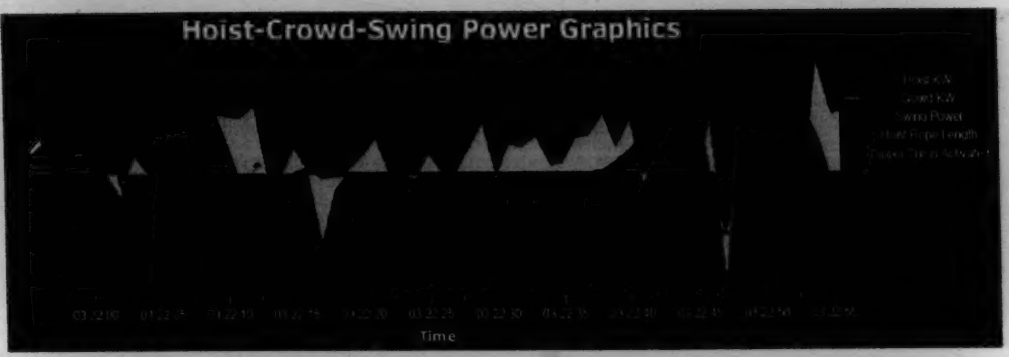

Figure 41: Digging Cycle Selection (Units are not in same scale)

Figure 43 shows the variations on crowd and hoist AC motors volt-ampere during the dig cycle. To measure the actual crowd and hoist AC motors voltage the equations on Appendix F has been applied. The third dig run is close to the theoretical Hoist-Crowd volt-time curve as drawn on this figure. Cross checking to Figure 42, it can be implied that the third dig run also has very good production very close to the average of whole shovel dig cycle as well as more uniform and managed hoist power usage.

And finally all data post processed by using the relations mentioned in Appendix E, the dipper position in a X-Y measured. As a sample example the above mentioned system shown in Figure 44. Also each individual dig cycle (Figure 45) has been shown on separate charts to verify the cutting force amount and it's direction with regard to dipper handle extent. Also it is tried to depict the correlation between the crowd/retract and hoisting while in dig mode to cutting force. Simple analysis can indicate that application of over-crowding while a uniform hoisting is in place causes the dig angle tend more toward the depth of digging face and consequently could create a negative force opposite to digging direction and trap the dipper in face and to release the dipper there is no other choice but applying retract, which in turn means reduction in dipper fill ratio. One can mention it is seen that the crowd power could not be used as good indicator to evaluate the digability and trajectory verification. Also to rationalize the algorithm of calculations in database sometimes multi conditions were considered

to measure the forces as actual as possible. Sometimes the AC motor working current direction is not in the same as the power direction; therefore, it is required with consideration of more criteria before come to final results.

Reports by others, including paper by Tannant, D.D. and Patnayak, S. (2005) performed on P&H electric shovels indicates that due to variations seen on crowd and hoist powers the best solution is that the averaging take place. By averaging the powers over fragments of cycle time the affect of shovel operator on predicting the digability can be reduced. To summarize this statement Figure 46 has been collected on some duration of the shovel dig cycle. As it can be seen over the course of time the local power variation that on previously shown figures was tangible, no longer cause a sensitive bench marking to the performance indicator such as hoist power.

Furthermore, it should be mentioned that on the exercise of calculating the cutting force and it's angle to the dipper handle, it found a bit challenging process to make sure that the measured force is correct as well as the angle. Cutting force directly correlates to hoist power and crowd power.

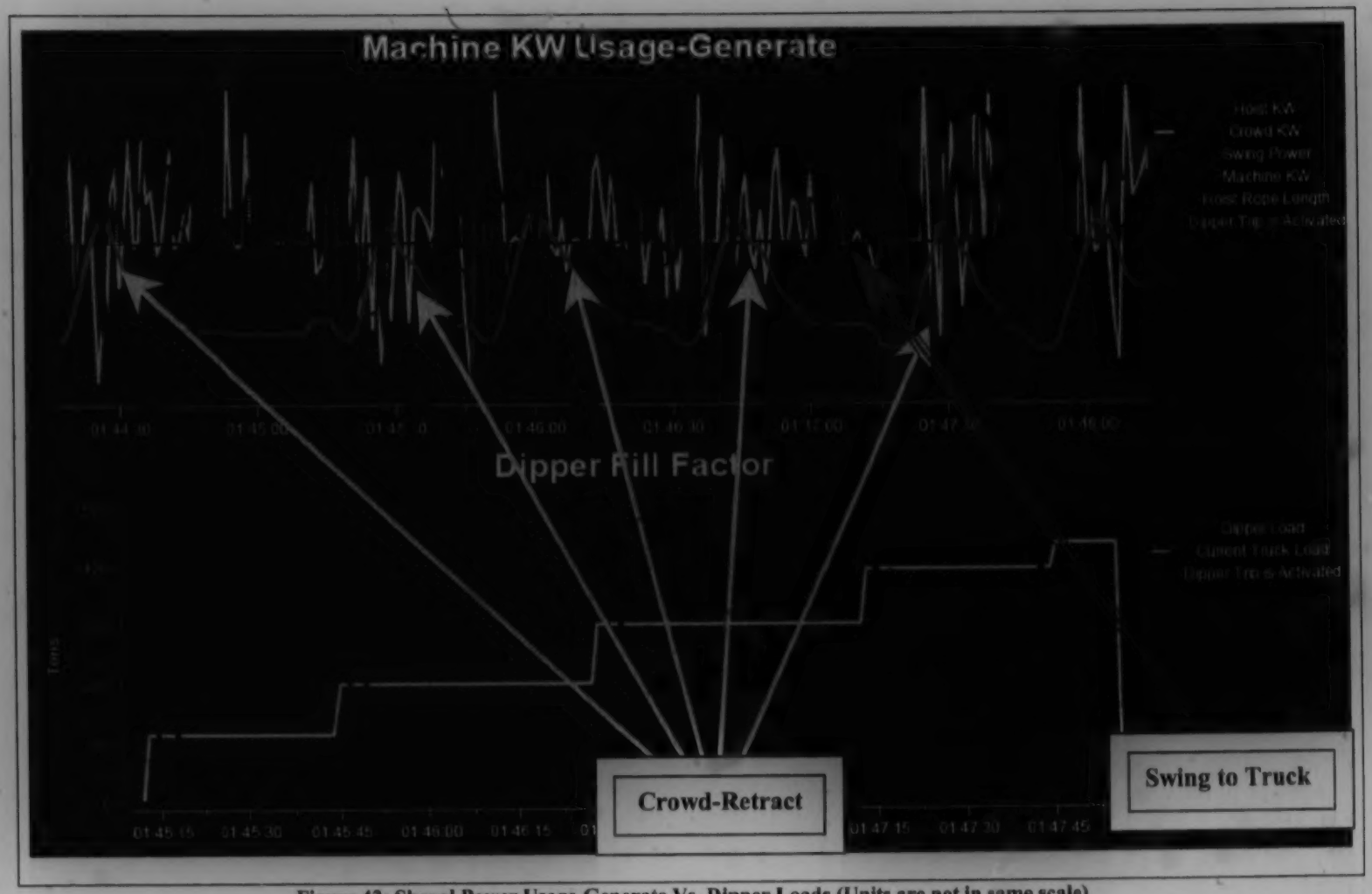

Figure 42: Shovel Power Usage-Generate Vs. Dipper Loads (Units are not in same scale)

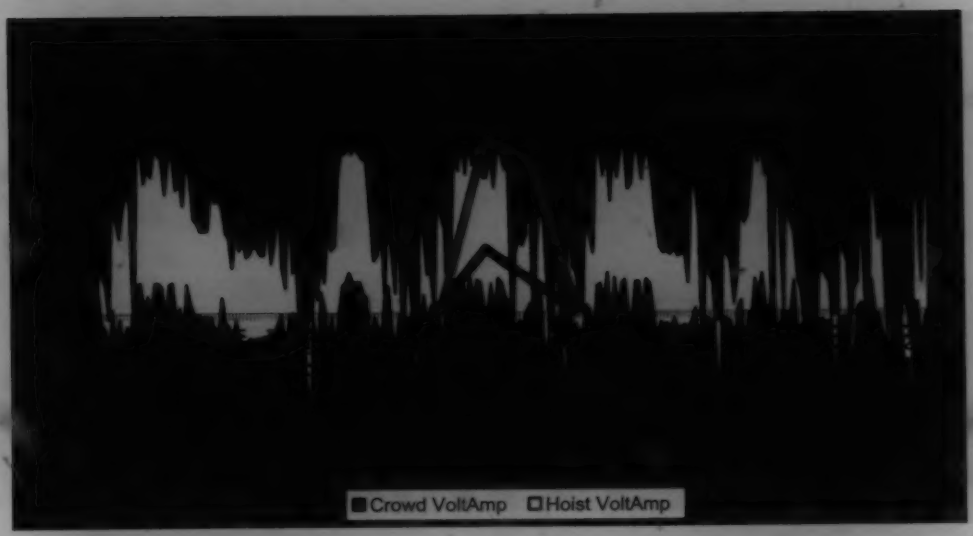

Figure 43: AC Motors Volt Amp Vs. Time

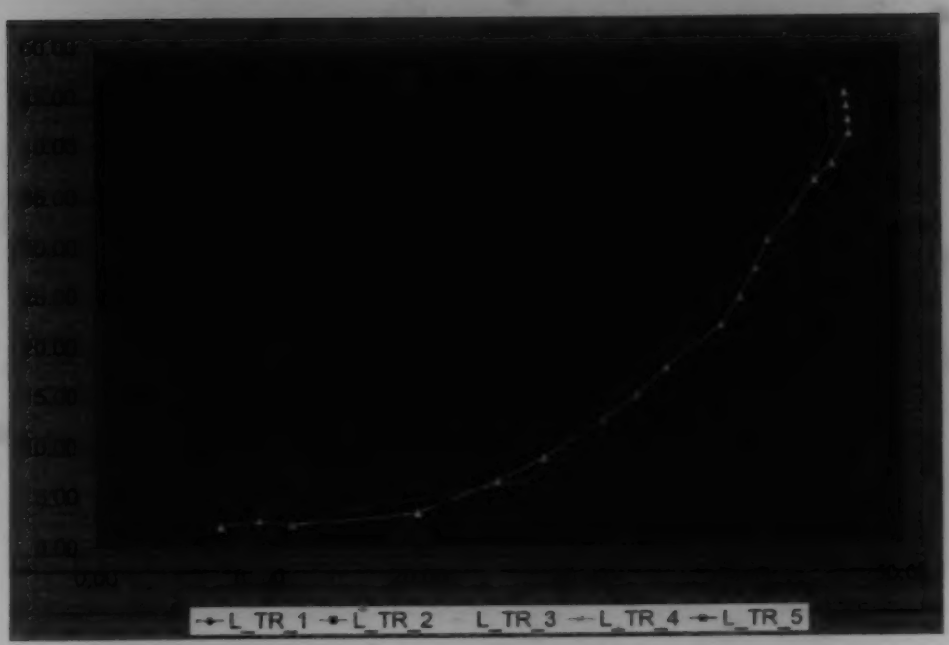

Figure 44: One Full Dig Cycle Trajectory

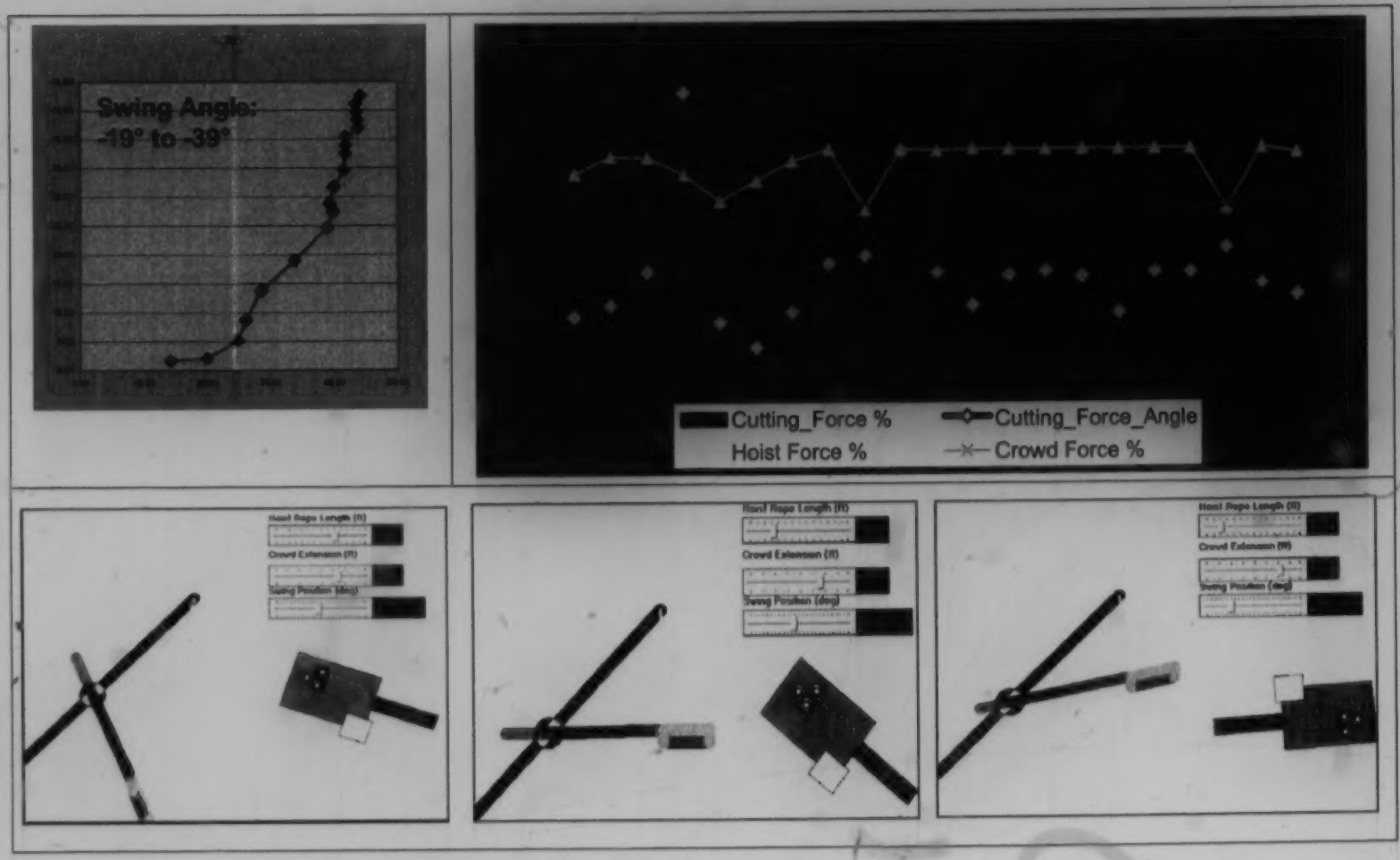
Swing Angle:
-19° to -39°
Cutting_Force %
Cutting_Force_Angle
Hoist Force %
Crowd Force %

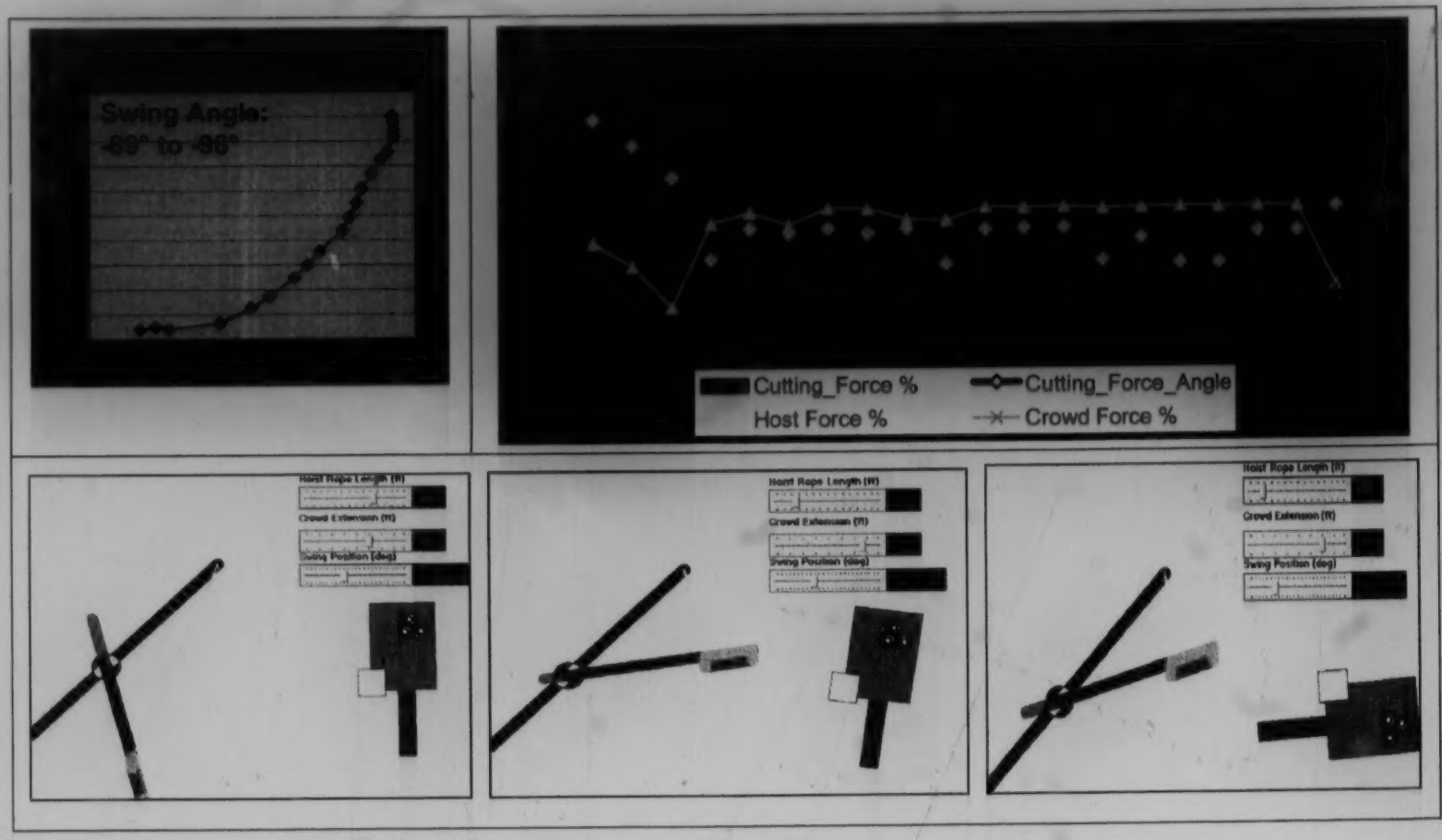
Swing Angle:
-89° to -98°
Cutting_Force %
Cutting_Force_Angle
Host Force %
Crowd Force %
Hoist Rope Length (ft)
Crowd Extension (ft)
Swing Position (deg)

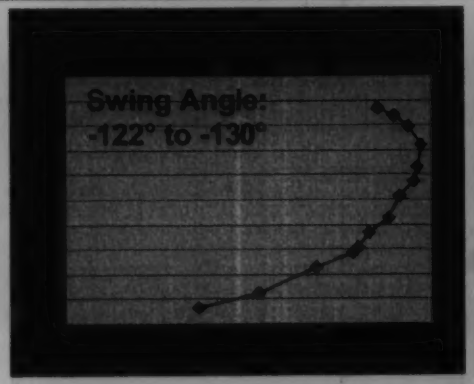
Swing Angle:
-122° to -130°

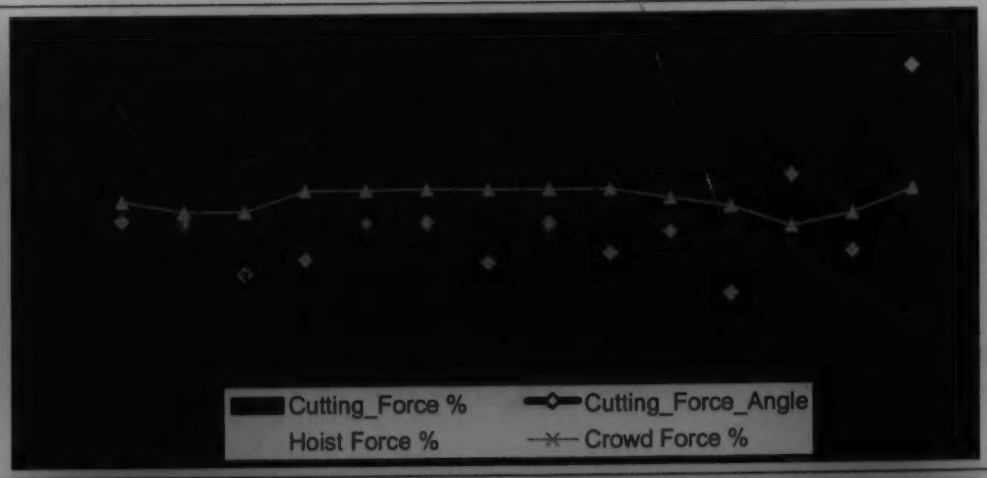
Cutting_Force %
Cutting_Force_Angle
Hoist Force %
Crowd Force %

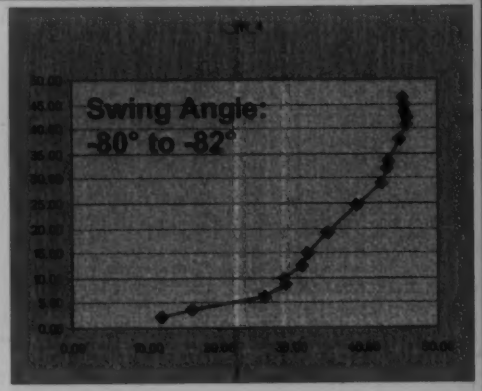
Swing Angle:
-80° to -82°

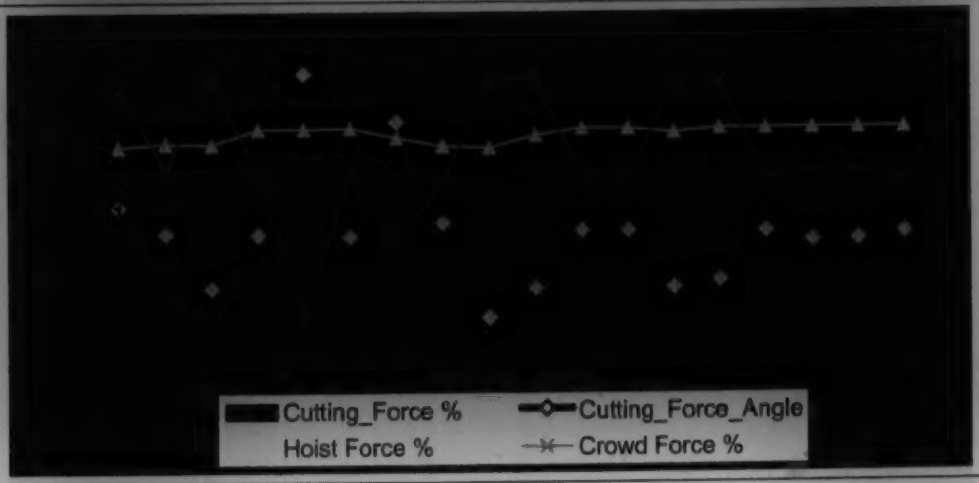
Cutting_Force %
Cutting_Force_Angle
Hoist Force %
Crowd Force %

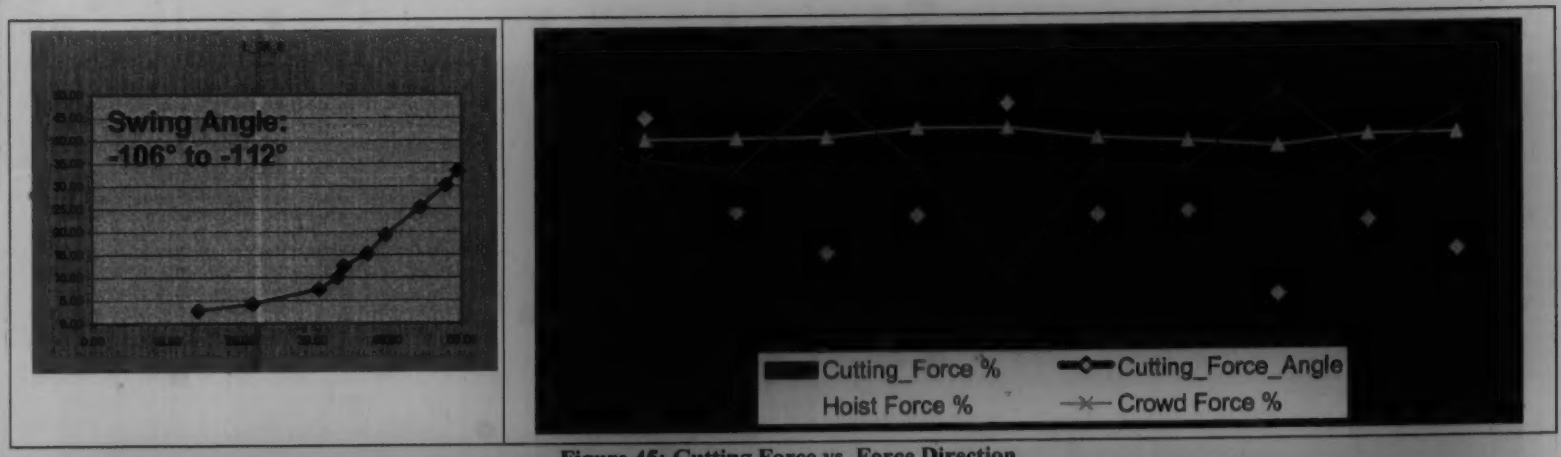

Figure 45: Cutting Force vs. Force Direction

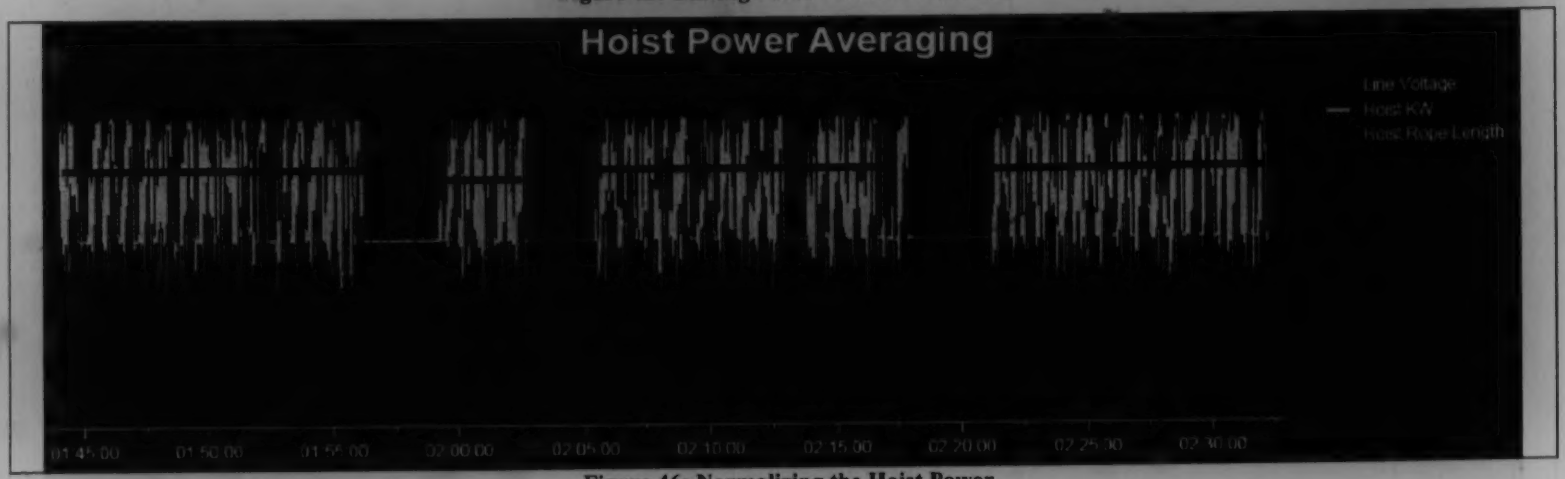

Figure 46: Normalizing the Hoist Power

6.2 Conclusion Summary

According what so ever described, following bullets can be accounted to summarize this text message:

- Video camera recording also carefully evaluated for cross checking
- Different shifts, seasons been sampled
- MIDAS Desktop applied to collect raw data
- MIDAS Desktop being used to cross check the validity of outputs (observation approach - QC)
- Physics and geometry applied to determine cutting force and its angle
- Dig trajectory also being drawn and evaluated
- Dig cycle been determined and interpreted
- The amount of hoist power significantly is bigger than crowd power
- Direct swing angle effect on trajectory
- Less weather condition effect on production
- To manage the face hardening applied support equipment (i.e. dozer equipped to ripper shank) to rip the frost above the face
- Hoist force direct relation to cutting force
- Crowd force direction counter relation to cutting force angle

6.3 Recommendations

The amount of hoist power significantly is bigger than crowd power; however, direction changes on crowd still has considerable impact as well as hoist (i.e. hoist to lowering) on cutting force direction and it can be found out how sensitive the trajectory could be to proper application of hoisting, lowering, crowding, and retracting. Basically the ground condition is a not negligible factor to determination of good dipper penetration, so less challenge on optimizing trajectory as there will be only operator's skill factor how to manoeuvre the dipper in the face.

On randomly sampled digging cycle data in a range of 49 consecutive digs, the histogram (Figure 47) of the cycle time shows a very close to normal distribution chart that the optimum cycle time is happening amongst the 15 seconds to 19 second of dig time with the best record of digging time on 16 seconds. As also depicted on Figure 48 the P50 and P80 can be well recognized that seconds of 16^{th} and 19^{th} are the range of optimized dig trajectory under this particular cutting conditions and operator. By plotting each shift histogram one can easily evaluate the production cycle times as well as production forecasters.

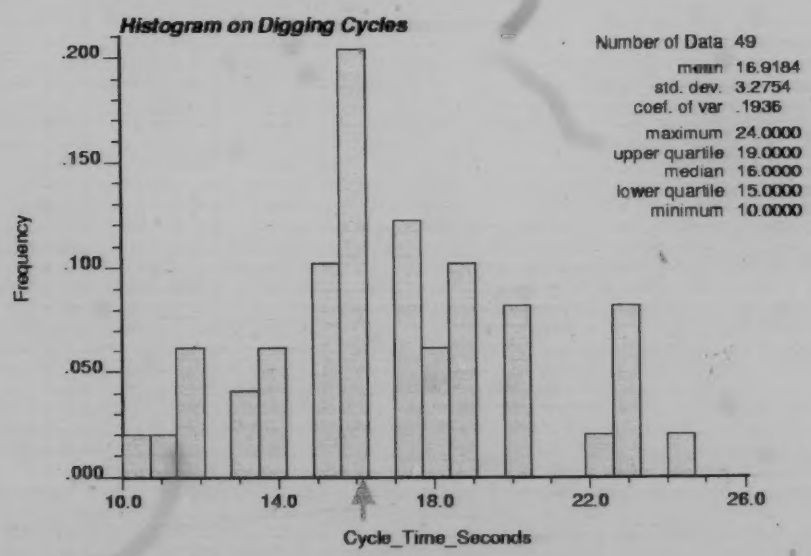

Figure 47: Sample Histogram of One Hour Digging

By cross checking all above-mentioned graphics, it can be said that while applying uniform hoist force to the face is essential to get best output, the importance of crowd force on affecting the dipper fill ratio must not be neglected as it can either acts on favour of cutting force or against it and causing the change of cutting force vector direction and trap the dipper into the face.

To gain the best result on combination of forces on face shovel operator needs to situate the shovel as described in chapter 5 and ensure that to avoid under cutting the face that can be happened if not good trajectory has been accomplished by extra crowding and less hoisting in first phase of dig cycle. The clear fact should never to be forgotten that the smoother digging trajectory always the less upsetting mechanical and hydraulic parts.

As indicated in this research results, the power usage on AC motors also directly relates on how the operator manage the control joystick in terms of proper timing on crowding, hoisting, and swinging.

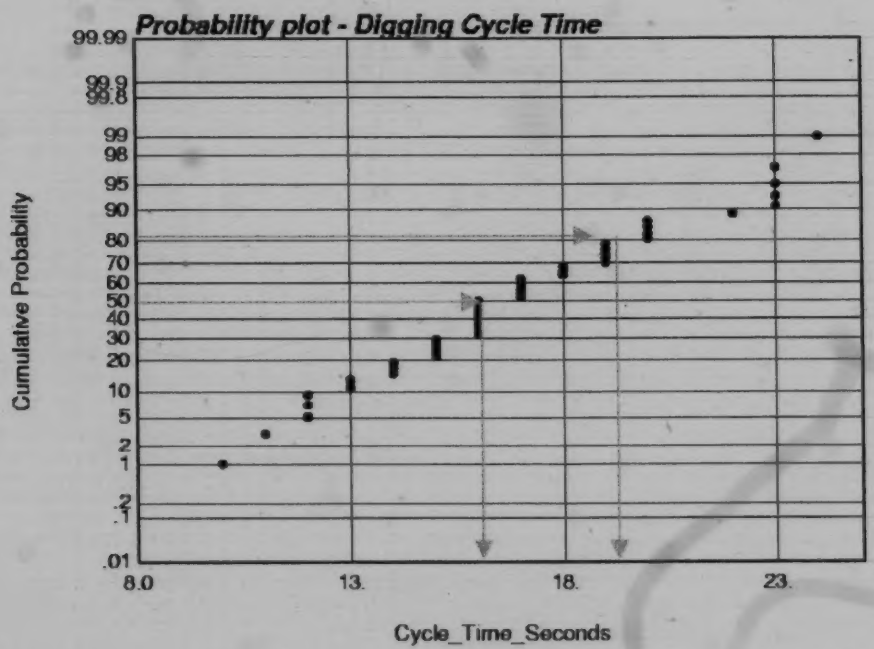

Figure 48: Dig Cycle Time Probability

As shown in Figure 49, the optimum cutting angle lies within range of 22 to 40 degrees and the batch of sampled data shows lognormal distribution proving that most of cutting forces directions were in favour of dig process.

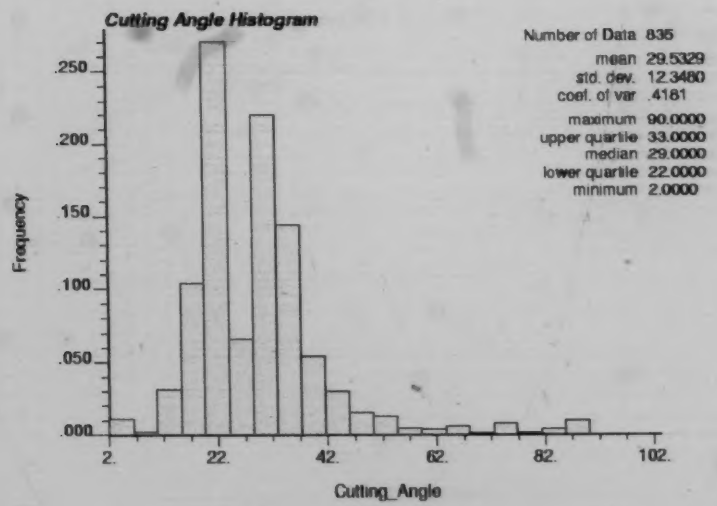

Figure 49: Cutting AngleDistribution Chart

And as a wrap up following bullets can be accounted for the brain of this research study summary of recommendations:

- Direction changes on crowd still has considerable impact as well as hoist (i.e. hoist to lowering) on cutting force direction
- Proper application of hoisting, lowering, crowding, and retracting
- Operator's skill factor how to maneuver the dipper in the face
- Optimum cycle time is happening amongst the 15 seconds to 19 second of dig time with the best record of digging time on 16 seconds

- Also depicted that P50 and P80 can be well recognized that seconds of 16th and 19th are the range of optimized dig trajectory under this particular cutting conditions and operator
- Optimum cutting angle lies within range of 22 to 40 degrees and the batch of sampled data showed lognormal distribution proving that most of cutting forces directions were in favour of dig process
- Application all sophisticated instrumentation and software such as MIDAS, all these can help to bench mark the shovel productivity performance
- Optimized trajectory when:
    - Shovel dipper teeth is less than 12" from face toe
    - Dipper handle angle of 35.5°
    - Shovel not too close nor too far to/from face
    - Less crowding in phase II of dipper digging travel

Finally one can say, with application all sophisticated instrumentation and software such as MIDAS, all these can help are to bench mark the shovel productivity performance and at the end of day this is the operator needs to have good knowledge over all this as shovel production is a manual control by him and no automated system has any touch on this area like those installed in airplanes allow the computer navigate the system.

At the end of this report I hope I could be able to picture the actual operating environment at face with regards to interactions of different forces and understanding the affecting parameters on helping operators and project managers to better understand the reasons for different production rates while using the same shovel and same material and conditions.

REFERENCES

1) Alekseeva, T.V., Artem'ev, K.A., Bromberg, A.A., Voitesekhovskii, R.I., Ui'yanov, N.A., 1985. Machines for Earthmoving Work - Theory and Calculations. Third revised and enlarged edition – Russian translation series. p. 28-88, 403-427

2) Awuah-Offei, K., 2004. Intelligent Excavation Scheme for Athabasca Oil Sands Excavtion. Ph.D. research report. School of mining and petroleum engineering, department of civil and environmental engineering, university of Alberta, p. 4-15.

3) Bucyrus-Erie Company, 1979. Surface Mining Supervisory Training Program Shovel/Truck. Chapters 5, 6, and 7.

4) Frimpong, S., Awuah-Offei, K., 2006. Numerical Simulation of Cable Shovel Resistive Forces in Oil Sands Excavation. International Journal of Mining, Reclamation and Environment, Vol. 20, No. 3, p. 223-238.

5) GILEWICZ, P., 1999. Shovels by numbers. World mining equipment, 23, p. 6.

6) Haddock, K., 2005. 125 Years, Making the Earth Move. Published by MBI publishing company. A full history of Bucyrus International Inc.

7) Hansen, J., 2001. Electric Rope Shovel Monitoring. CIM Bulletin, Vol. 94, p. 80-82.

8) Joseph, T.G., Hansen, G.W., 2002. Oil Sands Reaction to Cable Shovel Motion. CIM Bulletin, Vol. 95, p. 62-64.

9) Kuphaldt, T.R., 2006. Lessons in Electric Circuits Volume II AC – Sixth Edition, last update June 15, 2006 - (www.ibiblio.org/obp/electricCircuits)

10) Pasamehmetoðlu, A. G., Karpuz, C. and Muftiioglu, Y., International, Middle East Technical University, Mining Engineering Department, Ankara, Turkey, 1992. Performance assessment of hydraulic and cable shovels. International journal of surface mining, reclamation and environment, 6:2 p. 73-80.

11) Shi, N., M.A.Sc., 2005. A New Approach to Optimizing Cable Shovel Dipper Design for Cutting Soft Rock and Soils. Ph.D. research proposal. School of mining and petroleum engineering, department of civil and environmental engineering, university of Alberta, p. 4-17.

12) Siemens Industrial Solutions and Services. SIMINE^{CIS} SH Higher Reliability and Lower Costs with AC Drive Systems for Mining Shovels. Company web site: www.siemens.com

13) Tannant, D.D. and Patnayak, S., 2005. Performance Monitoring of Electric Cable Shovels. International journal of surface mining, reclamation and environment (Vol 19, No. 9, December 2005). p. 276-294.

Appendix A: Bucyrus-Erie Company Shovel Production History

In 1880, Daniel P. Ells of Cleveland Ohio, Haddock K. (2005) published, brought together a group of relatives and prominent business associates with the intention of forming a new company for the manufacture of railroad and mining equipment. The railroads were expanding west, and Ells saw an opportunity to benefit from the expansion and wanted to be on the forefront of the industry. The group Ells created purchased the former "Bucyrus Machine Company of Bucyrus", Ohio, and on December 1880, the new company was officially incorporated as "Bucyrus Foundry and Manufacturing Company". In 1882 Bucyrus first steam shovel came to life on its production line. This steam shovel purchased by Ohio Central Railroads. This shovel was given its name after his designer John Thompson, the manufacturing manager at the company at tat time. The company expanded into manufacturing other types of excavators. In 1883 Bucyrus first dipper dredge came to the market. Between 1889 and 1891, due to the market demand toward the larger capacity excavators, the Bucyrus facilities in Ohio was not big enough for such production line requirement. Also the company was seeking for new storage facility. In 1891, the South Milwaukee Company in charge of prompting an industrial town in South Milwaukee, presented a suitable location to Bucyrus need; therefore, Bucyrus made an outstanding move toward brilliant future of the corporation by uprooting the established company in Ohio and move it to the new location in South Milwaukee, Wisconsin. In 1893, the new South Milwaukee product plant commenced. This move also had another outcome of given a new name to the corporation. The new name of "Bucyrus Steam Shovel and Dredge Company of Wisconsin" last only for few years until 1896 that the new name came on board known as "Bucyrus Company". In Table 5, it is tried to put together a brief history of Bucyrus International Inc. shovel different models production as well as company name change.

TABLE 5: BUCYRUS INTERNATIONAL INC. SHOVEL PRODUCTION HISTORY

Bucyrus-Erie Company Shovel Production History

Manufactured/Event	Name	Type	Year	Location being Used	Remarks
First steam shovel		Steam	built in 1835	in railroads projects	
Bucyrus Foundry	Thompson Iron Steam Shovel	Steam	1882	Ohio central railroad	
Bucyrus Plant Relocation	Bucyrus Steam Shovel and Dredge Co. of Wisconsin		1891	From Ohio to South Milwaukee, Wisconsin	in 2 year the plant with 50 workers started the production line.
Company Name Change	The Bucyrus Company		1896	South Milwaukee, Wisconsin	2½ cubic yard (1.9 cubic meter) bucket shovel was the most popular size.
The Bucyrus Company	The Bucyrus Company	Steam	1895-1901	in mining and railroad excavation	12 different sizes of steam shovels were offered, ranging from 12 ton (11 tonne) model to gigantic 95 ton (86 tonne) machine. Shovel on standard gauge railroad tracks.
60-B	The Bucyrus Company	Steam	1897 - 1898		2½ cubic yard (1.9 cubic meter) bucket on shovel weighted 60 ton (54 tonne) machine which redesigned to 65 ton (59 tonne) in following year.
Independent Crowding Engine	The Bucyrus Company	Steam	1898		Independent thrusting (crowding) engines were added to 65 ton shovels.
Independent Slewing Engine	The Bucyrus Company	Steam	1901		Independent slewing engines were added to shovel with separate power for each of the three basic motions.
Introduction of Larger Shovels	The Bucyrus Company	Steam	1899		Weights of 75 ton (68 tonne), 85 ton (77 tonne), and 95 ton (86 tonne) with a 5 cubic yard (3.8 cubic meter) dipper.
Building the Panama Canal	The Bucyrus Company	Steam	1904-1908	Panama Canal Construction Site	70 ton (64 tonne) and 95 ton (86 tonne) plus another 100 more machines after the first two proved their merit were sold to this project owner.
New Revolving Machine	Marion and Vulcan	Steam	1908		Bucyrus two major competitors started to manufacture small revolving shovels.
New Partnership	Bucyrus-Vulcan Company		1910		
150-B First Stripping Shovel	Bucyrus-Vulcan Company	Steam-Stripping	1911		Dipper capacity of 2 ½ cubic yard (1.9 cubic meter) and 60 foot (18 meter) boom - rail mounted machine featured an equalizing beam on one side of the undercarriage providing a three-point suspension system with screw jacks for leveling.
175-B	Bucyrus-Vulcan Company	Stripping Shovel Steam or Electric Power	1911& 1951		Dipper capacity of 3 1/2 cubic yard (2.7 cubic meter) - the same info. as 150-B.
New Merger	The Bucyrus Company		1912		The Atlantic Equipment Company which was owned by American Locomotive Company, consolidated into this group.
225-B	The Bucyrus Company	Stripping Shovel Steam or Electric Power	1914		Weighted over 300 tons (272 tonnes) and carried a 6 cubic yard (4.6 cubic meter) dipper on a 75 foot (23 meter) boom. This was a new electrical-power system known as "Ward-Leonard" control as an alternative to steam on its largest stripping shovel, the 225-B.
30-B	The Bucyrus Company	Steam-Diesel	1920-1921	Strip mining of bituminous coal	1 cubic yard crawler mounted 30-B, Bucyrus first universal excavator was introduced to the market.
20-B & 50-B	The Bucyrus Company	Electric Drive	1922	Strip mining of bituminous coal	30-B model with an electric drive option appeared in production line. By application of Ward Leonard System, electric drive was introduced on these shovels.
320-B	The Bucyrus Company	Stripping Shovel Steam or Electric Power	1924	Query and hard rock mining	Weighting 390 tons (354 tonnes) and carrying a dipper of 8 cubic yard (6.1 cubic meter).
120-B	The Bucyrus Company	Electric Drive	1925	Query and hard rock mining	5 cubic yard (3.8 cubic meter) This was the first time to combine the advantages of the fully revolving shovel with proven heavy duty digging capability of the part swing railroad shovel. This machine was the forerunner of the present-day electric mining shovels.
100-B	The Bucyrus Company	Electric Drive	1926	Query and hard rock mining	3 1/2 cubic yard (2.7 cubic meter) dipper.

New Merger	Bucyrus-Erie Company		1927		The Erie Steam Shovel Company of Erie was the America's leader in small shovels.
750-B	Bucyrus-Erie Company	Electric-Stripping	1927	Michigan Limestone Company	Dipper capacity of 12 cubic yard (9 cubic meter). The machine designed based on a counterbalance hoist system.
75-B	Bucyrus-Erie Company	Electric Drive	1928	Query and hard rock mining	2 1/4 cubic yard (1.7 cubic meter) dipper. (1)
170-B	Bucyrus-Erie Company	Electric Drive	1929	Query and hard rock mining	6 1/2 cubic yard (5 cubic meter) dipper. (1)
85-B	Bucyrus-Erie Company	Electric Drive	1935	Query and hard rock mining	3 1/2 cubic yard (2.5 cubic meter) dipper.
950-B	Bucyrus-Erie Company	Electric-Stripping	1935	Shasta Coal Company in Bicknell, Indiana	30 cubic yard (23 cubic meter) dipper weighted 1,250 tons (1,134 tonnes) featured with counterbalance hoist system. The front end arrangement, with a single tubular dipper handle operated by wire ropes, was the most notable feature. **
1050-B	Bucyrus-Erie Company	Electric-Stripping	1941-2003	Old Ben Coal Company of Indiana	45 cubic yard (34 cubic meter) featured with "Knee-Action-Crowd"***.
New Acquisition	Bucyrus-Erie Company		1948		Bucyrus-Erie Company purchased the Milwaukee Hydraulic Corporation that was a big move toward the hydraulic excavators.
1650-B	Bucyrus-Erie Company	Stripping	1950s	Peabody Coal Company	Dipper capacity of 55 cubic yard (42 cubic meter) weighted 2,450 ton (2,223 tonne).
3850-B	Bucyrus-Erie Company	Stripping	1962	Peabody Coal Company	Dipper capacity of 115 cubic yard (88 cubic meter) weighted 9,000 ton (8,165 tonne).
260-B	Bucyrus-Erie Company		1962	Kaiser Steel's Eagle Mountain Iron Ore	
1950-B	Bucyrus-Erie Company	Stripping	1965	Hanna Coal Company, southern Ohio	105 cubic yard (81 cubic meter) dipper on a 200 foot (61 meter) boom. The machine weighted of 7,200 tons (6,532 tonnes).
295-B	Bucyrus-Erie Company	Electric-DC Motor	1972		Dipper capacity of 21 cubic yard (16 cubic meter).
395-B	Bucyrus-Erie Company	Electric-AC Motor	1979		Dipper capacity of 34 cubic yard (26 cubic meter). The first generation of electric shovel equipped with AC motors.
495-B	Bucyrus-Erie Company	Electric-AC Motor	1990	Albian Sands Energy	53 cubic yard (41 cubic meter) dipper.
New Acquisition	Bucyrus International, Inc.		1997		Bucyrus International, Inc. grew in 1997 through the acquisition of the Marion Power Shovel Company. Hence, the Bucyrus-Erie name changed to Bucyrus International Inc.
595-B	Bucyrus International, Inc.	Electric-AC Motor	1997	Suncor Energy	57 cubic yard (44 cubic meter) dipper. This machine is a renumbered of 351 M built by Marion's model.
495-HD/HR/HF	Bucyrus International, Inc.	Electric-AC Motor	2002		40-80 cubic yard dipper. HD 90 tons, HR & HF 110-120 tons.

* The Ward-Leonard System: Became standard on all electric shovels up to the advent of the modern AC-driven machines, consisted of DC motors for each motion (hoist, drag, and swing) powered by DC generators driven by constant-speed AC (synchronous) electric motors. The Ward-Leonard system offered power characteristics similar to steam in the DC motors' torque increased as their speed decreased, an appropriate solution on the cyclic nature of shovel loading.

**: In complementary on what mentioned for the 950-B model, there were more improvements done. A propelling motor was mounted in each of the four crawler assemblies, eliminating the previous complicated system of multiple gear trains, shafts, and jaw clutches. for the first time on Bucyrus-Erie machine, a hydraulic system was introduced, dispensing with the earlier screw types. this system automatically leveled the machine utilizing a pendulum device to control the oil in the four support cylinders. steering was effected through large horizontal hydraulic cylinders acting on the crawler assemblies.

*** Knee-Action-Crowd: Was a radial new design of front-end geometry for stripping shovels where the dipper handle was attached to a stiff leg pivoting at the boom foot, instead of the handle attached to the mid-point of the boom. The moveable stiff leg allowed the dipper to move in a long horizontal sweep at ground level, resulting in a long clean-up radius with the dipper teeth less likely to gouge into the coal being uncovered. its other advantages include reduced swing inertia due to the crowd machinery mounted near the machine's center of rotation and reduced bending stresses in the boom.

(1) notation: models 75-B and 170-B were included with several features that delivered to the customers satisfactory. Of these features, the most notable were the single tubular dipper handle with rope crowd, which replaced the former twin stick rack-and-pinion design, and the two-part boom that eliminated bending stresses.

Appendix B: Bucyrus Electric Shovels Spec. Sheets

Figure 50 can be applied as good source of information for geometrical calculations when one needs to evaluate the forces' vectors and end up to resistance forces at the face. An electric cable shovel a formed of major parts that each section includes group of components. Figure 51 shows the machinery house in which the electrical panels as well as all swing, hoist, and crowd units are installed on the main deck. The upper deck by the operator cabin has a unique design to avoid the crowd half sheave hit the body of the shovel when the crowd retreats and hoist is at upper limit.

One of the parts is worthwhile to be mentioned is the boom bumper. It is entirely dependent upon to the operator's experience how to maintain the control of shovel parts movement. One of those situations is when dipper comes to the rest point before start the dig cycle in front of the face. By over hoisting down and retreating the crowd back, this would generate an inertia cause dipper hit the boom.

It was also of advantage the use of to have better understanding of a 495HF electric cable shovel weights, dimensions and other characteristics might needed in this thesis research.

TABLE 6: HF BUCYRUS ELECTRIC CABLE SHOVEL SPECIFICATION SHEET

WEIGHTS

	Pounds	(Kilograms)
Working weight, with dipper and 125' (317.5 cm) links, approx.	2,963,500	(1,344,221)
Net weight, domestic, without ballast and without dipper, approx.	2,281,900	(1,035,052)
General purpose dipper - 66 yd³ (50.5 m³)	146,000	(66,225)
Ballast – furnished by customer	667,000	(302,546)

These weights will vary slightly depending upon dipper and optional equipment selection

ELECTRICAL

POWER REQUIREMENTS

Voltage	3 Phase, 60 Hz, 13,800v
Avg. 15 min. demand	877-1,228 kw
Peak Power	3,507 kw

Other voltage requirements available to suit customer requirements.
575v secondary

DISTRIBUTION SYSTEM REQUIREMENTS

Machine on separate system	4,000 kva

MAIN ELECTRICAL SYSTEMS

System voltage (nominal)		60 Hz, 13,800v
Trail cable (furnished by customer)		SHD-3-#2 @ 13,800v
Transformer, auxiliary	500 kva	13,800v primary
		575v primary
Lighting	2 @ 25 kva	120/240v secondary

ELECTRICAL EQUIPMENT – AC Variable Frequency Control

FRONT END

BOOM

Boom	welded, impact resistant steel	
Boom point sheaves	twin grooved flame hardened	
Boom point sheave diameters	96"	(243.84 cm)
Shipper shaft sheaves	twin grooved flame hardened	
Shipper shaft sheave diameters	72"	(182.88 cm)
Handle diameter	34"	(86.36 cm)
Wall thickness - Nominal	3"	(7.62 cm)

ROPE DATA

	No.	Diameter	Type	Constr.
Hoist	2	2-3/4" (69.8mm)	Twin Dual	6 x 37
Crowd	1	2-1/2" (63.5mm)	Single Dual	6 x 37
Retract	1	2-1/2" (63.5mm)	Single Dual	6 x 37
Boom Susp.	4	3-1/4" (82.6mm)	Equalized	Structural Strand
Dipper Trip	1	3/4" (19.1mm)	Single	6 x 37

MAIN STRUCTURES

PLANETARY PROPEL ..... Dual Motor Independent Drive

TURNTABLE

Forged rim alloy steel swing rack pitch dia.	17'-3"	(5.26 m)
Teeth external cut	9-1/2" face	(24.13 cm)
Tapered forged alloy steel roller rails dia.	15'-6"	(4.72 m)
Number of tapered rollers	50	
Tapered rollers diameter	10-3/4"	(27.31 cm)

REVOLVING FRAME (Center Section)

Welded impact resistant steel – Length	27'-6"	(8.38 m)
Width	12'-1"	(3.68 m)

CRAWLER MOUNTING

Overall width 125" (317.5 cm) treads (Std.)	41'-9"	(12.73 m)
Overall length of mounting	37'-6"	(11.43 m)

	Sq.Ft.	(m²)	Psi	(kpa)
Tot. effective bearing area (125" treads)	615	(57.13)	33.5	(231)
optional (140" treads)	689	(63.99)	30.1	(208)

No. and diameter of rollers – Lower	16 – 30.7"	(78.0 cm)
Lower rear	2 – 42"	(106.7 cm)
Upper	Slides	
Take-up tumblers diameter	63.8"	(162.00 cm)
Number and pitch of treads	94 – 20"	(50.8 cm)

Bucyrus International, Inc.

For more information, contact your local Bucyrus sales representative
or our corporate office located at:
1100 Milwaukee Avenue • P.O. Box 500 • South Milwaukee, WI 53172-0500 • 414.768.4000 • FAX 414.768-.4474 • An ISO 9001:2000 registered firm.
Visit us on the web at: www.bucyrus.com or e-mail: inquiry@bucyrus.com.

Bucyrus International, Inc. reserves the right to make changes in specifications or design which in its opinion are an improvement or are necessary because of unavailability of materials, without incurring any liability to make such changes on machines previously built. The description herein is for the purpose of identifying the type of machine only, and does not constitute an express warranty with regard to the machine or any aspect of it and does not limit or extend the express provisions in any contract of sale.

495HF

with Rope Crowd Shovel Specifications

Shovel – Standard Range – High Flotation **Lit 448**

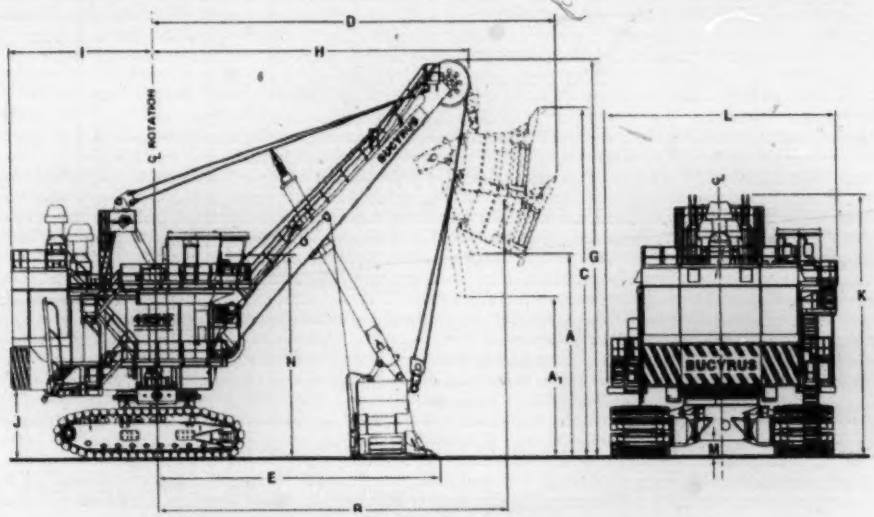

Dimensions, Working Ranges & Weight

Dipper Payload - tons nominal	110	(100 tonnes)	
[Available dipper payloads up to 120 tons (109 tonnes)* when specified]			
Dipper Capacity - yds³	40 - 80	(30.6 - 61.2 m³)	
Length of Boom	67'-0"	(20.4 m)	
Effective Length of Dipper Handle	35'-10"	(10.9 m)	
Overall Length of Dipper Handle	47'-0"	(14.3 m)	
OPTIMAL WORKING RANGES			
A Dumping Height	33'-0"	(10.05 m)	A
A_1 Dumping Height @ Maximum Radius	28'-3"	(8.61 m)	A_1
B Dumping Radius – Maximum	71'-0"	(21.64 m)	B
C Cutting Height – Maximum	59'-2"	(18.02 m)	C
D Cutting Radius – Maximum	82'-0"	(25.00 m)	D
E Radius of Level Floor	52'-11"	(16.11 m)	E
G Clearance Height – Boom Point Sheaves	68'-0"	(20.72 m)	G
H Clearance Radius – Boom Point Sheaves	64'-9"	(19.74 m)	H
I Clearance Radius – Revolving Frame	29'-11"	(9.12 m)	I
J Clearance Under Frame – to Ground	11'-11"	(3.63 m)	J
K Height of A-Frame	45'-7"	(13.89 m)	K
L Overall Width	42'-8"	(13.01 m)	L
M Clearance Under Lowest Point in Truck Frame/Propel Case	2'-8.5"	(0.82 m)	M
N Operator's Eye Level	30'-0"	(9.14 m)	N

Figure 50: 495HF Bucyrus Electric Shovel Dimensions

The Bucyrus-Erie design incorporates twin two par hoist ropes reeved through padlock sheaves that connect to the dipper sides. This gives maximum spacing between connections. Again when torsional forces are encountered, the natural stretching characteristics of the hoist wire ropes can absorb and reduce the torsional stresses. Figure 52 compares the torsion absorption offered by the Bucyrus-Errie design tubular dipper handle with that of the rack and pinion. A new feature to further assist has been the introduction of rotating or self-aligning bearing where the padlock sheaves connect to the dipper.

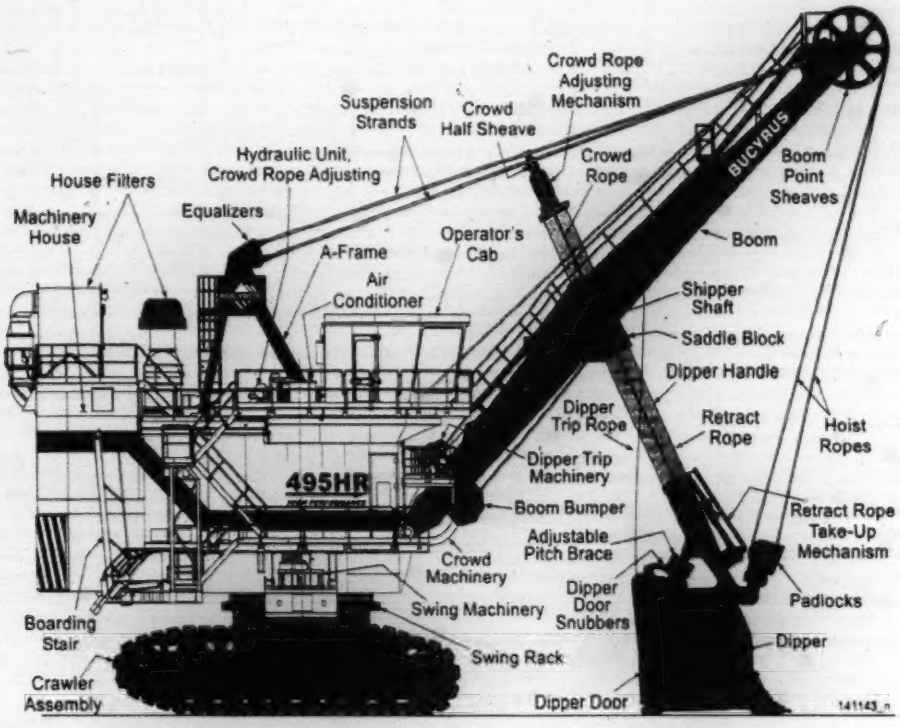

Figure 51: Schematic Bucyrus 495HR Parts Names

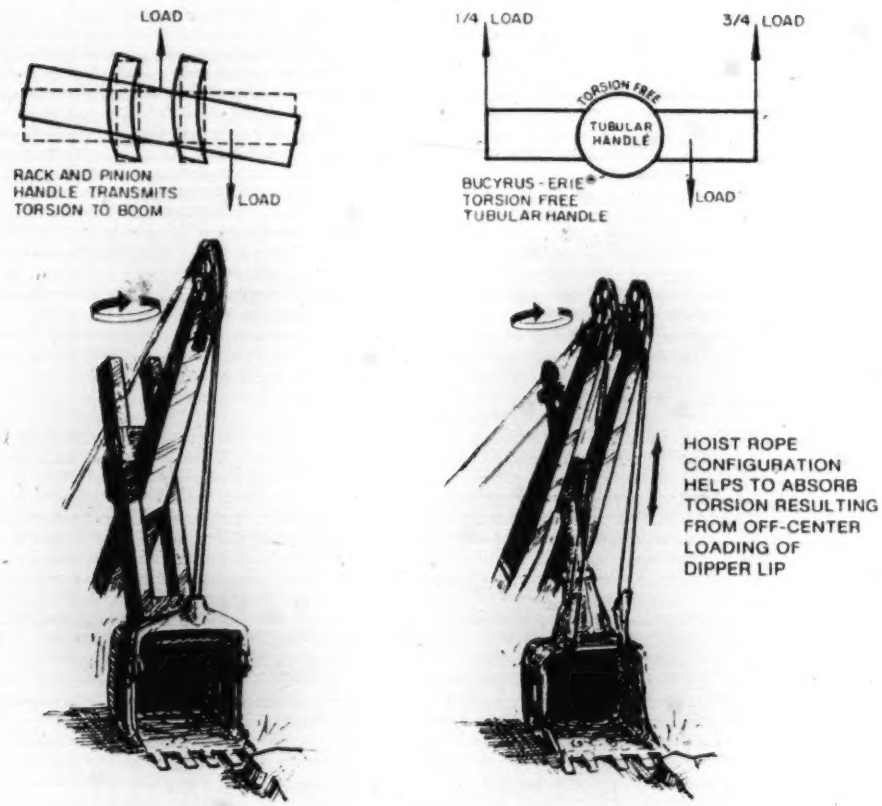

Figure 52: Tubular Dipper Handle Design Versus Rack& Pinion

In contrast, the rack and pinion (Figure 52), twin legged dipper handle design cannot rotate and consequently a heavier construction is required. In addition, the hoist ropes are centrally attached to the dipper with a bail bar. Commonly the crowd machinery for the rack and pinion system is mounted on the boom, which adds additional physical weight. There is also the additional weight required to reinforce the boom to resist stresses resulting during the crowd motion. All these factors give the Bucyrus-Erie shovel considerably less front-end weight, which translates into higher swing speed and higher production capability.

Appendix C: Soil Physical-Physicomechanical Properties

Porosity, which is in turn related to the number of pores, occupied by water and air can be described as percentage of the total volume of soil as shown in Equation 9.

Equation 9: Porosity Calculation

$$n = \left[1 - \frac{\gamma_g}{\Delta(1+0.01\omega)}\right] * 100 = \frac{\varepsilon}{1+\varepsilon} * 100\%$$

Where: Δ is the specific gravity of soil particles, g/cm^3:

$\Delta = \frac{weight\_of\_solid}{Volume\_of\_liquid}$ and Δ varies from 2.4 to 2.8 t/m3.

in Iron Δ is about 4 t/m^3 and in organics is about 1.2 to 1.4 t/m^3.

γ_g is the specific weight of wet soil, g/cm^3. γ_g is the ratio of the soil weight with natural moisture content g_0 to its volume V:

$\gamma_g = \frac{g_0}{V}$ and γ_g varies between 1.5 – 2.0 t/m^3.

ω is the moisture content by weight %;

ε is the coefficient of porosity. ε is the ratio of the volume of pores occupied by water and air to the volume of solid particles of the soil:

$$\varepsilon = \frac{n}{100-n} = \frac{\Delta(1+0.01\omega)}{\gamma_g} - 1$$

Moisture by weight is the ratio of the water g2 to the weight of dry soil g1:

$$\omega = \frac{g_2}{g_1} * 100\%$$

If not more than 1/3 of soil is saturated with water then that type of soil can be named a "dry soil". In turn it can be added that a soil between 1/3 to 2/3 of filled pores by water a "moist soil", and finally for amounts higher than 2/3 of pores become filled of water it is called "wet".

The specific weight of dry soil is given by:

$$\delta_0 = \frac{\gamma}{1 + \frac{\omega}{100}}$$

It is important to know the amount of the γ_g since it has effect on the energy expended in lifting and transporting soil while knowledge of δ_0 helps on determination of the degree of compaction of soil. The optimum moisture (ω_{opt}) is the moisture for which the maximum soil density can be achieved with minimum mechanical work. Plasticity of soil is the property of soil is its deformation under the external force(s) with holding its volume.

The force to cut the soil to overcome to the soil cohesion is determined by following equation:

P1=p1*F kgf

Where p1 is the specific cohesion (for clay p1=700-800 kg/m^2 and for loam p1=500-700 kg/m^2);

F is the area of contact surface between the cutting element of the machine and the soil, m2.

The specific weight of the soil decreases when it is loosened. This loosening is described by the coefficient of loosening k_r that varies between 1.08 and 1.32.

In design of the earthmoving machines the shear strength of soil plays the fundamental role which is derived by the coefficient of internal friction of soil $\mu_2 = \tan\varphi_2$ and the coefficient of cohesion of soil C, which in turn determines the resistance of a soil to shear stresses. C is totally dependent upon the soil moisture

content, particle size, and density. The Equation 10 is the basic determination of shear strength in soil.

Equation 10: Coulomb's Law

$$\tau = \sigma \tan \varphi_2 + C = \sigma * \mu_2 + C$$

Where τ is the shear strength of soils;

μ_2 is the coefficient of internal friction;

C is the cohesion coefficient of soil in shear, kg/cm^2. for dry soil, C=0;

σ is normal stress, kg/cm^2;

φ_2 is the angle of internal friction;

As shown in ,an increase in moisture by more than 10 to 12% lead to a sharp decrease in the angle of internal friction. Soil cohesion, for a given moisture content, increases with density and for a given density, falls with an increase in moisture content.

The angle of internal friction depends on moisture content and while the latter increases it will be decreased. As shown in Figure 53 –a by an increase in moisture more than 10% the internal friction drops rapidly. And as it shown in Figure 53 – b, soil cohesion under given moisture content, enhances with density and for a specific density being reduced with increase in moisture content. In this graph the values of moisture content varies and hence the cohesion factor: 1-- ω=8.9%; 2-- ω=13.7%; 3-- ω=15.9%; 4-- ω=19.2%; 5-- ω=25.8%.

Another term for soil property is the angle of natural repose (φ_0) that being used in the civil industry a lot. This is when we measure the vertex angle of the shaped cone by dumping the material. Or after the face of open cut opposed to the air during the course of time the face sloughs and come to the state of stability in an optimum angle of repose and after that point of time has minimal deformation at the face angle. Knowledge of the angle of repose plays major role in mining operations. The angle of repose depends on the condition of the soil as well as its

moisture content and its function of the angle of internal friction (φ_2) and cohesion coefficient (C).

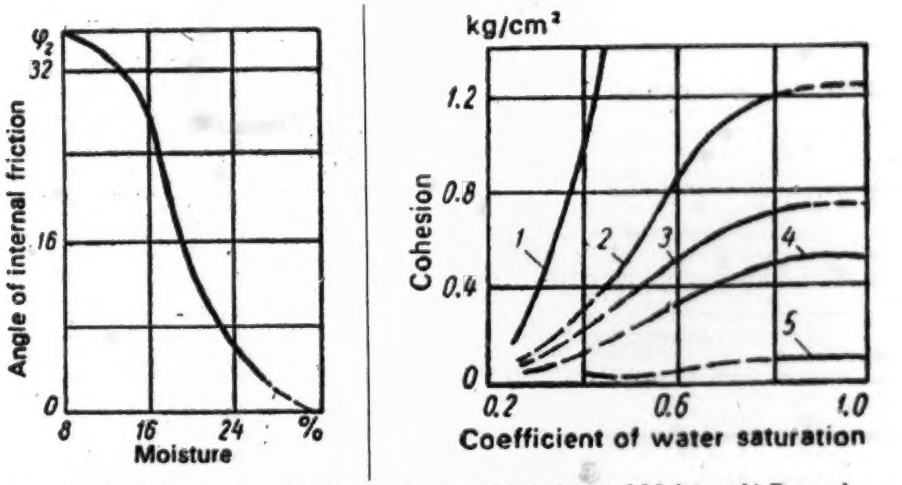

a) b)

Figure 53: a) Relation Between Angle of Internal Friction and Moisture b) Dependence of Cohesion on Coefficient of Saturation by Water (degree of compaction) and moisture

A soil particle is in equilibrium at the angle of repose if:

$$G_P \sin\varphi_0 \le \mu_2 G_P \cos\varphi_0 + CF;$$

Where G_p is the weight of the soil particle, kg/cm^2;

F is the surface area of contact with the plane of repose, cm^2.

It is obvious that the stability of repose in deprive of cohesion (C) is ensured while:

$$\mu_2 = \tan\varphi_2 \ge \tan\varphi_0$$

In the field, another coefficient, which is called coefficient of friction of soil with steel (μ_1), and mainly ups to condition and type of soil in contact with surface of steel and also depend on the manner of the surface of steel whether rough or smooth. μ_1 been determined values in the reference book by Alekseeva et al. of 0.25 to 1. This value increases when the surface of steel gets rougher and has increased in moisture content of soil. The μ_1 for broken soil structure is about 2/3

of the value of μ_1 when the soil has uniform structure. As said, moisture content has a major role in the magnitude of the μ_1 and can be expressed as the following equation introduced in the reference book by Alekseeva et al.:

$$\mu_1 = f_0 \frac{\ln \omega}{A}$$

where f_0 and A are constants: for loam, f_0=1.01, A=4.08; for clay f_0=0.95, A=5.33. and finally one can mention the correlation between the μ_1 and μ_2:

$$\mu_1 \approx 0.75\mu_2$$

Another important term is the modulus of deformation of soil (E) that usually determined from the soil resistance to compaction curve by a cylindrical ram:

Equation 11: Modulus of Deformation of Soil

$$E = \alpha \frac{\sigma D}{\lambda}$$

Where α is correction factor (usually equals to 1.25);

σ is the stress along the soil surface under the ram, kg/ cm^2 ;

D is the diameter of the ram, cm;

λ is settlement, cm.

Different values for E are given in Table 7 depend on the soil type.

TABLE 7: VALUES OF E FOR DIFFERENT SOILS

Soil Type	E, kg/ cm^2
Coarse Grained Sand	350 – 450
Medium Grained Sand	250 – 400
Fine Grained Sand	150 – 350
Very Fine Sand, Sandy Loam and Optimal Mixture	115 – 260

Silty Sand, Fine Non-Silty Sandy Loam	75 – 220
Loam, Heavy Loam, Light Clay and Heavy Clay	70 – 220
Silty Soils, Silty Sandy Loam, Loess	60 – 190

Temperature has a big affect on the elasticity of the soil as in negative temperatures the frost acts as cement in between the particles of the soil. In Table 8 shown the correlation in between the temperature, moisture content and shear strength of the frozen soils. The deformation on the frozen soil can be determined by the amount and magnitude of the external load and by the physical condition of the soil. Once the stress applies into the frozen soil, deformation can be occurred in either state of elastic or plastic. Elastic deformation on the frozen soil is expressed by the Poison's ratio and modulus of elasticity already discussed in this chapter. According to Alekseeva et al. the modulus of elasticity has direct relation to the size of particles (i.e. bigger size cause increase in E) and opposite relation to temperature. It means a frozen lump soil has higher E factor compare to its original state in plus temperatures. The abrasion strength or resistance to wear and tear of frozen soil is 70-200 times greater than that of unfrozen soil.

TABLE 8: TRANSIENT SHEAR STRENGTH OF FROZEN SOILS

Temperature, °C	Moisture by Weight, %	Transient Shear Strength, kg/cm^2
Clay Group		
-3	49.8	20.9
-6.3	42.0	28.5
-8.8	45.9	33.5
Loam Group		
-3	16.9	24.8
-6.7	19	44.2
-9.3	19	48.5

TABLE 9: ANGLE OF REPOSE FOR T = - 10 °C

Soil Type	Angle of Repose Soil-Soil, φ_2	Angle of Repose Soil-Metal, φ_1
Sand	24.0	25.5
Sandy Loam	26.5	26.0
Loam	30.0	28.0
Clay	31.0	32.0

In conclusion to this session, I found advantageous to bring in the table of angle of repose in different soils introduced by Alekseeva et al. as shown in Table 9. Plastic deformation can be found in clayey type soils with maximum amount of plastic deformation.

TABLE 10: VALUES OF ANGLES OF INTERNAL FRICTION φ_2

Soil Type	ω, %	Temperature (t), °C			
		-1	-10	-17	-40
Sand	15	26.5	24.0	24.0	22.0
Sandy Loam	21	27.0	26.5	22.0	17.0
Loam	25	33.0	30.0	29.0	29.0
Clay	33	32.0	31.5	30.5	31.0

Classifications of Soils

The strength of soil relates to its composition. It means that it relies mostly on its particle size as well as the moisture content as is shown in Table 10 and Table 11. As part of sandy soils characteristics one can be mentioned of having high coefficient of internal friction. It is also can be added the high permeability, incompressibility, no cement in between particles, have small capillary rise, are non plastic, and experience marginal decrease in resistance to load with increased moisture content. One of its features is difficulty of movement of the machines in

loose sand. Sandy silty soils are also deprive of cement in between the particles, non plastic and permeable to water. The unique feature of this type of soil is that it can be broken up and loose its load-bearing capacity if it carry a moisture content. The sandy loam type soil, carry small amount of clayey material in it that acts as cement and help the soil particles to bond together. While there is an increase in moisture content this type of soil resists against deformation compare to a more clayey type soil. Fine sandy loam type soil, holds a large amount of silt in between the particles that cause a weakness point in this type of soil when it been hit by moisture and becomes less stable and deform easily. Silty soils are prone to swelling when the moisture content increases and easily can be washed out by water streams. This type of soil has less resistance to loads when the moisture applies. Loamy soil is in plastic form and has high cohesive strength while is dry. But once the moisture applies it strength drops rapidly. Heavy loam soil is highly cohesive, has high plasticity and compressibility and low permeability to water. Clayey soil also has high cohesive strength, density and plasticity.

TABLE 11: CLASSIFICATION OF SOILS FOR ROADS

Type of Soil	Content of Fractions, wt%		
	Sand with particle Φ 2.0-0.05 mm	Silt with particle Φ 0.05-0.005 mm	Clay with particle Φ > 0.005 mm
Sandy soil	---	<15	<3
Sandy silty soil	---	15-20	<3
Sandy loam	> 50% (particles of Φ 2.0-0.25 mm)	Less than sandy soil	3-12
Fine sandy loam	< 50% (particles of Φ 2.0-0.25 mm)	Less than sandy soil	3-12
Silty soil	---	More than sandy soil	<12
Loamy soil	More than silty soil	---	12-18
Heavy loam soil	More than silty soil	---	18-25
Silty loam soil	---	More than sandy soil	12-25
Clayey soil	---	---	> 25

Physical Properties of Soil

It is tried to introduce several important properties of soils in appreciation of relationship between the soil and steel when the dipper digs into the soil. Depend upon the soil type, moisture content, temperature, compaction rate, angle of repose, angle of internal friction all these play major role in determination of the cutting resistance forces that eventually drive the cutting force to be produced by the shovel AC motors. However, the geometry and design of shovel parts also can lead to better penetration in conjunction to the soil state (i.e. temperature, frost in frozen soil acts as a strong cement and in turn the machine need more breaking force). By looking at the real data collected from field of shovel operation, it is clearly understandable that how the frost can act as resistive force against the breaking force of the machine. That is why having proper knowledge of the soil type and state of the mine pit area helps the shovel operator better handle the machine control. For instance, if he is digging in an area with deep frost, by application of too much force on crowd hoping fracture the lumps sometimes does not work the way we expect and cause the trapping the dipper and increased cycle time. Some times we need ripping tool (e.g. big dozers like D8-9-10 or smaller hoes by installing ripper shank on them) rip the frost on advancing faces or even by blasting some hard frozen faces we can increase the productivity on the machine drastically.

Working Parts of Shovel and Its Interaction with Soil

In a shovel in order to facilitate the penetration into soil, design engineers designated the teeth on the bucket to separate and collect the soil. For the tooth the following angles will be used for dipper calculations as well as force vectors at tooth. Cutting angle δ, lip angle β, back angle α as part of the machine geometry are such angles being used in cutting force calculations. As mentioned in section 3.2 the behaviour of soil in response to the cutting tool like dipper depends on different factors like moisture content and basically properties of the media (soil) as well as the digging tool geometry and design. In Figure 54 shown the variations of chip soil when a wedge penetrate into face and depend upon the

above mentioned factors, the manner of the chipped cut would be totally not identical in each case.

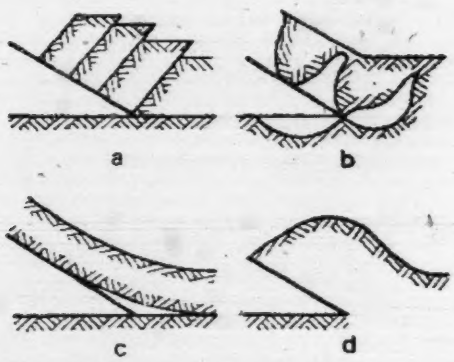

a—Soil of average moisture and cohesion; b—Dry cohesive soil;
c—Viscous and moist soil; d—Dense soil.

Figure 54: Deformation of Soil Under Action of Wedge

Before to move on and continue the discussion, it is matter of better understanding in this report on different angles been used to calculate the cutting force. Hence, as shown in Figure 55, these angles of interaction between the tooth and soil that considered the same in most of the reference books and reports, illustrated in favour of this research study. In this picture, the angle of α is the back angle of cutting, β is the tooth lip angle, and δ is the minimum cutting angle. Also a is the width of the tooth, h is thickness of the chip of the soil, Pp is the soil's resistance to cutting, and Pn is the resistance to movement of the prism of soil, and soil movement in the bucket.

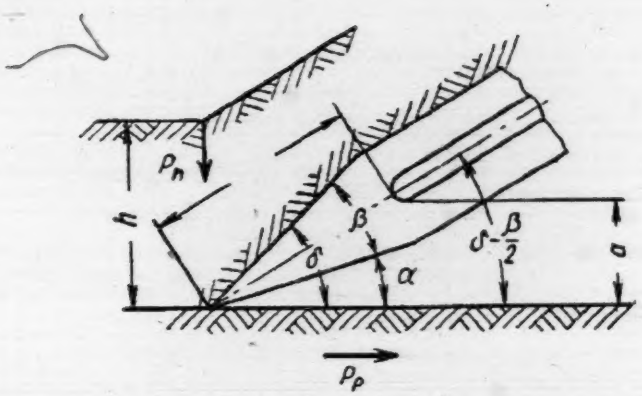

Figure 55: Determination of Tooth Parameters

It is mentioned by Alekseeva et al. that the theories of cutting of soils can be divided to two categories:

Theories based on the experimental results data.

Theories based on fundamental principles of continuum mechanics and the strength of materials.

Theories of Cutting of Soils Based on Experimental Studies

Based on the introduced equations and experimental results by Alekseeva et al., having the teeth in rectangular buckets of 0.6-0.75 m wide gives a 25% reduction in cutting resistance; however, by increasing the length of cutting edge the effect of blades would increase. Therefore, for large buckets with capacities more than 5 m3 (horizontal cutting edge greater than 1.8m) teeth are not very effective. That is why designers will never bring the teeth on the cutting edge of the buckets. The back angle of cutting α should not be less than 5 to 7 degrees otherwise; soil reaction in terms of resistance to cutting can be escalated by 10%. The tooth lip angle β usually is manufactured as equal to 25° for the strength point of view. Therefore, the minimum cutting angle of δ can be somewhere between 30 to 32 degrees. The current teeth installed on the buckets give a cutting angle of 25 to 55 degrees. As Alekseeva et al. mention, the soil cutting resistance develops by 1.5%

for each degree of increase in cutting angle. As a wrap up to this section, as the result of the experimental studies on collected data mentioned by Alekseeva et al., the factors affect the cutting process can be deemed the following items:

Dimensions of the cut including width and thickness

The extent of interaction between the soil and digging tool

Wear and tear of the cutting edge

Cutting angles which is the angle between the trajectory and leading edge of the cutting wedge

The wear and tear on the cutting device causes the increase in cutting resistance. In buckets with continuous edge, allowable tear and wear can easily cause an increase of about 90-200% in cutting resistance. The same problem can cause an increase of 60 to 100 percent in cutting resistance in excavators' bucket with teeth.

When the depth of the cut (thickness of slit) increases with the presence of areas with the wear and tear, additional cutting resistance occur. As shown in Figure 56 the resistance force varies depend upon the depth of cut and never meet the zero point while the cutting depth is at zero. Also better not to neglect the effect of the cutting angle as already discussed about it. By increasing this angle to 40° to 60° it will double up the cutting resistance in front of the cutter.

Also as mentioned earlier in this chapter, very small cutting angle dose not work in or favour either and can cause increase in soil resistance to the cutting force specially when the direction of the dig is against the bedding (stratification). Hence, as recommended by Alekseeva et al., the optimum cutting angle can be deemed in the range of 30° to 40°.

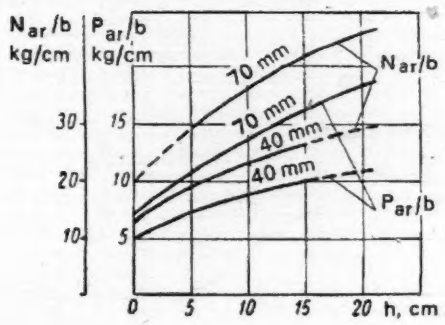

Figure 56: Additional Resistance to Cutting as Function of Area of Blunting at Different Cutting Depth

Theories of Soil Cutting Based on the Concept of Limiting Equilibrium of a Loose Medium

What is given in previous section is based on experimental data. In this section it is tried to develop equations based on the interaction between the soil and the digging device like shovel. As the geometrical dimensions of the digging tool is a know parameter to us we can then measure the resistive forces against the generated cutting force by the machine. Also having the knowledge of soil properties such as internal angle of friction, soil density and coefficient of cohesion are necessary to establish a comprehensive formula to describe the nature of forces during the cut function. There is always two force vectors for the cutting resistance at the tip of the digging device like bucket tooth. Normal (vertical) and tangential (horizontal) components of this force that in this section it is tried to simply show how to measure them.

Digging of Soil by Excavators

Based on the theoretical analysis the cutting resistance is composed of two vectors, tangential resistance to the digging and normal resistance in the soil. In the reference book by Alekseeva et al., it is mentioned that the tangential resistance is derived of three forces:

Equation 12: Tangential Resistance Force

$$P_{01} = P_p + P_m + P_n$$

Where P_0 is the resistance force to digging (Figure 57);

Pp is the soil's resistance to cutting;

Pm is the resistance of the working tool with the ground;

Pn is the resistance to movement of the prism of soil, and soil movement in the bucket

Equation 12 can also shown in more detail as follows:

Equation 13: Detailed Form of Tangential Equation

$$P_{01} = kbh + \mu_1 N_1 + \varepsilon(1 + q_{np})qk_n$$

Where k is the specific resistance to cutting, kg/cm^2;

B and h are the width and thickness of the dug soil, cm;

μ_1 is the coefficient of friction of the bucket with the ground, kg;

N_1 is the pressure of the bucket on the soil, kg;

Q_{np} is the volume of the prism of soil expressed as a fraction of the volume of the bucket, q;

ε is the coefficient of resistance to filling of the bucket and movement of the prism of soil;

k_n is the coefficient of filling of the bucket – ratio of the volume of dug soil in the bucket to the geometric volume of the bucket.

Equation 13, Alekseeva et al., can be addressed in the following form :

Equation 14: Summarized Form of Tangential Equation

$$P_{01} = k_1 bh = k_1 F$$

Where k_1 is the specific digging force, which includes not only frictional cutting resistance but also all other resistive forces like friction of the bucket at the rear, soil resistance when moving in the bucket. This parameter is an experimental value need to be taken from Table 12.

In Table 12 if the ratio of chip thickness (h) over width (b) rest between 0.05 - 0.5 then the values for k_1 would increase by 20-25%.

As shown in Figure 57, the digging resistance force (P_0) happens at a different angle from what we saw for the tangential resistance force; thus, the best is measure the normal component of the P_0, P_{o2} from which can be calculated as follows:

Equation 15: Digging Resistance Normal Component

$$P_{02} = \psi P_{01}$$

Where ψ is the function of digging and feeding as well as the digging angle and the wear and tear of the cutting edge. For excavators under usual conditions the ψ varies from 0.1 to 0.45. we should apply the bigger corresponding coefficient (close to 0.45) when digging on going with thinner soil chips or under steep digging angle or worn and torn cutting edge.

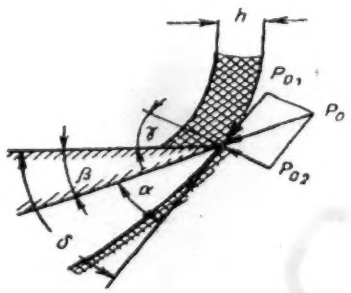

Figure 57: Digging Resistance Force Vectors

Alekseeva et al. suggest that applying sharp teeth on an excavator rectangular cutting edge with a minimum cutting angle of δ=25°-55°, this makes the cutting

resistance to be reduced by 10-25% while the digging resistance drops by 6-15%. This would lead to have also less wear and tear on bucket wall due to improved concentration of forces at the teeth into the soil. However, installing the teeth on the semicircular cutting edge would increase the digging resistance. Based on Figure 55 the following equation can be used for selecting the bucket tooth. This is while a should be less than 40-50% of h.

Equation 16: Normal Tooth Length

$$l_t = \frac{a}{\sin(\frac{\beta}{2} + \alpha)}$$

TABLE 12: SPECIFIC RESISTANCE TO CUTTING, K, AND DIGGING, K_1 FOR EXCAVATOR

Soil Category	Soil Type	K, kg/cm^2	k_1, kg/ cm^2						A	A_1
			Excavators, Single Bucket			Excavators, Multi-buckets				
			Shovel	Dragline	Scraper Loader	Chain Transverse Digging	Rotor	Trencher		
I	Sand, Sandy Loam	0.1-0.55	0.16-0.8	0.3-0.8	0.4-1.3	0.5-1.8	0.4-1.3	0.7-0.23	5	1.1
II	Loam without Inclusions	0.57-1.1	0.7-1.6	1.2-2.0	1.4-2.0	1.5-3.0	1.2-2.5	2.1-4.0	10	2.8
III	Compact Loam, Medium Clay	1.1-1.7	1.2-2.5	1.6-3.0	1.8-3.2	2.4-4.5	2.0-3.5	3.8-6.0	16	3.6
IV	Hard Loam with Rubber or Pebbles, Hard Clay and Very Hard and Wet Clay	1.6-2.4	2.2-3.6	2.5-4.2	2.7-4.5	3.7-6.0	3.0-4.5	5.5-8.0	26	4.5

Effect of Speed of Movement of the Digging Tool

Experimentally it is learned that the speed of cutting tool at higher velocities could cause increase in digging resistance. One of the reasons can be some of the energy requires to be expend on throwing the cut soil away from front of the digging tool. Also with a fast cutting, the loosed material fall behind the applied load on the cutter; hence, we cannot expect the magnitude of the deformation we expect from the dig/cut operation. As per Alekseeva et al. citation from others, developing the speed from 1.0 to 7.0 m/sec for δ=40° leads to escalation in cutting resistance by 28%. The related increase for δ=55° is 78%. When the δ=22-35° with a logical cutting edge shape on the bucket, as long as we keep the cutting speed around 5-6 m/s, the cutting resistance will not exceed 10-15%.

Appendix D: Dynamics Behaviour of Cable Shovel

Figure 58 is schematic of the free-body of the dipper handle and illustration of existing force vectors of hoist and crowd versus the resistance force components. It is tried to analyse these force vectors on Cartesian coordinate system. The following nomenclature is what is being used in this figure:

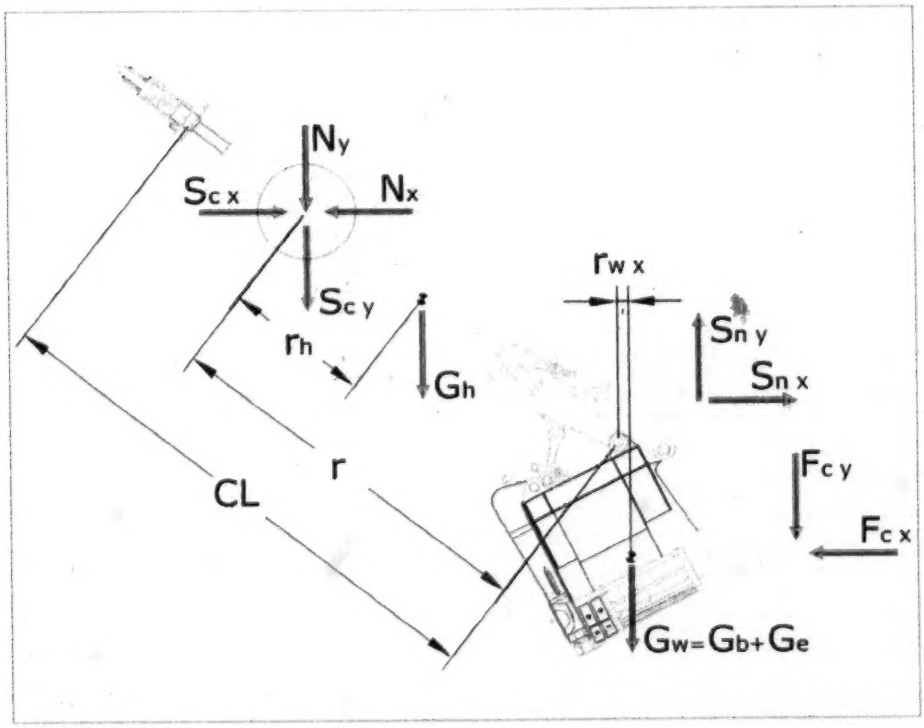

Figure 58: Crowd Free Body Diagram and Bucket Assembly (Awuah-Offei, K., 2004)

Sc x is the x-component of crowd force;

Sc y is the y-component of crowd force;

Sn x is the x-component of hoist force;

Sn y is the y-component of hoist force;

Fc x is the x-component of resistance force;

Fc y is the y-component of resistance force;

Nx is the x-component of normal reaction force on the shipper shaft;

Ny is the y-component of normal reaction force on the shipper shaft;

Gh is the centroid of weight of the handle;

Gw is the centroid of weight of the dirt in bucket plus the dipper.

With respect to introduced angles of hoist and crowd in Figure 13 of chapter 3.3, and application of those angles into Figure 58, the upcoming dynamic equations based on Newton laws can be determined for the crowd and bucket of a cable shovel:

Equation 17: Summation of Forces in X-Y Directions

$$\sum F_X = M * A_{CX}$$
$$\sum F_Y = M * A_{CY}$$

Equation 18: Result of Momens Around Centre of Mass of Handle

$$\sum M = I * \alpha$$

Equation 19: Correlation of Force X-Y Components

$$\frac{Sc_Y}{Sc_X} = Tan(2\pi - \theta_4)$$
$$\frac{Sn_Y}{Sn_X} = Tan\theta_3$$
$$\frac{N_Y}{N_X} = Tan(\theta_4 - \frac{3\pi}{2})$$

And prior to develop the combined dynamic model equations, there is one more to show to describe the acceleration of centre of mass in Equation 17 which being derived by differentiation of the position vector of the centre of the mass as follows (Awuah-Offei, K., 2004):

Equation 20: Position Vector of Centre of Mass of the Handle

$$R_h = (r_h Cos\theta_4)i + (r_h Sin\theta_4)j$$

And:

Equation 21: Acceleration Characteristics of the Crowd Arm

$$A_{CX} = -r_h\omega^2 c - 2\dot{r}\,\omega s + \ddot{r}\,c - (r_h s)\alpha$$
$$A_{CY} = -r_h\omega^2 s + 2\dot{r}\,\omega c + \ddot{r}\,s - (r_h c)\alpha$$

And to result the combined dynamic model of the cable shovel forces system, we need to introduce the system of Differential-Algebraic Equations (DAE) (Awuah-Offei, K., 2004 referenced to Haug,1992) in here: $\Omega x = b$ Where:

$$\Omega = \begin{bmatrix}
-M_4 & 0 & 0 & 0 & 1 & 0 & 1 & 0 & -1 & 0 \\
0 & -M_4 & 0 & 0 & 0 & -1 & 0 & 1 & 0 & -1 \\
0 & 0 & 0 & -I & -r_h|s_4| & r_h c_4 & (r_4 - r_h)|s_4| & (r_4 - r_h)c_4 & r_h|s_4| & r_h c_4 \\
0 & 0 & 0 & 0 & Tan(2\pi - \theta_4) & -1 & 0 & 0 & 0 & 0 \\
0 & 0 & 0 & 0 & 0 & 0 & t_{Sn} & -1 & 0 & 0 \\
1 & 0 & 0 & r_h s_4 & 0 & 0 & 0 & 0 & 0 & 0 \\
0 & 1 & 0 & -r_h c_4 & 0 & 0 & 0 & 0 & 0 & 0 \\
0 & 0 & (r_3 s_3 - r_2 s_2) & r_4 s_4 & 0 & 0 & 0 & 0 & 0 & 0 \\
0 & 0 & (r_3 c_3 - r_2 c_2) & r_4 c_4 & 0 & 0 & 0 & 0 & 0 & 0 \\
0 & 0 & 0 & 0 & 0 & 0 & 0 & 0 & Tan(\theta_4 - 1.5\pi) & -1
\end{bmatrix}$$

$$x = \begin{bmatrix} A_{C4X} & A_{C4Y} & \alpha_3 & \alpha_4 & Scx & Scy & Snx & Sny & Nx & Ny \end{bmatrix}^T$$

$$b=\begin{bmatrix} F_{CX} \\ F_{CY}+W \\ W((r_4-r_{C2})c_4+P_{WX})+F_{CY}(r_4-r_{C2}+BSL)c_4+F_{cx}(r_4-r_{C2}+BSL)|s_4| \\ 0 \\ 0 \\ -r_h c_4\omega_4^2-2\omega_4\dot{r}s_4+\ddot{r}c_4 \\ -r_h s_4\omega_4^2-2\omega_4\dot{r}c_4+\ddot{r}s_4 \\ (c_2r_2\omega_3-c_3r_3\omega_3-2s_3\dot{r}_3)\omega_3-(c_4r_4\omega_4+2s_4\dot{r}_4)\omega_4+c_3\ddot{r}_3+c_4\ddot{r}_4 \\ (s_3r_3\omega_3-s_2r_2\omega_3-2c_3\dot{r}_3)\omega_3-(s_4r_4\omega_4+2c_4\dot{r}_4)\omega_4+s_3\ddot{r}_3+s_4\ddot{r}_4 \\ 0 \end{bmatrix}$$

Another set of equations for the cable shovel kinematics and dynamics are brought in here for referencing to the text (Frimpong S. et al., 2005). To develop these following equations, Equation 14 considered as schematics of the crowd handle-boom motion parts. Furthermore, Newton-Euler method is applied (Frimpong S. et al., 2005) to evaluate the kinematics and dynamics of the cable shovel as well as computing the crowd force and hoist torque. This method embraces with accounting the velocities and accelerations on one hand and forces and torques on the other hand. In introducing the following equations the related nomenclature is showed as follows:

$0\omega_0$ is the angular velocity and $0\dot{\omega}_0=\dfrac{d^0\omega_0}{d_t}$ angular acceleration of the boom;

$i\omega_i$ is the angular velocity and $i\dot{\omega}_i$ angular acceleration of the gravity centre (i=1 is crowd arm; i=2 is dipper);

$1\dot{\omega}_1$ is the angular moment of the crowd arm;

$1\dot{v}_{C1}$ is linear acceleration at the gravity centre of the crowd arm;

$\dot{0v_0} = g\hat{y}_0$ is the gravity effect;

$\dot{iv_i}$ is the linear acceleration at the connection point (i=1 is crowd arm; i=2 is dipper);

iN_i is torque at the gravity centre (i=1 is crowd arm; i=2 is dipper);

iFi is the inertial for at the gravity centre (i=1 is crowd arm; i=2 is dipper);

${}^1_0R$ is the transformation matrix from base frame to the crowd arm coordinates;

${}^2_1R$ is the transformation matrix from crowd arm coordinates to the dipper based coordinate;

${}^3_2R$ is the transformation matrix from dipper to the dipper tip based coordinate;

$\dot{\theta}$ is the rotation angular velocity of the crowd arm base coordinate relative to the base frame;

$\ddot{\theta}$ is the rotation angular acceleration of the crowd arm based coordinate relative to the base frame;

$0P_1$ is the position vector to locate the rotation point of the crowd arm;

$1P_{C1}$ is the position vector to locate the centre of the mass of the crowd arm;

$\dot{d}_i$ is the linear velocity and $\ddot{di}$ is the linear acceleration (i=1 is crowd arm; i=2 is dipper);

$\hat{X}_i, \hat{Y}_i, \hat{Z}_i$ (i=1,2) are displacement vectors along the i_{th} 3D Cartesian coordinate system;

if_i is inward iteration force (i=1 is crowd arm; i=2 is dipper);

in_i is torque balance (i=1 is crowd arm; i=2 is dipper);

f_{31}, f_{32} are respective x and y components of the interaction force between soil

and dipper tip;

Ii is moment of inertia of link I about centeroidal axis parallel to Zi-axis;

Since the boom is a fixed structure with no rotation; hence:

$$0\omega_0 = \begin{bmatrix} 0 \\ 0 \\ 0 \end{bmatrix},\ 0\dot{\omega}_0 = \frac{d^0\omega_0}{d_t} = \begin{bmatrix} 0 \\ 0 \\ 0 \end{bmatrix}$$

With regards to dynamics of the crowd arm:

$$1\omega_1 = {}^1_0R\,{}^0\omega_0 + \dot{\theta}_1\,1\hat{Z}_1 = \begin{pmatrix} c1 & s1 & 0 \\ -s1 & c1 & 0 \\ 0 & 0 & 1 \end{pmatrix}\begin{pmatrix} 0 \\ 0 \\ 0 \end{pmatrix} + \begin{pmatrix} 0 \\ 0 \\ \dot{\theta}_1 \end{pmatrix} = \begin{pmatrix} 0 \\ 0 \\ \dot{\theta}_1 \end{pmatrix}$$

$$1\dot{\omega}_1 = {}^1_0R\,{}^0\dot{\omega}_0 + \ddot{\theta}_1\,1\hat{Z}_1 + {}^1_0R\,{}^0\omega_0 \times \dot{\theta}_1\,1\hat{Z}_1 = \begin{pmatrix} c1 & s1 & 0 \\ -s1 & c1 & 0 \\ 0 & 0 & 1 \end{pmatrix}\begin{pmatrix} 0 \\ 0 \\ \ddot{\theta}_1 \end{pmatrix} + \begin{pmatrix} c1 & s1 & 0 \\ -s1 & c1 & 0 \\ 0 & 0 & 1 \end{pmatrix}\begin{pmatrix} 0 \\ 0 \\ \dot{\theta}_1 \end{pmatrix} \times \begin{pmatrix} 0 \\ 0 \\ \dot{\theta}_1 \end{pmatrix} = \begin{pmatrix} 0 \\ 0 \\ \ddot{\theta}_1 \end{pmatrix}$$

$$1\dot{v}_1 = {}^1_0R\left(0\dot{\omega}_0 \times 0P_1 + 0\omega_0 \times (0\omega_0 \times 0P_1) + 0\dot{v}_0\right) + 2 * 1\omega_1 \times \dot{d}_1\,1\hat{X}_1 + \ddot{d}_1\,1\hat{X}_1 = \begin{pmatrix} gs_1 + \ddot{d}_1 \\ gc_1 + 2\dot{d}_1\dot{\theta}_1 \\ 0 \end{pmatrix}$$

$$1\dot{v}_{C1} = 1\dot{\omega}_1 \times 1P_{C1} + 1\omega_1 \times (1\omega_1 \times 1P_{C1}) + 1\dot{v}_1 = \begin{pmatrix} -d_1\dot{\theta}_1^2 + \ddot{d}_1 + gs_1 \\ d_1\ddot{\theta}_1 + 2\dot{d}_1\dot{\theta}_1 + gc_1 \\ 0 \end{pmatrix}$$

$$1N_1 = c1I_1\,1\dot{\omega}_1 + 1\omega_1 \times c1I_1\,1\omega_1 = \begin{pmatrix} 0 & 0 & 0 \\ 0 & 0 & 0 \\ 0 & 0 & I_{ZZ1} \end{pmatrix}\begin{pmatrix} 0 \\ 0 \\ \ddot{\theta}_1 \end{pmatrix} + \begin{pmatrix} 0 \\ 0 \\ \dot{\theta}_1 \end{pmatrix} \times \left(\begin{pmatrix} 0 & 0 & 0 \\ 0 & 0 & 0 \\ 0 & 0 & I_{ZZ1} \end{pmatrix}\begin{pmatrix} 0 \\ 0 \\ \dot{\theta}_1 \end{pmatrix}\right) = \begin{pmatrix} 0 \\ 0 \\ I_{ZZ1}\ddot{\theta}_1 \end{pmatrix}$$

And based on the Newton's second law the crowd inertial force is:

$$1F_1 = m_1 {}^1\dot{v}_{C1} = \begin{pmatrix} -m_1 d_1 \dot{\theta}_1^2 + m_1 \ddot{d}_1 + m_1 g s_1 \\ m_1 d_1 \ddot{\theta}_1 + m_1 2\dot{d}_1 \dot{\theta}_1 + m_1 g c_1 \\ 0 \end{pmatrix}$$

With regards to the dipper dynamics also we can writ similar equations as the above:

$$2\omega_2 = {}^2_1R\,{}^1\omega_1 + \dot{\theta}_2\, 2\hat{Z}_2 = \begin{pmatrix} c2 & s2 & 0 \\ -s2 & c2 & 0 \\ 0 & 0 & 1 \end{pmatrix}\begin{pmatrix} 0 \\ 0 \\ \theta_1 \end{pmatrix} + \begin{pmatrix} 0 \\ 0 \\ 0 \end{pmatrix} = \begin{pmatrix} 0 \\ 0 \\ \dot{\theta}_1 \end{pmatrix}$$

$$2\dot{\omega}_2 = {}^2_1R\,{}^1\dot{\omega}_1 + \dot{\theta}_2\, 2\hat{Z}_2 + {}^2_1R\,{}^1\omega_1 + \ddot{\theta}_2\, 2\hat{Z}_2 = \begin{pmatrix} c2 & s2 & 0 \\ -s2 & c2 & 0 \\ 0 & 0 & 1 \end{pmatrix}\begin{pmatrix} 0 \\ 0 \\ \dot{\theta}_1 \end{pmatrix} \times \begin{pmatrix} 0 \\ 0 \\ 0 \end{pmatrix} + \begin{pmatrix} c2 & s2 & 0 \\ -s2 & c2 & 0 \\ 0 & 0 & 1 \end{pmatrix}\begin{pmatrix} 0 \\ 0 \\ \ddot{\theta}_1 \end{pmatrix} + \begin{pmatrix} 0 \\ 0 \\ 0 \end{pmatrix} = \begin{pmatrix} 0 \\ 0 \\ \ddot{\theta}_1 \end{pmatrix}$$

$$2\dot{v}_2 = {}^2_1R(1\dot{\omega}_1 \times 1P_2 + 1\omega_1 \times (1\omega_1 \times 1P_2) + 1\dot{v}_1) + 2 * 2\omega_2 \times \dot{d}_2\, 2\hat{X}_2 + \ddot{d}_2\, 2\hat{X}_2$$

$$= \begin{pmatrix} -l_1 \dot{\theta}_1^2 c_2 + \ddot{d}_1 c_2 + l_1 \ddot{\theta} s_2 + 2\dot{d}_1 \dot{\theta}_1 s_2 + g s_{12} \\ l_1 \dot{\theta}_1^2 s_2 - \ddot{d}_1 s_2 + l_1 \ddot{\theta} c_2 + 2\dot{d}_1 \dot{\theta}_1 c_2 + g c_{12} \\ 0 \end{pmatrix}$$

$$2\dot{v}_{C2} = 2\dot{\omega}_2 \times 2P_{C2} + 2\omega_2 \times (2\omega_2 \times 2P_{C2}) + 2\dot{v}_2 = \begin{pmatrix} -(l_1 c_2 + d_2 C_{C2})\dot{\theta}_1^2 + (l_1 s_2 - d_2 S_{C2})\ddot{\theta}_1 + 2\dot{d}_1 \dot{\theta}_1 s_2 + \ddot{d}_1 c_2 + g s_{12} \\ (l_1 s_2 + d_2 s_{C2})\dot{\theta}_1^2 + (l_1 c_2 - d_2 c_{C2})\ddot{\theta}_1 + 2\dot{d}_1 \dot{\theta}_1 c_2 + \ddot{d}_1 s_2 + g c_{12} \\ 0 \end{pmatrix}$$

$$2N_2 = c2 I_2\, 2\dot{\omega}_2 + 2\omega_2 \times c2 I_2\, 2\omega_2 = \begin{pmatrix} 0 & 0 & 0 \\ 0 & 0 & 0 \\ 0 & 0 & I_{ZZ2} \end{pmatrix}\begin{pmatrix} 0 \\ 0 \\ \ddot{\theta}_1 \end{pmatrix} + \begin{pmatrix} 0 \\ 0 \\ \dot{\theta}_1 \end{pmatrix} \times \left(\begin{pmatrix} 0 & 0 & 0 \\ 0 & 0 & 0 \\ 0 & 0 & I_{ZZ4} \end{pmatrix}\begin{pmatrix} 0 \\ 0 \\ \dot{\theta}_1 \end{pmatrix} \right) = \begin{pmatrix} 0 \\ 0 \\ I_{ZZ2} \ddot{\theta}_1 \end{pmatrix}$$

And based on the Newton's second law the dipper inertial force is:

$$2F_2 = m_2 2\dot{v}_{C2} = \begin{pmatrix} -m_2(l_1 c_2 + d_2 C_{C2})\dot{\theta}_1^{*2} + m_2(l_1 s_2 - d_2 S_{C2})\ddot{\theta}_1 + m_2 2\dot{d}_1 \dot{\theta}_1 s_2 + m_2 \ddot{d}_1 c_2 + m_2 g s_{12} \\ m_2(l_1 s_2 + d_2 s_{C2})\dot{\theta}_1^{*2} + m_2(l_1 c_2 - d_2 c_{C2})\ddot{\theta}_1 + m_2 2\dot{d}_1 \dot{\theta}_1 c_2 + m_2 \ddot{d}_1 s_2 + m_2 g c_{12} \\ 0 \end{pmatrix}$$

So far all forces and torques on the dipper and crowd arm are computed. Now is time to combine these in terms of the forces and moment balance equations based on the free body diagrams of the crowd arm and the dipper (Figure 59). In this figure the following parameters are being defined:

θ_b is the angle between dipper bottom and $\overline{O_2 D}$;

θ_{C2} is the angle between $\overline{O_2 D}$ and $\overline{O_2 C_2}$;

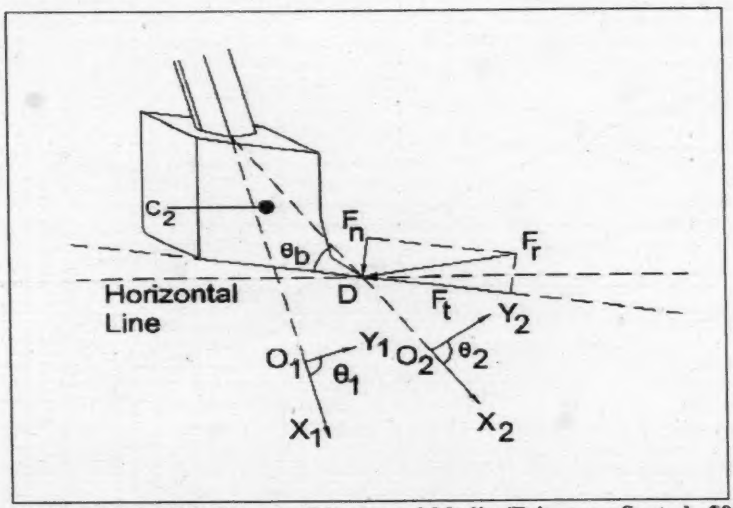

Figure 59: Interaction Between Dipper and Media (Frimpong S. et al., 2005)

Therefore, for the dipper following can be written:

$$
{}^{2}f_{2} = {}^{3}_{2}R\,{}^{3}f_{3} + {}^{2}F_{2}
$$

$$
= \begin{pmatrix} -m_2(l_1 c_2 + d_2 C_{c2})\dot{\theta}_1^{2} + m_2(l_1 s_2 + d_2 s_{c2})\ddot{\theta}_1 + 2m_2 \dot{d}_1 \dot{\theta}_1 s_2 + m_2 \ddot{d}_1 c_2 + F_t c_{\theta_b} - F_n s_{\theta_b} + m_2 g s_{12} \\ m_2(l_1 s_2 + d_2 s_{c2})\dot{\theta}_1^{2} + m_2(l_1 c_2 + d_2 c_{c2})\ddot{\theta}_1 + 2m_2 \dot{d}_1 \dot{\theta}_1 c_2 + m_2 \ddot{d}_1 s_2 + F_t s_{\theta_b} - F_n c_{\theta_b} + m_2 g c_{12} \\ 0 \end{pmatrix}
$$

$$
{}^{2}n_{2} = {}^{2}N_{2} + {}^{2}_{3}R\,{}^{3}n_{3} + {}^{2}P_{C2} \times {}^{2}F_{2} + {}^{2}P_{3} \times {}^{2}_{3}R\,{}^{3}f_{3}
$$

$$
= \begin{pmatrix} 0 \\ 0 \\ I_{ZZ2}\ddot{\theta}_1 + m_2 l_1 d_2 s_{2_{C2}}\dot{\theta}_1^{2} + m_2(l_1 c_{2_{C2}} + d_2)d_2\ddot{\theta}_1 + 2m_2 d_2 \dot{d}_1 \dot{\theta}_1 c_{2_{C2}} - m_2 d_2 \ddot{d}_1 s_{2_{C2}} \end{pmatrix}
$$

$$
+ \begin{pmatrix} 0 \\ 0 \\ m_2 d_2 g c_{12_{C2}} + F_t l_2 s_{2\theta_b} + F_n l_2 c_{2\theta_b} \end{pmatrix}
$$

Also with the same procedure we can write inward iteration for the crowd arm:

$$
{}^{1}f_{1} = {}^{2}_{1}R\,{}^{2}f_{2} + {}^{1}F_{1}
$$

$$
= \begin{pmatrix} -(m_1 d_1 + m_2(l_1 + d_2 C_{2c2}))\dot{\theta}_1^{2} - m_2 d_2 s_{2c2}\ddot{\theta}_1 + (m_1 + m_2)\ddot{d}_1 + F_t c_{2\theta_b} - F_n s_{2\theta_b} + (m_1 + m_2) g s_1 \\ -m_2 d_2 s_{2c2}\dot{\theta}_1^{2} + (m_1 d_1 + m_2)(l_1 + d_2 c_{2c2})\ddot{\theta}_1 + 2(m_1 + m_2)\dot{d}_1 \dot{\theta}_1 + F_t s_{2\theta_b} - F_n c_{2\theta_b} + (m_1 + m_2) g c_1 \\ 0 \end{pmatrix}
$$

$$
{}^{1}n_{1} = {}^{1}N_{1} + {}^{2}_{1}R\,{}^{2}n_{2} + {}^{1}P_{C1} \times {}^{1}F_{1} + {}^{1}P_{2} \times {}^{1}_{2}R\,{}^{2}f_{2}
$$

$$
= \begin{pmatrix} 0 \\ 0 \\ (I_{ZZ1} + I_{ZZ2})\ddot{\theta}_1 \end{pmatrix}
$$

$$
+ \begin{pmatrix} 0 \\ 0 \\ (m_1 d_1^2 + m_2(l_1^2 + 2l_1 d_1 c_{2C2} + d_1^2))\ddot{\theta}_1 + 2(m_1 d_1 + m_2(l_1 + d_2 c_{2c2}))\dot{d}_1 \dot{\theta}_1 - m_2 d_2 \ddot{d}_1 s_{2C2} \end{pmatrix}
$$

$$
+ \begin{pmatrix} 0 \\ 0 \\ (m_1 d_1 c_1 + m_2(l_1 c_1 + d_2 c_{12C2}))g \end{pmatrix} + \begin{pmatrix} 0 \\ 0 \\ F_t(l_1 + l_2)s_{2\theta_b} + F_n(l_1 + l_2)c_{2\theta_b} \end{pmatrix}
$$

And the crowd inertial force and torque:

$$F_1 = (m_1 + m_2)\ddot{d}_1 - (m_1 d_1 + m_2(l_1 + d_2 c_{2C2}))\dot{\theta}_1^2 - m_2 d_2 s_{2C2}\ddot{\theta}_1$$
$$+ (m_1 + m_2)gs_1 + F_t c_{2\theta_b} - F_n s_{2\theta_b}$$

$$\tau_1 = (I_{ZZ1} + I_{ZZ2})\ddot{\theta}_1 + (m_1 d_1^2 + m_2(l_1^2 + 2l_1 d_1 c_{2C2} + d_1^2))\ddot{\theta}_1$$
$$+ 2(m_1 d_1 + m_2(l_1 + d_2 c_{2C2}))\dot{d}_1\dot{\theta}_1 - m_2 d_2 \ddot{d}_1 s_{2C2}$$
$$+ (m_1 d_1 c_1 + m_2(l_1 c_1 + d_2 c_{12C2}))g + F_t(l_1 + l_2)s_{2\theta_b} + F_n(l_1 + l_2)c_{2\theta_b}$$

Appendix E: MIDAS Post Processed Data Sheets

MIDAS software is available in two different applications. MIDAS Desktop and MIDAS Report. The two software receive their master database from coded file generated by on board-installed device on shovel so called SiRAS remote technology. All production parameters will be captured and recorded at any given second as long as shovel become online on dispatch system. On perception the concept of evaluating the shovel KPI's, the following high-level spreadsheet as shown in Table 13 is prepared. Decoded MIDAS database was used to input the shovel operating values to the equations and calculations. Then by using the mathematical/geometrical equations and correlation between different angles (Figure 60) the major forces including hoist, crowd, and cutting forces calculated. Shown variable angles can be easily calculated based on the law of sins and cosines in triangle. Then simply can determine the position of dipper at any given second and draw the position of it in a X-Y system. As well, the trajectory, which is a function of time and position of dipper can be illustrated:

$$A = f(t, X, Y)$$

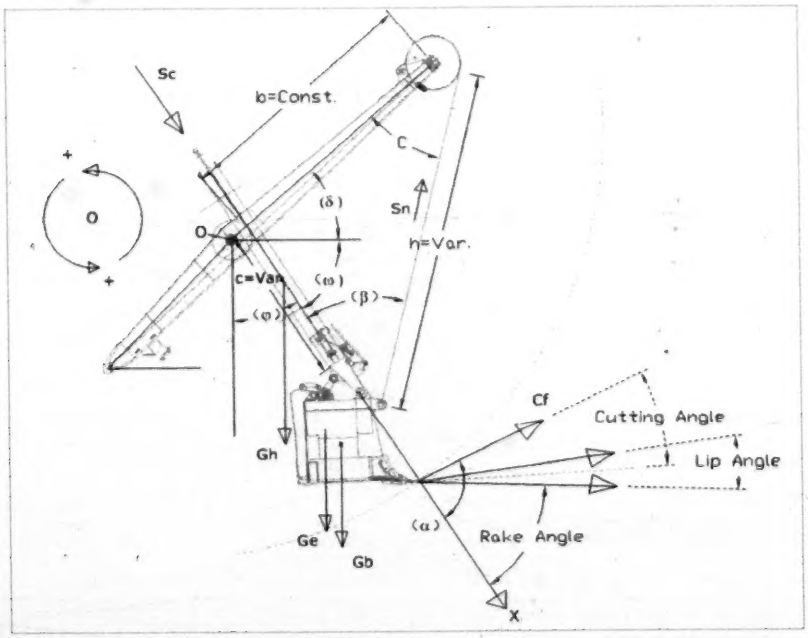

Figure 60: Handle Free Body Geometry

To measure the cutting force as well as its direction at any given second following relations has been used in this research study. In order to depict the relationship of these angles one can add:

$$\varphi = 90 - \omega$$

$$\omega = H - \delta$$

$$\begin{cases} C = Cos^{-1}\left(\dfrac{b^2 + h^2 - c^2}{2bh}\right) \\ H = Cos^{-1}\left(\dfrac{b^2 + c^2 - h^2}{2bc}\right) \\ \beta = Cos^{-1}\left(\dfrac{c^2 + h^2 - b^2}{2ch}\right) \end{cases} \quad \text{And} \quad \begin{cases} \Sigma Fx = 0 \\ \Sigma Mo = 0 \end{cases}$$

$$\therefore \begin{cases} Cf * Cos\alpha = Sc + Sn * Cos\beta - \Sigma Gi * Cos\varphi \\ Cf * R_{Cf} * Sin\alpha = Sn * Rc * Sin\beta - \Sigma Gi * Ri * Sin\varphi \end{cases}$$

$$\Rightarrow \begin{cases} Sin\alpha = \dfrac{Sn * Rc * Sin\beta - \Sigma Gi * Ri * Sin\varphi}{Rc_f * Cf} \rightarrow (\mathrm{I}) \\ Cos\alpha = \dfrac{Sn * Cos\beta - Sc - \Sigma G * Cos\varphi}{Cf} \rightarrow (\mathrm{II}) \end{cases}$$

$$\Rightarrow \alpha = Tang^{-1}\left(\frac{\mathrm{I}}{\mathrm{II}}\right)$$

And cutting force simply can be calculated from one of the two above-mentioned equations.

In above relations where:

δ is the boom angle to horizontal axis coincide to dipper handle;

Cf cutting force, RCf distance from centre of rotation to tangent vector of cutting force;

Ri the distance from centre of rotation "O" to each of centre of mass on boom, dipper and material in dipper, and

Sn Hoist force, Rc is the crowd extent, and Sc is the crowd force.

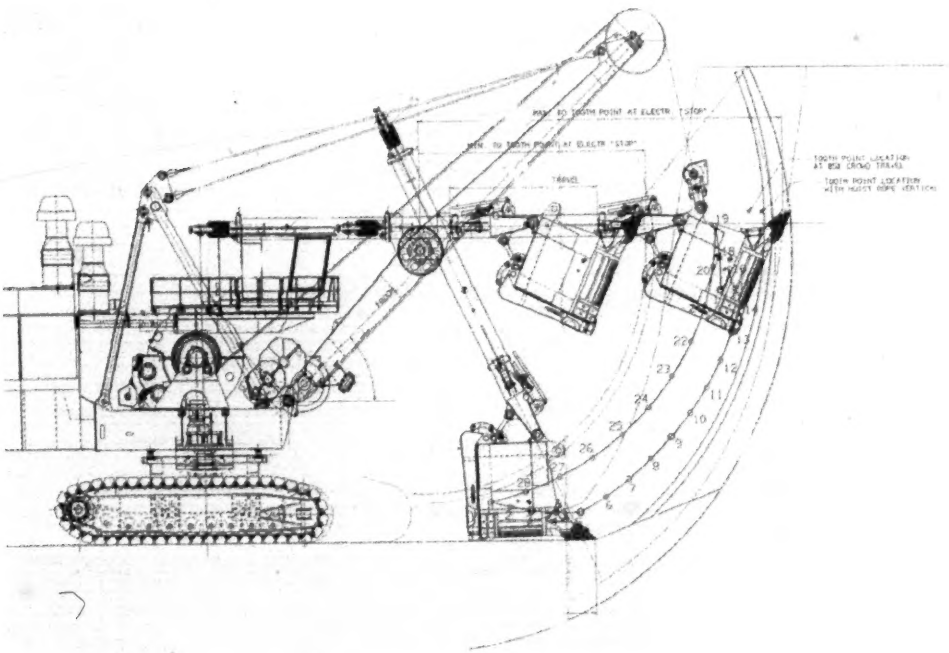

Figure 61: Tooth Point Trajectory

Also, in developed database, it was essential to detect the filling rate in dipper to allocate dipper weigh at any given second during the cut cycle. Figure 61 is good indication of trajectory of dipper teeth each second of dig cycle. As shown in this figure, dipper trajectory is divided into three sections. Positions are based on dipper tooth point. Position 1 to 5 is called beginning of dig cycle, 5 to 13 is where the majority of dirt fills into the dipper and position 13 to 14 end of the dig cycle. Usually it takes two times of dipper length to make it full of material.

It also should be mentioned that when dipper handle reaches to its end limits (maximum axial travel to the shipper shaft) the electrical system slows down and followed by electrical stop applies. The same mechanism engages when the handle gets close to minimum travel through the shipper shaft.

In bench marking the data the boom considered a solid static part hence the boom angle deemed a constant number. Also to evaluate the dig cycles the data filtered down to only those digging in the face and not the ones for which time consumed for floor clearing and wait time for truck.

To calculate the values of the digging force, the crowd and hoist force need to be measured. Since the software only collects the data recorded from electric motors and rope drums (i.e. torques, amps, powers, etc.), the engineering design conversion ratios have been entered in calculations to translate the motor torques into crowd/hoist forces. With the same approach the crowd and hoist speed measured by converting the crowd and hoist drums RPM's with consideration of the ration of crowd/hoist RPM to motor speed (RPM). Also by having the maximum design limit numbers on crowd/hoist forces on each main positions of the dipper one can QA the integrity of the calculations on spreadsheets.

As mentioned in chapter 4, to determine the dig cycle from collected data hoist length was found good indicator of beginning of the dig when it approaches its maximum length with a rapid change in direction of crowd power from negative to positive. This is; however, need to be carried on with another satisfying condition, which in turn is the constant change of the hoist power from negative to positive, meaning the dipper engaged in the soil removal and trying to penetrate in dirt and overcome to cutting resistance. Once the dipper comes to end of its travel in face, retract engages, and the hoist power turns to its minimum positive value.

Based on operating key indicators' values in the database piggy backing to the MIDAS Report one can easily anatomize the digging process on any given second on different shifts, operators, faces, and weather and hydrological conditions to evaluate the share and effect of each of those mentioned on shovel operation productivity. For this goal, I scrutinized several shovels operating data and analyzed their KPI's as well as trajectories in an attempt to come to level of results needed for this research study.

TABLE 13: NORMALIZED RAW DATA TO BE REPORTABLE TO PUBLIC

Date	Time		Normalized Raw Data (Devided by Average of Each Population)													
Value/Average		Load Cycle Time	Crowd Speed	Crowd Torque	Percent Crowd Torque	Crowd Working Current	Crowd Power	Crowd Extension	Hoist Speed	Hoist Torque	Percent Hoist Torque	Hoist Working Current	Hoist Power	Hoist Rope Length	Percent Swing Torque	Swing Working Current
1-Dec-04	4:05:13 AM	0	-917.2589179	1173.26082	1173.26082	2038.891731	-898.7312678	22	231.2060132	113.428531	113.428531	103.603599	-259.3578242	56	-723.4999094	-1005.218688
1-Dec-04	4:05:14 AM	1	-914.0253377	-1657.230909	-1657.230909	-3058.337597	1136.836695	24	-299.8538793	225.0275696	225.0275696	210.3567474	254.4357049	55	-39.10810321	-448.0403295
1-Dec-04	4:05:15 AM	2	-315.8129999	-263.9836846	-263.9836846	-505.3663265	259.1147292	26	-421.7724896	230.5160469	230.5160469	216.821612	403.4244696	53	0	-109.138029
1-Dec-04	4:05:16 AM	3	-2.69465017	-1789.222751	-1789.222751	-2892.786559	23.34366929	27	-421.7724896	230.5160469	230.5160469	220.1369271	403.4244696	51	0	0
1-Dec-04	4:05:17 AM	4	328.7473208	-1583.902107	-1583.902107	-2544.258058	23.34366929	27	-359.1656357	228.6865545	228.6865545	213.6720626	340.9514171	49	0	-109.138029
1-Dec-04	4:05:18 AM	5	-2.69465017	-1319.918423	-1319.918423	-2204.442769	11.67183465	27	-343.7885137	228.6865545	228.6865545	216.821612	326.5636838	47	0	0
1-Dec-04	4:05:19 AM	6	-159.5232901	-1730.55971	-1730.55971	-2718.522308	212.4273906	28	-331.1573063	228.6865545	228.6865545	216.821612	316.9087574	46	0	-109.138029
1-Dec-04	4:05:20 AM	7	-143.8943191	190.6548833	190.6548833	-339.8152885	343.1519386	28	-293.8128671	228.6865545	228.6865545	216.821612	292.8660978	44	0	0
1-Dec-04	4:05:21 AM	8	328.7473208	-879.9456152	-879.9456152	-1524.812192	0	28	-293.8128671	228.6865545	228.6865545	216.821612	273.7455575	43	0	0
1-Dec-04	4:05:22 AM	9	-128.8042781	351.9782461	351.9782461	-165.551038	140.0620158	29	-306.4440745	228.6865545	228.6865545	216.821612	292.8660978	41	0	0
1-Dec-04	4:05:23 AM	10	-315.8129999	-1715.89395	-1715.89395	-2718.522308	294.1302331	29	-337.7475014	228.6865545	228.6865545	216.821612	302.5210241	39	0	0
1-Dec-04	4:05:24 AM	11	-478.5698702	-1686.562429	-1686.562429	-2718.522308	627.944704	30	-337.7475014	228.6865545	228.6865545	216.821612	321.8308767	38	0	-109.138029
1-Dec-04	4:05:25 AM	12	-521.6842729	-1730.55971	-1730.55971	-2718.522308	721.3193812	32	-331.1573063	228.6865545	228.6865545	216.821612	312.1759504	36	0	0
1-Dec-04	4:05:26 AM	13	-536.7743139	-1701.228189	-1701.228189	-2718.522308	697.9757119	33	-312.4850867	226.8570621	226.8570621	216.821612	254.4357049	35	0	-109.138029
1-Dec-04	4:05:27 AM	14	-579.8887166	-1686.562429	-1686.562429	-2718.522308	758.669252	34	-337.7475014	228.6865545	228.6865545	213.6720626	312.1759504	33	0	0
1-Dec-04	4:05:28 AM	15	-9.161810578	-659.9592114	-659.9592114	-1359.261154	-11.67183465	35	-456.3710141	226.8570621	226.8570621	223.2864765	384.3039293	31	0	0
1-Dec-04	4:05:29 AM	16	266.7703668	1466.576025	1466.576025	1524.812192	0	35	-568.9535146	181.1197512	181.1197512	226.6017917	422.7343222	29	2463.810502	3699.204771
1-Dec-04	4:05:30 AM	17	1104.80657	630.6276909	630.6276909	1184.996904	473.8764867	34	-518.9778681	-67.69122013	-67.69122013	-129.4630573	19.12054032	25	2405.148347	3590.066742
1-Dec-04	4:05:31 AM	18	604.1405681	-1070.600499	-1070.600499	-1359.261154	-1136.836695	32	30.75424403	151.8478722	151.8478722	129.4630573	0	24	2229.161883	3251.164442
1-Dec-04	4:05:32 AM	0	-2.69465017	439.9728076	439.9728076	505.3663265	0	32	252.6241474	142.70041	142.70041	135.9279219	4.732807011	24	2131.391625	3360.302471
1-Dec-04	4:05:33 AM	0	334.1366211	469.3043281	469.3043281	679.630577	0	32	241.6404888	135.3824403	135.3824403	129.4630573	4.732807011	24	2014.067315	3136.282306
1-Dec-04	4:05:34 AM	0	334.1366211	527.9673691	527.9673691	679.630577	0	32	236.1486595	146.3593949	146.3593949	139.0774713	4.732807011	24	1955.40516	2912.262141
1-Dec-04	4:05:35 AM	0	-355.6938225	-1701.228189	-1701.228189	-2718.522308	282.4583985	32	247.1323181	142.70041	142.70041	135.9279219	4.732807011	24	1740.310593	2803.124112
1-Dec-04	4:05:36 AM	0	-1107.50122	-14.66576025	-14.66576025	-165.551038	11.67183465	33	225.165001	-113.428531	-113.428531	-119.6828776	110.3690595	25	-606.1755997	-448.0403295
1-Dec-04	4:05:37 AM	0	-230.1231245	689.2907319	689.2907319	1184.996904	-497.220156	35	-56.01665878	228.6865545	228.6865545	213.6720626	0	25	-2092.283522	-3360.302471
1-Dec-04	4:05:38 AM	0	336.8312713	0	0	0	0	35	-447.0349043	221.3685848	221.3685848	207.207198	379.38181	24	-1916.297057	-3027.144277
1-Dec-04	4:05:39 AM	0	797.6164504	1745.22547	1745.22547	2544.258058	770.3410867	35	-746.8887837	133.5529478	133.5529478	216.821612	413.0793959	21	-2463.810502	-3923.224936
1-Dec-04	4:05:40 AM	0	1098.339409	263.9836846	263.9836846	505.3663265	282.4583985	33	-243.8372206	-62.20274282	-62.20274282	-61.49909636	-129.6789121	18	-2385.594296	-3699.204771
1-Dec-04	4:05:41 AM	0	42.57547269	-1070.600499	-1070.600499	-1524.812192	-105.0465118	32	225.165001	53.05528064	53.05528064	55.03423178	0	18	-2150.945676	-3360.302471
1-Dec-04	4:05:42 AM	0	334.1366211	395.9755269	395.9755269	505.3663265	0	32	236.1486595	67.69122013	67.69122013	64.64864577	0	18	-1994.513264	-3136.282306

Appendix F: AC Motor Formulas and Calculations

Rockwell Automation
Allen-Bradley

AC Motor Formula

To Find Amperes when HP is known:

Single Phase	Two Phase - *(4 - wire)	Three Phase
$I = \frac{746 * HP}{E * Eff * PF}$	$I = \frac{746 * HP}{2 * E * Eff * PF}$	$I = \frac{746 * HP}{1.73 * E * Eff * PF}$

To find Amperes when KW is known:

Single Phase	Two Phase - *(4 - wire)	Three Phase
$I = \frac{1000 * KW}{E * PF}$	$I = \frac{1000 * KW}{2 * E * PF}$	$I = \frac{1000 * KW}{1.73 * E * PF}$

To find Amperes when KVA is known:

Single Phase	Two Phase - *(4 - wire)	Three Phase
$I = \frac{1000 * KVA}{E}$	$I = \frac{1000 * KVA}{2 * E}$	$I = \frac{1000 * KVA}{1.73 * E}$

To find Kilowatts Input:

Single Phase	Two Phase - *(4 - wire)	Three Phase
$KW = \frac{E * I * PF}{1000}$	$KW = \frac{2 * E * I * PF}{1000}$	$KW = \frac{1.73 * E * I * PF}{1000}$

To find Kilovolt Amperes:

Single Phase	Two Phase - *(4 - wire)	Three Phase
$KVA = \frac{E * I}{1000}$	$KVA = \frac{2 * E * I}{1000}$	$KVA = \frac{1.73 * E * I}{1000}$

To find Horsepower Output:

Single Phase	Two Phase - *(4 - wire)	Three Phase
$HP = \frac{E * I * Eff * PF}{746}$	$HP = \frac{2 * E * I * Eff * PF}{746}$	$HP = \frac{1.73 * E * I * Eff * PF}{746}$

* For two phase three wire balanced circuits, the Amperes in common conductor = 1.41 times that in either of the two.

Synchronous Speed:

$$n_s = \frac{120 * f}{P}$$

Frequency:

$$f = \frac{P * n_s}{120}$$

Number of poles:

$$P = \frac{120 * f}{n_s}$$

Relation between horsepower, torque and speed:

$$HP = \frac{T * n}{5250}$$

$$T = \frac{5250 HP}{n}$$

$$n = \frac{5250 HP}{T}$$

Motor Slip:

$$\%Slip = \frac{n_s - n}{n_s} * 100$$

Motor Formulas

Here are some ***motor formulas*** that may be useful.

Options:

- Useful Formulas Formulas
- Transformer Formulas

Calculating Motor Speed:

A squirrel cage induction motor is a constant speed device. It cannot operate for any length of time at speeds below those shown on the nameplate without danger of burning out.

To Calculate the *speed of a induction motor*, apply this formula:

$$Srpm = \frac{120 \times F}{P}$$

S*rpm* = synchronous revolutions per minute.
120 = constant
F = supply frequency (in cycles/sec)
P = number of motor winding poles

Example: What is the synchronous of a motor having 4 poles connected to a 60 hz power supply?

$$Srpm = \frac{120 \times F}{P}$$

$$Srpm = \frac{120 \times 60}{4}$$

$$Srpm = \frac{7200}{4}$$

$$Srpm = 1800 \text{ rpm}$$

Calculating Braking Torque:

Full-load motor torque is calculated to determine the required braking torque of a motor.

To Determine *braking torque* of a motor, apply this formula:

$$T = \frac{5252 \times HP}{rpm}$$

T = full-load motor torque (in lb-ft)
5252 = constant (33,000 divided by 3.14 x 2 = 5252)
HP = motor horsepower
rpm = speed of motor shaft

Example: What is the braking torque of a 60 HP, 240V motor rotating at 1725 rpm?

$$T = \frac{5252 \times HP}{rpm}$$

$$T = \frac{5252 \times 60}{1725}$$

$$T = \frac{315,120}{1725}$$

$$T = 182.7 \text{ lb-ft}$$

Calculating Work:

Work is applying a force over a distance. Force is any cause that changes the position, motion, direction, or shape of an object. Work is done when a force overcomes a resistance. Resistance is any force that tends to hinder the movement of an object. If an applied force does not cause motion the no work is produced.

To calculate the amount of work produced, apply this formula:

$$W = F \times D$$

W = work (in lb-ft)
F = force (in lb)
D = distance (in ft)

Example: How much work is required to carry a 25 lb bag of groceries vertically from street level to the 4th floor of a building 30' above street level?

$$W = F \times D$$
$$W = 25 \times 30$$
$$W = 750 \text{ lb}$$

Calculating Torque:

Torque is the force that produces rotation. It causes an object to rotate. Torque consist of a force acting on distance. Torque, like work, is measured is pound-feet (lb-ft). However, torque, unlike work, may exist even though no movement occurs.

To calculate torque, apply this formula:

$$T = F \times D$$

T = torque (in lb-ft)
F = force (in lb)
D = distance (in ft)

Example: What is the torque produced by a 60 lb force pushing on a 3' lever arm?

$$T = F \times D$$
$$T = 60 \times 3$$
$$T = 180 \text{ lb ft}$$

Calculating Full-load Torque:

Full-load torque is the torque to produce the rated power at full speed of the motor. The amount of torque a motor produces at rated power and full speed can be found by using a horsepower-to-torque conversion chart. When using the conversion chart, place a straight edge along the two known quantities and read the unknown quantity on the third line.

To calculate motor full-load torque, apply this formula:

$$T = \frac{HP \times 5252}{rpm}$$

T = torque (in lb-ft)
HP = horsepower
5252 = constant
rpm = revolutions per minute

Example: What is the FLT (Full-load torque) of a 30HP motor operating at 1725 rpm?

$$T = \frac{HP \times 5252}{rpm}$$
$$T = \frac{30 \times 5252}{1725}$$
$$T = \frac{157,560}{1725}$$
T = 91.34 lb-ft

Calculating Horsepower:

Electrical power is rated in horsepower or watts. A horsepower is a unit of power equal to 746 watts or 33,0000 lb-ft per minute (550 lb-ft per second). A watt is a unit of measure equal to the power produced by a current of 1 amp across the potential difference of 1 volt. It is 1/746 of 1 horsepower. The watt is the base unit of electrical power. Motor power is rated in horsepower and watts.
Horsepower is used to measure the energy produced by an electric motor while doing work.

To calculate the horsepower of a motor when current and efficiency, and voltage are known, apply this formula:

$$HP = \frac{V \times I \times Eff}{746}$$

HP = horsepower
V = voltage
I = curent (amps)
Eff. = efficiency

Example: What is the horsepower of a 230v motor pulling 4 amps and having 82% efficiency?

$$HP = \frac{V \times I \times Eff}{746}$$
$$HP = \frac{230 \times 4 \times .82}{746}$$
$$HP = \frac{754.4}{746}$$
HP = 1 Hp

Eff = efficiency / HP = horsepower / V = volts / A = amps / PF = power factor

Horsepower Formulas				
To Find	Use Formula	Example		
		Given	Find	Solution
				HP = 240V x 20A x 85%

HP	HP = I X E X Eff / 746	240V, 20A, 85% Eff.	HP	746 HP=5.5
I	I = HP x 746 / E X Eff x PF	10HP, 240V, 90% Eff., 88% PF	I	I = 10HP x 746 / 240V x 90% x 88% I = 39 A

To calculate the horsepower of a motor when the speed and torque are known, apply this formula:

$$HP = \frac{rpm \times T(torque)}{5252(constant)}$$

Example: What is the horsepower of a 1725 rpm motor with a FLT 3.1 lb-ft?

$$HP = \frac{rpm \times T}{5252}$$
$$HP = \frac{1725 \times 3.1}{5252}$$
$$HP = \frac{5347.5}{5252}$$
$$HP = 1\ hp$$

Calculating Synchronous Speed:

AC motors are considered constant speed motors. This is because the synchronous speed of an induction motor is based on the supply frequency and the number of poles in the motor winding. Motor are designed for 60 hz use have synchronous speeds of 3600, 1800, 1200, 900, 720, 600, 514, and 450 rpm.

To calculate synchronous speed of an induction motor, apply this formula:

$$rpm_{syn} = \frac{120 \times f}{Np}$$

rpm_{syn} = synchronous speed (in rpm)
f = supply frequency in (cycles/sec)
Np = number of motor poles

Example: What is the synchronous speed of a four pole motor operating at 50 hz.?

$$rpm_{syn} = \frac{120 \times f}{Np}$$
$$rpm_{syn} = \frac{120 \times 50}{4}$$
$$rpm_{syn} = \frac{6000}{4}$$
$$rpm_{syn} = 1500\ rpm$$

Check out these Online Calculators!

If there is anything you would like to add or if you have any comments please feel free to email E.T.E.

Back to Main Page

1997, Electricians Toolbox Etc...

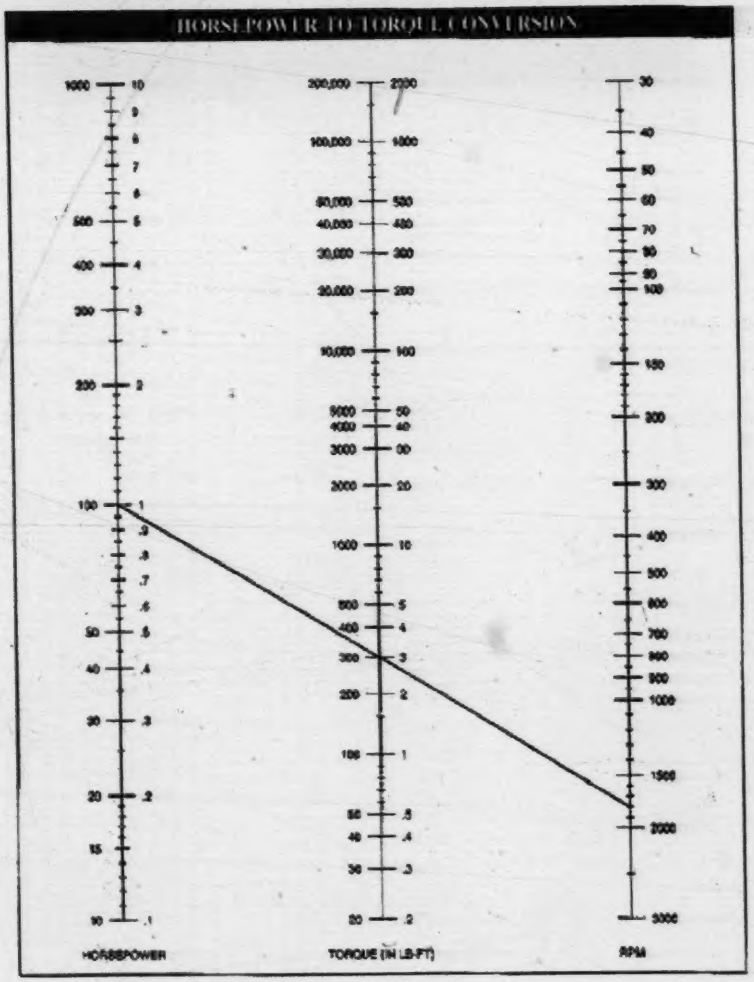
HORSEPOWER TO TORQUE CONVERSION
HORSEPOWER
TORQUE (IN LB-FT)
RPM